

THIS REPORT HAS BEEN DELIM.TED
AND CLEARED FOR PUBLIC RELEASE
UNDER DOD DIRECTIVE 5200.20 AND
NO RESTRICTIONS ARE IMPOSED UPON
ITS USE AND DISCLOSURE.

DISTRIBUTION STATEMENT A

APPROVED FOR PUBLIC RELEASE;
DISTRIBUTION UNLIMITED.

UNCLASSIFIED

AD

401 112

*Reproduced
by the*

DEFENSE DOCUMENTATION CENTER

FOR

SCIENTIFIC AND TECHNICAL INFORMATION

CAMERON STATION, ALEXANDRIA, VIRGINIA



UNCLASSIFIED

NOTICE: When government or other drawings, specifications or other data are used for any purpose other than in connection with a definitely related government procurement operation, the U. S. Government thereby incurs no responsibility, nor any obligation whatsoever; and the fact that the Government may have formulated, furnished, or in any way supplied the said drawings, specifications, or other data is not to be regarded by implication or otherwise as in any manner licensing the holder or any other person or corporation, or conveying any rights or permission to manufacture, use or sell any patented invention that may in any way be related thereto.

R62-36

401 112

**FLOW INDUCED VIBRATION
OF FLAT PLATES:**

THE MECHANISM OF SELF-EXCITATION

by

P. S. Eagleson

J. W. Dally

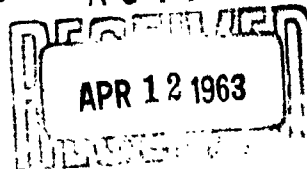
G. K. Noutsopolous

CATALOGED BY ASTIA
AS AD 401112

HYDRODYNAMICS LABORATORY

Report No. 58

ASTIA



Prepared Under

BUREAU OF SHIPS FUNDAMENTAL HYDROMECHANICS RESEARCH PROGRAM

Project S-R009 01 01

Contract No. Nonr-1841 (21)

TECHNICALLY ADMINISTERED BY THE

DAVID TAYLOR MODEL BASIN

U. S. Department of the Navy

Washington, D. C.

February, 1963

MIT

**DEPARTMENT
OF
CIVIL
ENGINEERING**

**SCHOOL OF ENGINEERING
MASSACHUSETTS INSTITUTE OF TECHNOLOGY
Cambridge 39, Massachusetts**

R 62-36

HYDRODYNAMICS LABORATORY
Department of Civil Engineering
Massachusetts Institute of Technology

FLOW-INDUCED VIBRATION OF FLAT PLATES:
THE MECHANISM OF SELF-EXCITATION

by

P.S. Eagleson, J.W. Daily and G.K. Noutsopolous

February 1963

Report No. 58

Prepared Under
Bureau of Ships Fundamental Hydromechanics Research Program
Project S-R009 01 01
Contract No. Nonr - 1841 (21)

Technically Administered by the
David Taylor Model Basin
U.S. Department of the Navy
Washington, D.C.

(Reproduction of this report in whole or in part is permitted for any purpose of the United States Government.)

ACKNOWLEDGEMENTS

This study was conducted as part of a general investigation of wake mechanics sponsored by the David Taylor Model Basin, U. S. Department of the Navy, under Contract No. Nonr - 1841 (21). Contract administration was provided by the Division of Sponsored Research of M.I.T. under DSR 7579.

The work was performed in the Hydrodynamics Laboratory of the Department of Civil Engineering at M.I.T. under the general direction of Dr. James W. Daily, Professor of Hydraulics. Dr. Peter S. Eagleson, Associate Professor of Civil Engineering, served as project technical supervisor.

The work was carried out by Mr. Georges K. Noutsopolous, Research Assistant in Civil Engineering.

ABSTRACT

Study is made of the vibrational behavior of flat plates when placed parallel to a uniform stream and allowed one degree of freedom torsional oscillation around a vertical axis through their leading edge.

The experimental work was carried out in the 7-1/2" x 9" test section of an open-circuit water tunnel in the Hydrodynamics Laboratory of the Civil Engineering Department at M.I.T. Four test plates were used, each 1/4 inch thick and 2 inches in chord, but having different trailing edge geometries. Measurements were made of the amplitude and frequency of plate vibration and of the fluctuating total head in the wake over the range of free-stream velocity producing significant vibrational excitation. Measurable vibrations are found to occur in three distinct regions surrounding the natural resonant frequencies of the system.

An equation of motion of the plate-spring system is developed incorporating the hydrodynamic loads given by the linearized potential theory, and the unknown, vortex-induced, forcing moments. Using this linear model and the experimental data, forcing moment coefficients are obtained which show a unique (for all plates) and piecewise linear dependence upon a "self-excitation" parameter consisting of the ratio of the mean transverse velocity of the trailing edge to the free-stream velocity. This dependence of moment coefficient on vibrational amplitude is equivalent to a negative damping and thus yields eigenvalues of frequency at which the amplitude tends to grow without bound.

These critical frequencies and the free-stream velocities at which they occur are predicted knowing only the physical system constants, the body's steady-state Strouhal number, and the slope of the moment coefficient function. They are shown to agree with the bounds of the region of large amplitude motion and variable Strouhal number obtained in these experiments and in those of other investigators.

Major conclusions of this study are:

1. Controlled variation of the system parameters, i.e., increasing the combined structural-viscous damping and increasing the steady-state Strouhal number, allows design of a system in which self-excitation is avoided.
2. The primary role of trailing edge geometry in flow-induced vibrations is in determining the free-stream velocity for resonant response through establishment of the steady-state Strouhal number.
3. Self-excitation, the increase in moment coefficient with increasing vibrational amplitude, is due both to increasing two-dimensionality of the wake and to increasing strength of the discrete vortices.

TABLE OF CONTENTS

	<u>Page</u>
I. INTRODUCTION	1
A. Flow Induced Vibrations	1
B. Scope of the Investigation	1
II. LITERATURE REVIEW	2
A. Engineering Aspects of Flow-Induced Vibrations	2
B. Wake Studies	4
III. EXPERIMENTAL EQUIPMENT	6
A. Water Tunnel	6
B. Test Plates	6
C. Torsion Spring and Plate Mounting Device	6
1. Basic Design Criteria	6
2. Description of the Mounting Assembly	8
D. Measurement of Plate Motion	10
1. Strain Gages	10
2. Amplifier	10
3. Oscilloscope	10
4. A.C. Voltmeter	10
5. Vibration Analyzer	10
E. Velocity Measurements	12
F. Measurements of Total Head Fluctuations	12
IV. FORMULATION OF THE LINEARIZED VIBRATIONAL PROBLEM	15
V. PRESENTATION AND DISCUSSION OF RESULTS	20
A. System Constants	20
B. Exploratory Tests	23
1. Experimental Procedure	23
2. Vibrational Characteristics	23
3. Wake Characteristics	24
4. Conclusions	26
C. Final Tests - Vibrational Measurements	26
1. Experimental Procedure	26
2. Qualitative Vibrational Characteristics	27
3. The Strouhal Number	29
4. Vibrational Amplitude versus Ambient Velocity	31
5. Reproducibility of Results	31
6. The Response Curves	32

TABLE OF CONTENTS (continued)

	<u>Page</u>
7. The Forcing Moment Coefficient	32
8. Range I - The Frequency Range of Large Vibrational Amplitudes	36
9. The Critical Value of c_{sv}	40
10. Range II - The Velocity Range of Large Vibrational Amplitudes	41
11. Range III - The Velocity Range of Small Varying Amplitude Vibrations	48
12. The Influence of Ambient Velocity on the Viscous Damping	49
13. The Self-Excited Nature of the Vibrations	50
D. Final Tests - Wake Measurements	53
1. Experimental Procedure	53
2. Interpretation of Wake Measurements	53
3. Correlation of Wake Measurements with Vibrational Characteristics	55
4. The Periodic Flow Field in the Wake	56
VI. SUMMARY AND CONCLUSIONS	60
VII. APPENDICES	62
A. Experimental Results	A-0
B. Spring Calibration and Free Oscillation Tests	B-1
C. References	C-1

LIST OF FIGURES

<u>No.</u>		<u>Page</u>
1.	Water Tunnel and Distribution Circuit	7
2.	Test Plates	8
3.	Plate Mounting Assembly	9
4.	Test Section	9
5.	Plate and Spring Mounting Assembly	9
6.	Interior of Test Section	11
7.	Electrical Components for Vibrational Measurements	11
8.	Block Diagram of Instrumentation for Vibrational Measurements	11
9.	Traversing System	13
10.	Electrical Components for Total Head Fluctuation Measurements	14
11.	Block Diagram of Instrumentation for Total Head Fluctuation Measurements	14
12.	The Theodorsen Function	17
13.	Coordinate System	23
14.	Graphical Representation of Equation $F_1(\omega_0) - F_2(\omega_0) = 0$	38
15.	Form of Frequency-Velocity Relationship in Range II	47
16.	Moment Coefficient	49
A1	Mean Velocity Distributions in the Wake	A-1
A2	Normalized Spectral Distributions of $(\overline{H'^2_t})^{1/2}$	A-2
A3	Normalized Spectral Distributions of $(\overline{H'^2_t})^{1/2}$	A-2
A4	Normalized Spectral Distributions of $(\overline{H'^2_t})^{1/2}$	A-3
A5	Normalized Spectral Distributions of $(\overline{H'^2_t})^{1/2}$	A-3
A6	Frequency-Amplitude versus Ambient Velocity, Plate A	A-4
A7	Frequency-Amplitude versus Ambient Velocity, Plate B	A-4
A8	Frequency-Amplitude versus Ambient Velocity, Plate C	A-5
A9	Frequency-Amplitude versus Ambient Velocity, Plate D	A-5
A10	Vibrational Signal, Plate B - Range II	A-6
A11	Vibrational Signal, Plate B - Range II	A-6
A12	Vibrational Signal, Plate B - Point of Intermittency	A-6

LIST OF FIGURES (continued)

<u>No.</u>		<u>Page</u>
A13	Vibrational Signal, Plate B - Point of Intermittency	A-6
A14	Vibrational Signal, Plate D - Range I	A-7
A15	Vibrational Signal, Plate D - Range II	A-7
A16	Vibrational Signal, Plate D - Range II	A-7
A17	Vibrational Signal, Plate D - Range II	A-7
A18	Vibrational Signal, Plate C	A-8
A19	Vibrational Signal, Plate C	A-8
A20	Normalized response curve, Plate B	A-9
A21	Normalized response curve, Plate C	A-9
A22	Normalized response curve, Plate D	A-9
A23	Reproducibility of results, Plate B - Spring II	A-10
A24	Response curve, Plate A	A-11
A25	Response curve, Plate B	A-11
A26	Response curve, Plate C	A-12
A27	Response curve, Plate D	A-12
A28	Reduced Response curve, Plate A	A-13
A29	Reduced Response curve, Plate B	A-13
A30	Reduced Response curve, Plate C	A-14
A31	Reduced Response curve, Plate D	A-14
A32	The Moment Coefficient	A-15
A33	The Moment Coefficient, Expanded Scale	A-15
A34	The Moment Coefficient, Hysteresis Effect	A-16
A35	Prediction of Critical Frequencies	A-16
A36	Prediction of Critical Velocities	A-17
A37	Transverse Wake Profiles - Fluctuating Total Head, Plate B	A-18
A38	Transverse Wake Profiles - Fluctuating Total Head, Plate C	A-18
A39	Transverse Wake Profiles - Fluctuating Total Head, Plate D	A-19
A40	Transverse Wake Profiles - Fluctuating Total Head, Plate D	A-19

LIST OF FIGURES (continued)

<u>No.</u>		<u>Page</u>
A41	Vibrational Signal versus Total Head Fluctuation Signal	A-20
B1	Sample of Spring Calibration	B-2
B2	Free Oscillation Test in Air	B-2
B3	Free Oscillation Test in Still Water	B-2
B4	Calibration of Oscilloscope versus Vibration Analyzer	B-5

LIST OF TABLES

<u>No.</u>		<u>Page</u>
I.	System Constants	22
II.	Results of Exploratory Tests	25
III.	Strouhal Numbers	30
IV.	Moment Coefficient Constants (Nominal Values)	35
V.	Critical Frequencies	40
VI.	Critical Structural plus Viscous Damping	41
VII.	Criterion for Determination of Upper Critical Velocity	45
VIII.	Free Stream Total Head Fluctuations and Vibrational Amplitudes	58

LIST OF SYMBOLS

- a = longitudinal spacing between successive vortices on one side of the von Karman vortex street.
- 2b = plate chord; 2 inches.
- c_c = critical damping coefficient; lbs-in-sec.
- c_p = $(3/2)\pi\rho b^3HV(1+C(K))$, Theodorsen damping coefficient; lbs-in-sec.
- c_s = structural damping coefficient; lbs-in-sec.
- c_t = $c_p + c_s + c_v$; total damping coefficient; lbs-in-sec.
- c_v = viscous damping coefficient; lbs-in-sec.
- c_{sv} = $c_s + c_v$; structural plus viscous damping coefficient; lbs-in-sec.
- c_{svc} = critical value of c_{sv} ; lbs-in-sec.
- C, C_I, C_{II} = dimensional moment coefficient constants; lbs-sec².
- C_{1I}, C_{1II} = dimensionless moment coefficient constants.
- C_{2I}, C_{2II} = dimensionless moment coefficient constants.
- f = frequency of forcing moment; cps.
- f_L = lower critical frequency; cps.
- f_n = natural frequency, cps.
- f_o = fundamental vibrational frequency, cps.
- f_v = frequency of vortex shedding; cps.
- f_{vo} = fundamental frequency of vortex shedding; cps.
- f_{v2}, f_{v3} = second and third harmonics of shedding frequency, cps.
- f_u = upper critical frequency; cps.
- f_a = vibrational frequency; cps.
- f_{ao} = fundamental vibrational frequency; cps.
- f_{a3} = third harmonic of vibrations; cps.
- F = strain gage factor; 2.
- F(K) = real part of Theodorsen function.
- $F_1(\omega_o),$
 $F_2(\omega_o)$ = functions of frequency as defined.

- e = 2.7182.
- \bar{e} = vibration analyzer calibration signal, RMS voltage; volts.
- e_m = amplified total head fluctuation gage signal, input to the measuring instruments; millivolts.
- e_p = voltage output of the total head fluctuation gage-pre-amplifier system; millivolts.
- e_t = instantaneous output signal of the total head fluctuation gage; millivolts.
- $e(n)$ = spectral distribution of input signal to the vibration analyzer; volts² per cps.
- E = battery voltage; volts.
- $E(f_v)$ = spectral distribution of total head fluctuation energy density; ft² of water per cps.
- g = gravitational acceleration; 32.2 ft/sec².
- G_a = amplifier gain.
- G_p = preamplifier gain.
- G_s = spring sensitivity; $\frac{\text{millivolts}}{\text{rad.volt.of battery}}$.
- h = transverse spacing between opposite rows of vortices in a Karman vortex street.
- H = spanwise length of plate; inches.
- H_t = instantaneous total head; ft. of water.
- H_t' = fluctuating total head; ft. of water.
- \bar{H}_t = mean total head; ft. of water.
- i = $\sqrt{-1}$.
- i = electrical current through Wheatstone bridge; amperes.
- I_p = apparent moment of inertia; lbs-in-sec².
- I_s = structural moment of inertia; lbs-in-sec².
- I_t = $I_p + I_s$, total moment of inertia; lbs-in-sec².
- K_G = total head fluctuation gage sensitivity; $\frac{\text{millivolts}}{\text{ft.of water}}$.
- K_p = $\pi p b^2 H V^2 C(K)$, Theodorsen spring coefficient; lbs-in.
- K_s = structural spring coefficient; lbs-in.
- K_t = $K_s + K_p$; total spring coefficient; lbs-in.
- l = length of spring surface element; inches.
- L = spring length; inches.

$$m = \frac{2g \int_0^{\delta/t} \overline{(H_t')^2}^{1/2} d\left(\frac{y}{t}\right)}{V^2 \cdot \frac{\delta}{t}} .$$

- m_f = forcing moment coefficient; dimensionless.
 m_{fo} = amplitude of forcing moment coefficient; dimensionless.
 $\overline{m_{fo}}$ = $m_{fo}/\sqrt{2}$, RMS of forcing moment coefficient; dimensionless.
 $\overline{m_{foI}}$ = RMS of forcing moment coefficient in range I; dimensionless.
 $\overline{m_{foII}}$ = RMS of forcing moment coefficient in range II; dimensionless.
 m_{fz} = two-dimensional forcing moment coefficient; dimensionless.
 M = vortex-induced forcing moment; lbs-in.
 M_p = Theodorsen moment; lbs-in.
 M_t = $M + M_p + M_v$, total moment; lbs-in.
 M_v = viscous moment; lbs-in.
 n_c = tuned frequency of the vibration analyzer; cps.
 p = instantaneous static pressure; lbs/ft².
 p' = fluctuating static pressure; lbs/ft².
 \bar{p} = mean static pressure; lbs/ft².
 r = outside radius of spring; inches.
 R, R_1, R_2, R_3, R_4 = resistances of strain gages; ohms.
 R_d = reading of vibration analyzer voltmeter.
 S = length of strain gages; inches.
 S_t = Strouhal number; dimensionless.
 t = plate thickness; 1/4 inches.
 t = time; seconds.
 T = period of oscillation; seconds.
 u = mean local velocity in the wake; fps.
 u' = fluctuating longitudinal velocity; fps.
 U = mean velocity outside the wake; fps.
 v = transverse plate velocity; inches per sec.
 v' = transverse fluctuating velocity; fps.
 V = mean ambient flow velocity; fps. or inches/sec.

- V_L = lower critical velocity; fps or inches/sec.
 V_r = mean ambient velocity at the maximum vibrational amplitude; fps.
 V_u = upper critical velocity; fps or inches/sec.
 V^* = $2b\omega_0\bar{\alpha}_0/V$, "self-excitation" parameter; dimensionless.
 w' = spanwise fluctuating velocity; fps.
 x = longitudinal coordinate, origin at trailing edge.
 x' = longitudinal coordinate, origin at the rotational axis.
 y = transverse coordinate, origin at plate centerline.
 z = spanwise coordinate, origin arbitrary.
 α = angular plate displacement; radians.
 $\dot{\alpha}$ = angular plate velocity; rad/sec.
 $\ddot{\alpha}$ = angular plate acceleration; rad/sec².
 α_0 = amplitude of plate motion; radians.
 $\bar{\alpha}_0$ = RMS of vibrational amplitude; radians.
 $\bar{\alpha}_3$ = RMS amplitude of the third harmonic; radians.
 γ = specific weight of fluid; lbs/ft³.
 δ = width of the wake; inches.
 δ' = boundary layer thickness; inches.
 Δ = an increment.
 ΔE = voltage output of the strain gages Wheatstone bridge; millivolts.
 θ = deflection angle of spring surface element; radians.
 K = $\frac{2\pi f \alpha^b}{V}$, Theodorsen reduced frequency.
 λ_1, λ_2 = proportionality constants.
 μ_1, μ_2, μ_3 = vibration analyzer constants.
 π = 3.1415.
 ρ = mass density of fluid; $\frac{\text{lbs-sec}^2}{\text{ft}^4}$ or $\frac{\text{lbs-sec}^2}{\text{inches}^4}$.
 ϕ = phase angle between forcing moment and plate motion; radians.
 ω_c = frequency at $c_{sv} = c_{svc}$; rad/sec.
 ω_L = lower critical frequency; rad/sec.

ω_n = natural frequency; rad/sec.
 ω_o = fundamental vibrational frequency; rad/sec.
 ω_u = upper critical frequency; rad/sec.
 R_t = Vt/ν , body Reynolds number.
 ν = Kinematic fluid viscosity; ft^2/sec .
RMS = root-mean-square.

I. INTRODUCTION

A. Flow-Induced Vibrations

It is an observed fact that structural members subjected to a flow field may, under certain conditions, suffer considerable vibrations. Vibration of a structure is undesirable for many reasons, one of which is the danger of collapse from fatigue of the material. It is the aim of the structural designer to avoid such a possibility.

Vibrations of smokestacks, pipe-lines, telephone wires, submarine periscopes, television antennas, turbine and propeller blades, vanes and the flutter of aircraft wings, are but a few examples of flow-induced vibrations.

This phenomenon has long attracted the attention of engineers and scientists and is still not completely understood, remaining a stimulating field of analytical and experimental research. From the fluid mechanics point of view structures can be classified into two categories: 1. Streamlined structures in which the fluid follows continuously the geometric contour of the body and 2. Unstreamlined or "bluff" structures in which the flow becomes separated from the boundary. Structures of the first category are used extensively in aerodynamics and well established theories exist for the computation of their dynamic loads. Structures of the second category are used extensively in civil and mechanical engineering practice. Separation of flow occurs in such structures and since there is no complete theory for computation of the resulting dynamic loads, experimental work becomes the basic source of information.

The shedding of discrete vortices in the wake of an unstreamlined body submerged in a uniform stream has been recognized as instrumental in creating transverse periodic forces on the body. The periodic discharge of discrete vortices in the wake gives rise to periodic circulation around the body and thus to a periodic lift force, the magnitude of which is proportional to the strength of the discrete vortices. As the frequency of periodic lift forces approaches a natural vibrational mode of the structure substantial vibrations may occur. It is thus obvious that a detailed knowledge of the flow field in the wake of the body is of paramount importance in estimating the frequency and magnitude of the periodic lift forces.

B. Scope of the Investigation

The investigation reported herein is part of a fundamental research program on wake mechanics undertaken in the Hydrodynamics Laboratory, Department of Civil Engineering, at MIT under the sponsorship of the David Taylor Model Basin, Office of Naval Research. It is the general

aim of this project to contribute to the understanding of the problem of flow-induced vibrations. The flat plate has been selected as the structural element to be tested since it constitutes the most simple structural element similar in form to the blades and vanes of primary interest to the Naval hydrodynamicist. Previous investigators have found the trailing edge geometry to be of tremendous importance in the vibrational problem, which accounts for its selection as a primary variable in the present tests.

In order to simplify the problem and to reduce the important factors to a minimum, the plates are tested at zero mean angle of attack (parallel to the ambient flow). The plates are provided with an external elastic restoring force and the motion of the plate is restricted to one degree of freedom, that of oscillatory motion around an axis containing the leading edge.

The first phase of this project dealt with an exploratory experimental investigation of the vibrational behavior of the plates as related to trailing edge geometry, externally supplied restraint and mean ambient flow velocity. A theoretical review of the vibrational problem and comparison of the experimental results with the theoretical concepts closed this phase (1).

The second phase dealt with an experimental investigation of the early wake structure of the plates when vibrational motion was prevented (2)(3)(4).

It is the aim of the present investigation to provide a quantitative estimate of the periodic forces acting on the plate and to correlate them with pertinent wake characteristics. For this purpose provision is made for experimental determination of the structural characteristics (natural frequency and damping) of the plate-spring system. Amplitudes and frequencies of vibration are measured to establish experimentally the response curve of every plate-spring system throughout the velocity range of measurable vibrational excitation. Root-mean-square and spectral measurements of the power density of the total head fluctuations are made in the early wake.

II. LITERATURE REVIEW

Fairly exhaustive surveys of previous work in the areas of flow-induced vibrations and wake mechanics are given elsewhere (1)(2)(4), thus only a brief summary is included here.

A. Engineering Aspects of Flow-Induced Vibrations

The vast majority of studies have treated either the circular cylinder or the thin flat plate and have centered around one or more of the following questions:

1. What is the origin of the exciting force?
2. Are the large amplitude vibrations self-excited or do they represent a forced vibration at a resonant structural frequency?
3. What means can be employed to prevent large amplitude vibrations?

Dockstader (5) attributes the vibrations of steel stacks caused by wind to forces induced by the von Karman vortices. Parmakian and Jacobson (6) reporting on vibrations of a slow-speed hydraulic turbine attribute the vibrations to vortex shedding at the trailing edge of the blades.

Donaldson (7), Heskestad and Olberts (8), Ippen, et al. (1), point out the importance of the trailing edge geometry on the maximum amplitudes obtained in tests with flat plates and consider the vibrations as induced by the vortex shedding.

The singing of propellers is attributed by Conn (9) to torsional vibrations of the blades caused by hydrodynamic forces which change in magnitude, direction, and location. Hughes (10) attributes the singing of propellers to a rapid change of forces as the propeller blade passes through the variable wake. Gongwer (11), from experimental studies on vanes singing in water, reaches the conclusion that singing is caused by the action of the von Karman vortex street.

Dickey and Woodruff (12) reporting on field data of steel stack vibrations consider the important question to be whether the vibrations are of the self-excited type (negative air damping) or forced vibrations at a structural resonance. Strouhal numbers computed from the field data differ appreciably from the experimentally determined values for rigid cylinders, being in general smaller.

Penzien (13) from experiments in a wind tunnel with cylinders concludes that the vibration of tall stacks are self-excited rather than forced. Marris (14) from experiments on cantilever-supported probes concludes that negative hydrodynamic damping is responsible for the large amplitude vibrations in the vicinity of structural resonance.

From the above brief survey of the literature it can be deduced that while the shedding of vortices in the wake is recognized as the initiating mechanism of what is truly a forced vibration, other effects, such as negative hydrodynamic or aerodynamic damping, may become important as the amplitude of vibration grows. Under these latter conditions the motion may be considered self-excited with the amplitude growing continuously until limited by an increase in the damping or until structural failure occurs.

Means of preventing flow-induced vibrations have been studied. The enclosure of a cylinder in a concentric perforated shroud has been found as an effective suppressor of vibrations by Price (15) after extensive tests in a wind tunnel. Design criteria for helical aerodynamic

spoilers have been formulated by Weaver (16) for cylinders. Baird (17) reporting on the vibration of a pipe-line suspension bridge excited by wind indicates that the use of a sawtooth paneling around the pipe-line proved very satisfactory in minimizing the vibrations. Reduction of the thickness of the trailing edge of the blades proved satisfactory in reducing the vibrations of turbines (6). Sharp and thin leading edge of the propeller blades is suggested as a remedy for the singing of propellers by Shannon (18) and Hughes (10).

B. Wake Studies

The shedding of vortices in the wake of a body submerged in a uniform stream was understood to be the initiating mechanism of vibrations in many cases of flow-induced vibrations. Thus the wake studies and the detailed description of the flow field in the wake is of basic importance in estimating the vortex induced forces on a structure.

A thorough survey of wake flows for cylinders and flat plates is given in References (1)(2)(4). In the present brief summary the aspects of wake flow related to the vibrational problem will be stressed. It should be stated that a complete theoretical model for the wake flows does not exist and we must rely heavily upon experimental information.

The first mathematical model for the description of the wake of a bluff body was given by Kirchhoff (19) in 1869 and was a big advance in classical hydrodynamics, removing the obstacle of D'Alembert's paradox. Based on this model and using the momentum principle, the drag coefficient on the body can be obtained. Many of the basic assumptions of this model are not substantiated experimentally and drag computations underestimate the true experimental values.

The second mathematical model is the one presented by von Karman (20)(21) in 1911-12. It represents the wake by two parallel rows of equally spaced and staggered point vortices in an otherwise irrotational field of flow; the important parameters being the longitudinal and transverse spacing of vortices and the strength of the individual vortex. Von Karman proved that the only stable configuration of this form is the one with a spacing ratio $h/a = 0.281$. Rosenhead (22) substantiated the above stability ratio and proved that the configuration possesses instabilities of higher order. Most of the experimental work done on wake flows is centered on the above model and provides data both supporting and rejecting and applicability of the model.

The von Karman model provides adequate explanation of the periodic nature of the wake which is instrumental in creating periodic transverse forces on the body.

Theoretical and experimental efforts were made in two directions; in establishing the actual spacing ratio h/a of the vortex street and in predicting the strength of the individual vortex.

Experimental work (23)(24)(25)(26)(27) has proved that the transverse spacing of the vortex street increases downstream in the wake and Birkhoff (28) justifies this widening on mathematical grounds. Efforts were made to connect the transverse spacing of the vortices to the body thickness.

Heisenberg (29) and Prandtl (30) attempted to connect the strength of the individual vortex with the rate of vorticity discharge into the wake from each side of the body by the separated shearing layers.

The Strouhal number, a parameter of importance in the description of periodic wakes, has received special attention. For a certain body geometry it has been established that the Strouhal number is a function of body Reynolds number. Reported experimental values of Strouhal number are given for different body geometries and Reynolds numbers in References (31)(32)(33)(34), (1)(3)(8)(11). The variety of these experimental values reveals the importance of body geometry and their range for the same body studied by different investigators suggests a sensitivity to experimental method.

The wake flow is usually classified by the body Reynolds number. A thorough experimental work for cylinders is reported by Roshko (31) and sufficient information for the flat plate by Taneda (25). While the shedding of vortices gives an easy explanation of periodic transverse forces acting on the body, rigorous theoretical prediction of these forces has not yet been developed. Actual direct measurements of vortex induced lift forces have been reported (35)(36)(37) only for cylinders in spite of the importance in design of other, more streamlined, body shapes.

Most of the theoretical and experimental efforts toward a description of the wake have been centered around two-dimensional models while in actuality, the total vortex induced lift forces acting on a body are integral quantities over the span of the body. Thus three-dimensional effects can greatly influence their value. Thorough investigations of the three-dimensional structure of wakes do not exist. Roshko (31) reports some experimental observations on cylinders.

Thus far the above discussion has been based on wakes of stationary bodies, however, the lift forces associated with the shedding of vortices can cause body vibrations which may greatly influence the wake structure.

The problem of the thin flat plate oscillating in a uniform incompressible flow has been solved by Theodorsen (38) on the basis of linearized potential theory and this solution constitutes the basis of flutter analysis in aerodynamics. For bluff bodies where separation and shedding of vortices occurs such a solution does not exist.

III. EXPERIMENTAL EQUIPMENT

A. Water Tunnel

The experiments reported herein were performed in a closed-jet, open circuit water tunnel which has been described in detail in References (1)(39). A schematic view is presented in Fig. 1.

An effort was made to minimize the free turbulence level in the test section. It was proved that by using pump No. III (rated capacity 3000 GPM at $H = 45'$ and 1175 RPM) and running the water through the longest approach path, a minimum free turbulence level in the test section is obtained ($\sqrt{u'^2}/V \approx 3\%$ or 4%).

The uniformity of the flow in the test section was checked and the tunnel contraction was recalibrated for flow measuring purposes.

B. Test Plates

Four flat plates with different trailing edge geometries were used. The cross section of the plates and the trailing edge configurations are shown in Fig. 2. The plates are mounted vertically in the test section, parallel to the flow in such a way as to permit rotation about the center of their semi-circular leading edge. They are fabricated of aluminum and all but plate D have been electroplated to prevent corrosion. Plate D has a somewhat rougher surface than the three others due to corrosion resulting from its use in a previous investigation (2).

C. Torsion Spring and Plate Mounting Device

1. Basic Design Criteria

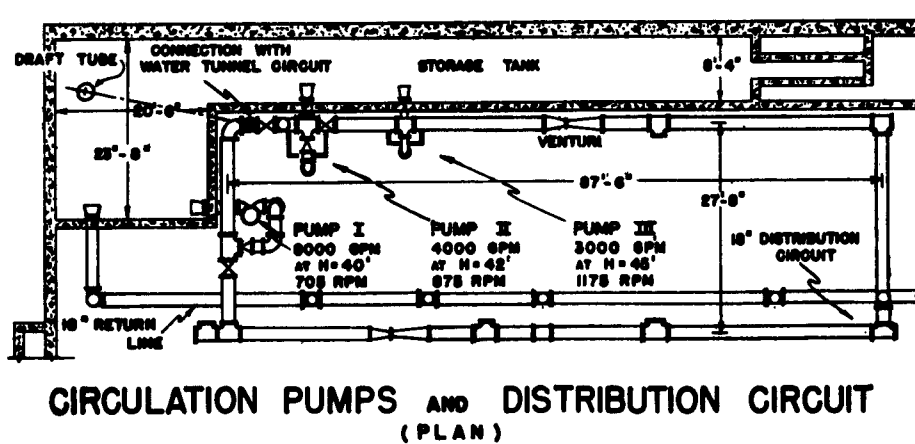
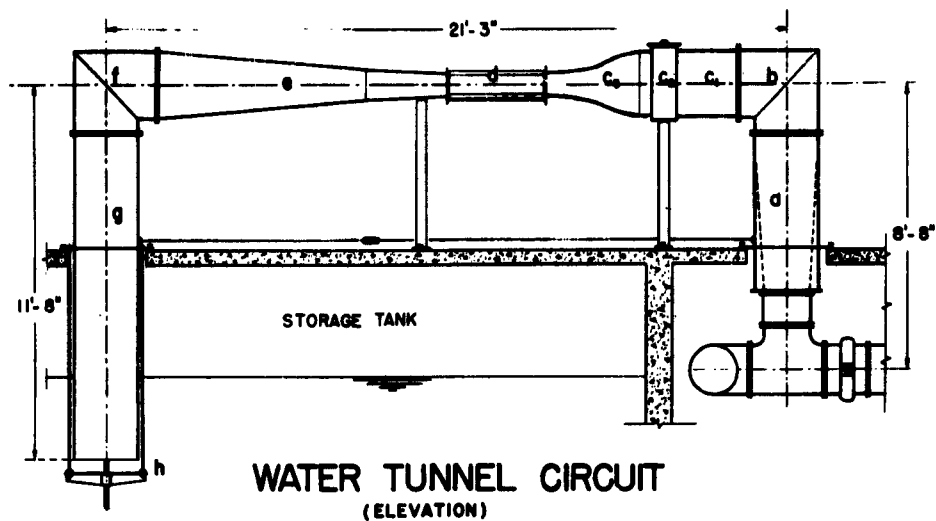
The experimental results reported in Reference (1) served as a guide in the design of the spring and plate mounting assembly. The criteria adopted were the following:

a) Single degree of freedom motion of the plate. Oscillatory motion of the plate as a rigid body around an axis through the center of the semi-circular leading edge will be permitted. No other motion should be permitted in order to avoid coupled oscillations.

b) The spring should be sensitive enough to provide for accurate measurement of very small angular displacements of the plate.

c) The plate-spring system and the whole mounting assembly should provide for the minimum possible structural damping.

d) Measurement of moments should be made on the flow side of any water seals.



Pump I



Pump II and III

Fig. 1 Water Tunnel and Distribution Circuit

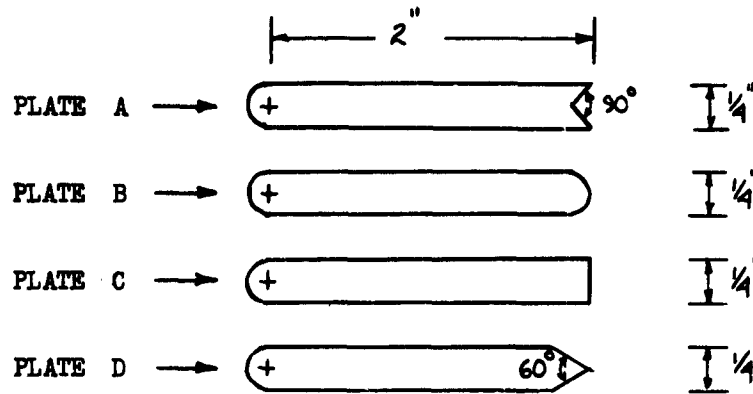


Fig. 2 Test Plates

2. Description of the Mounting Assembly

The plate mounting device is shown in Figs. 3, 4, and 5.

Two rectangular slots on the upper and lower lucite faces of the test section permit the plate to be inserted vertically. A cylindrical shaft is clamped tightly on each end of the plate, the axis of the shafts coinciding with the axis of rotation previously specified. Each shaft carries a stainless steel, doubly shielded, radial ball bearing, which fits a counterbored hole in an aluminum plate attached to the wall of the test section. Sealing of both plates is provided by O-rings and their exact positioning is insured by keying. A flanged aluminum pipe is pinned and fastened to the upper aluminum plate. The top of the pipe is covered with an aluminum plate carrying a central hole for insertion of the torsion spring.

The spring consists of a hollow cylindrical stainless steel tube 1/2" OD and one foot long. The first spring (I) used had a wall thickness of 0.035" and the second one (II), 0.049". At its lower end the tube is rigidly fixed to a cylindrical aluminum piece which carries a square hole to receive the end of the upper test plate shaft. At its upper end the spring tube is welded to a stainless steel plate which is fastened to the cover of the aluminum pipe. The aluminum pipe has two small circular openings to facilitate the placement of screws clamping the spring to the shaft and the in-place calibration of the spring.

The whole mounting device is assembled in place after setting the plate at zero angle of attack (± 0.001 rad). To prevent leakage through the lower shaft-bearing a sealed cover plate is used. The whole upper device is enclosed in a lucite casing. Electrical leads from the torsion spring strain gages are passed through a sealed hole in this casing.

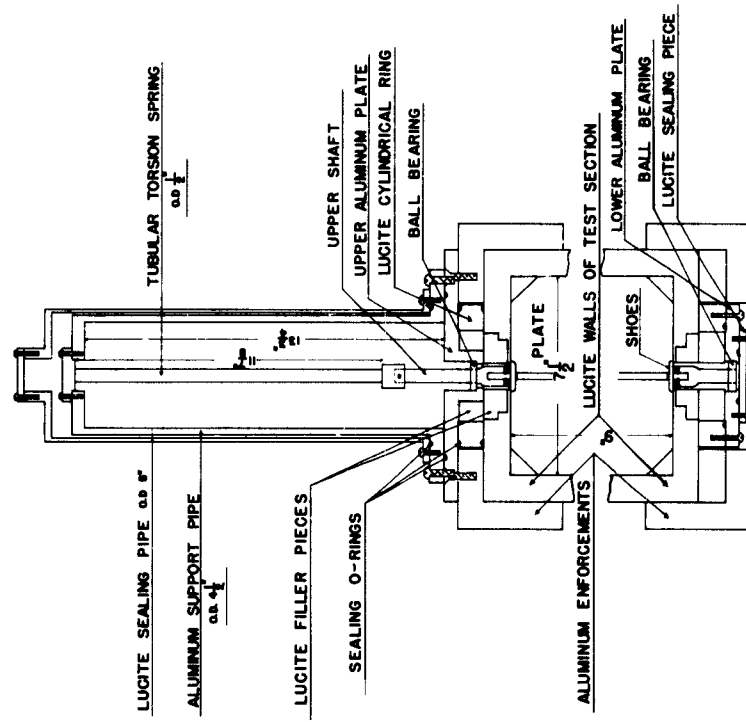


Fig. 5 Plate and Spring Mounting Assembly

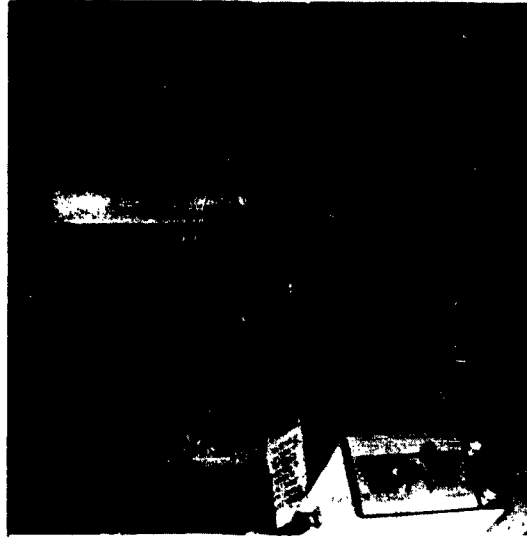


Fig. 4 Test Section

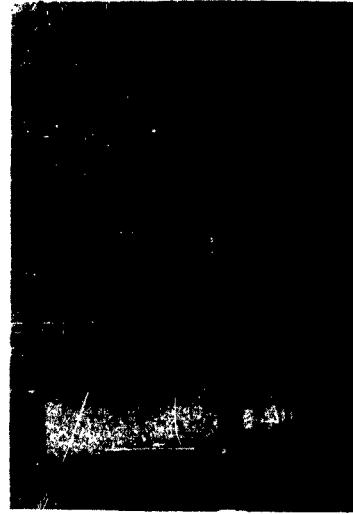


Fig. 3 Plate Mounting Assembly

All cavities in the test section walls are plugged with specially made lucite pieces in order to avoid major disturbances of the flow. The shoes described in Reference (4) were used to minimize end effects (see Fig. 6).

D. Measurement of Plate Motion

1. Strain Gages

Tatnall type, C9-121-R2C, strain gages were cemented and water-proofed on the surface of the torsion springs in the conventional array for torsion measurement. The four gages form a Wheatstone bridge circuit supplied by a 12 Volt automobile battery. A variable resistance in the circuit provides for balancing of the bridge. The voltage output of the bridge is proportional to the angle of rotation of the spring. (See Appendix B).

2. Amplifier

The voltage output of the Wheatstone bridge is amplified with a KIN-TEL DC Amplifier. This amplifier has a flat response over the operating range of frequencies (0 to 750 cps). The design gain accuracy is $\pm 1\%$ from DC to 2KC.

3. Oscilloscope

A Dumont dual-beam oscilloscope was used during the tests for visual observations of the vibrational signal.

4. AC Voltmeter

The total output of the Wheatstone bridge was measured with a Balantine vacuum tube voltmeter, which is a true RMS indicating meter for sinusoidal wave forms.

5. Vibration Analyzer

The analyzer used was a General Radio Type 762-B Vibration analyzer. It is a constant percentage band width tunable voltmeter with a logarithmic scale. Its operating range of frequencies is from 2.5 to 750 cps. This instrument is battery supplied, therefore frequent calibrations were made. Calibration procedure is described in Reference (43). A damping capacitance was inserted in parallel with the analyzer meter to reduce needle fluctuations. Vibrational frequencies as well as amplitudes of every component were measured. The electrical components for vibrational measurements are shown in Figs. 4 and 7. A schematic block diagram of instrumentation for vibrational measurements is shown in Fig. 8.



Fig. 6 Interior of Test Section



Fig. 7 Electrical Components for Vibrational Measurements

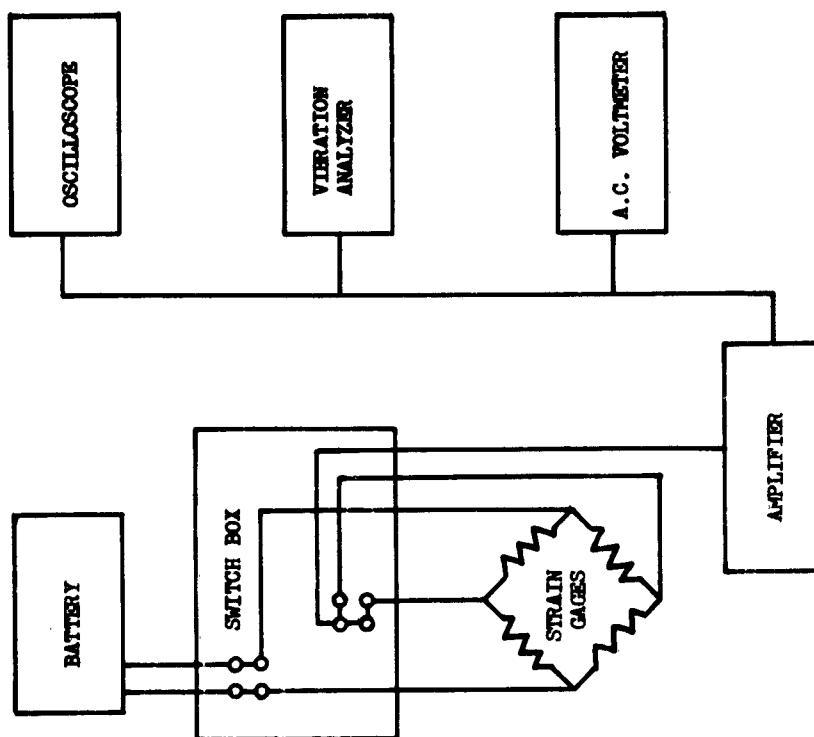


Fig. 8 Block Diagram of Instrumentation for Vibrational Measurements

E. Velocity Measurements

The mean velocity in the test section (ambient velocity) was measured using the water tunnel contraction as a flow meter (1). A differential manometer with Meriam fluid No. D-8325 (specific gravity 1.75) and water was used. Mean local velocities in the wake of the plate were measured with the total head and static pressure tubes described in Reference (2) (see Fig. 9), using open mercury manometers.

F. Measurements of the Total Head Fluctuations

The gage for measuring the total head fluctuations has been described in detail in Reference (2) and (40), along with the electrical components required. The measuring system consists of:

1. instantaneous total head gage,
2. electrometer preamplifier,
3. Kin-Tel amplifier,
4. oscilloscope for visual observation of the signal,
5. vibration analyzer for spectral analysis,
6. thermocouple voltmeter which is a true RMS indicating meter for a signal of any wave form.

The electrical components for total head fluctuation measurements are shown in Fig. 10. A schematic block diagram of the above components is shown in Fig. 11. Calibration of the gage is reported in References (2) and (3). The only difference in the calibration procedure followed in the present tests was that the Gage-Preamplifier-Amplifier (at $G_a = 50$) were connected together. The gage was calibrated at the beginning and at the end of the tests.

The gage sensitivity obtained in the present tests and used in the analysis of the data taken is:

$$K_G = 14.60 \frac{\text{mv}}{\text{ft. water}}$$

The preamplifier gain was also checked and found to be

$$G_p = 0.350 \frac{\text{mv}}{\text{mv}} .$$

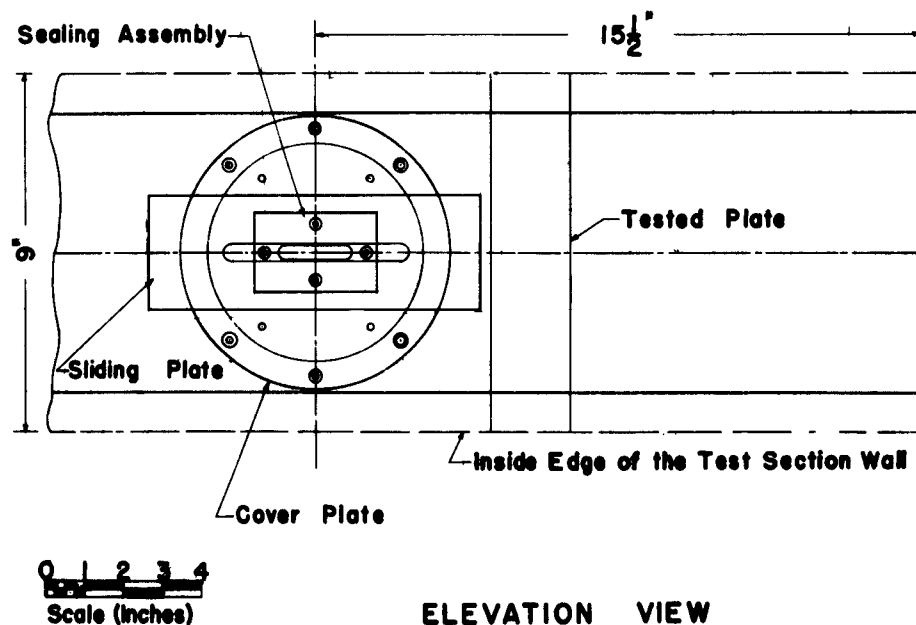
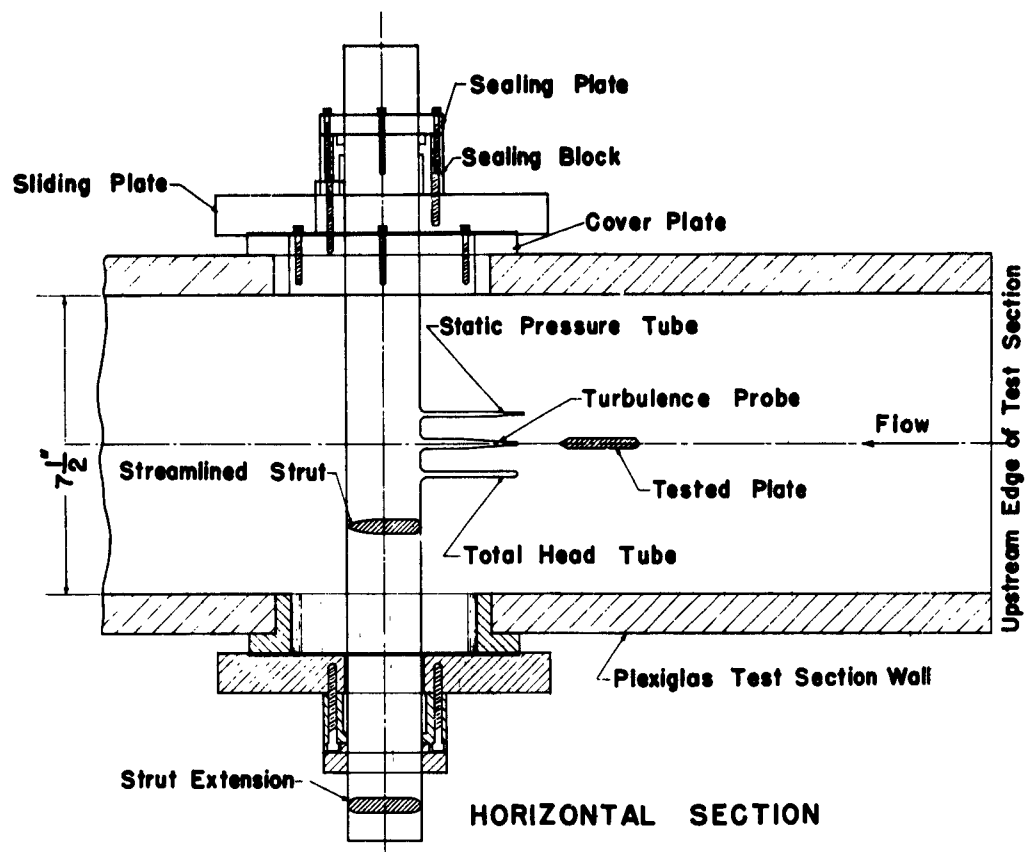
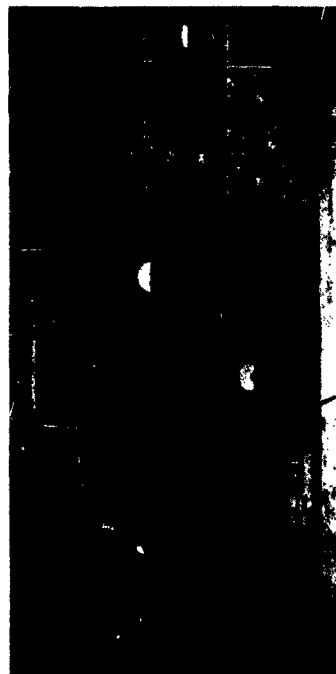


Fig. 9 Traversing System



a. Preamplifier, Filter, Amplifier



b. Switch Box, Thermocouple Voltmeter, Vibration Analyzer, Oscilloscope

Fig. 10 Electrical Components for Total Head Fluctuation Measurements

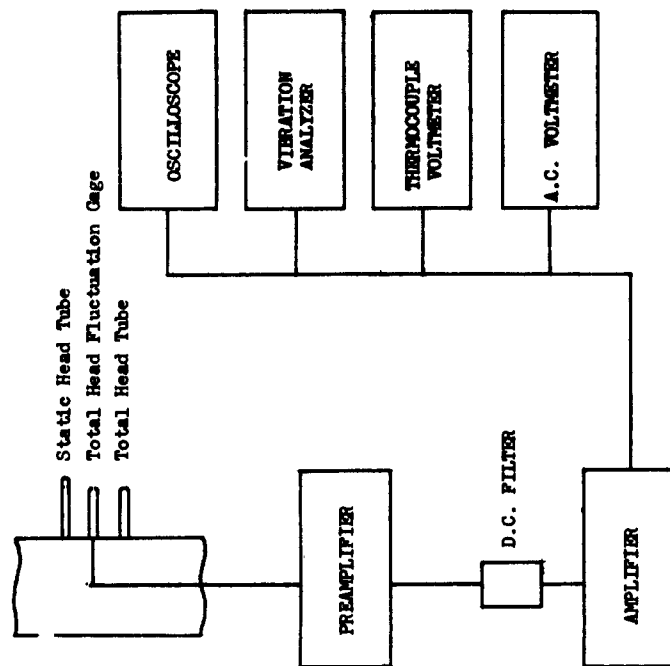


Fig. 11 Block Diagram of Instrumentation for Total Head Fluctuation Measurements

IV. FORMULATION OF THE LINEARIZED VIBRATIONAL PROBLEM

The plate-spring system employed in the present tests was designed to insure a single degree of freedom torsional oscillation about the leading edge of the plate.

Assuming linear damping, the equation of motion for this plate-spring system can thus be written in the form:

$$I_s \ddot{\alpha} + c_s \dot{\alpha} + K_s \alpha = M_t \quad (1)$$

in which:

$\alpha, \dot{\alpha}, \ddot{\alpha}$ represent the angular plate displacement, velocity, and acceleration respectively (in radians, rad. per sec. and rad/sec²)

I_s = polar moment of inertia of the plate about the rotational axis,

c_s = structural damping coefficient,

K_s = structural spring coefficient,

and M_t is the total hydrodynamic moment acting on the plate.

The moment M_t may be thought of as consisting of several parts:

$$M_t = M_{\text{Theodorsen}} + M_{\text{viscous}} + M_{\text{forcing}} \quad (2)$$

Theodorsen Moment

The Theodorsen moment (38) is that moment due to the potential-flow pressure distribution about the oscillating plate. For thin flat plates undergoing small amplitude, torsional, simple harmonic oscillations about the leading edge in a uniform stream of incompressible fluid, Bisplinghoff et al. (41) show this moment to be:

$$\begin{aligned} M_{\text{Theodorsen}} = & -1.125\pi\rho b^4 H \ddot{\alpha} \\ & - \frac{3}{2} \pi\rho b^3 H V (1 + C(K)) \dot{\alpha} \\ & - \pi\rho b^2 H V^2 C(K) \alpha \end{aligned} \quad (3)$$

in which

b = half chord of plate (1" in the present tests)

H = plate span (8.625" in the present tests)

V = ambient free stream velocity

$C(K)$ = Theodorsen function

$$C(K) = F(K) + i G(K) \quad (\text{see Fig. 12}) \quad (3)$$

and

$$K = \frac{2\pi f_a b}{V} \quad (4)$$

where f_a is the frequency of plate oscillation in cps. For the present plate geometry ($2b = 2"$ and $t = 1/4"$), $b = 4$ plate thicknesses or $b = 4t$. Thus utilizing the plate thickness Strouhal number:

$$S_t = \frac{f_a t}{V} \quad (5)$$

we find:

$$K = 8\pi S_t \quad (6)$$

Using the subscript "p" for "potential" we may write the Theodorsen moment:

$$M_{\text{Theodorsen}} = M_p = -I_p \ddot{\alpha} - c_p \dot{\alpha} - K_p \alpha \quad (7)$$

in which:

Inertia coefficient (real)

$$I_p = 1.125 \pi \rho b^4 H \quad (8)$$

Damping coefficient (complex)

$$c_p = \frac{3}{2} \pi \rho b^3 H V (1 + C(K)) \quad (9)$$

and

Spring coefficient (complex)

$$K_p = \pi \rho b^2 H V^2 C(K) \quad (10)$$

For the range of Strouhal numbers obtained in the present tests $K > 2.5$. Under these conditions the real part of the Theodorsen function $C(K)$ tends to the value of $1/2$ while the imaginary part becomes very small. We will thus neglect the imaginary part whereupon, $C(K) \approx 1/2$.

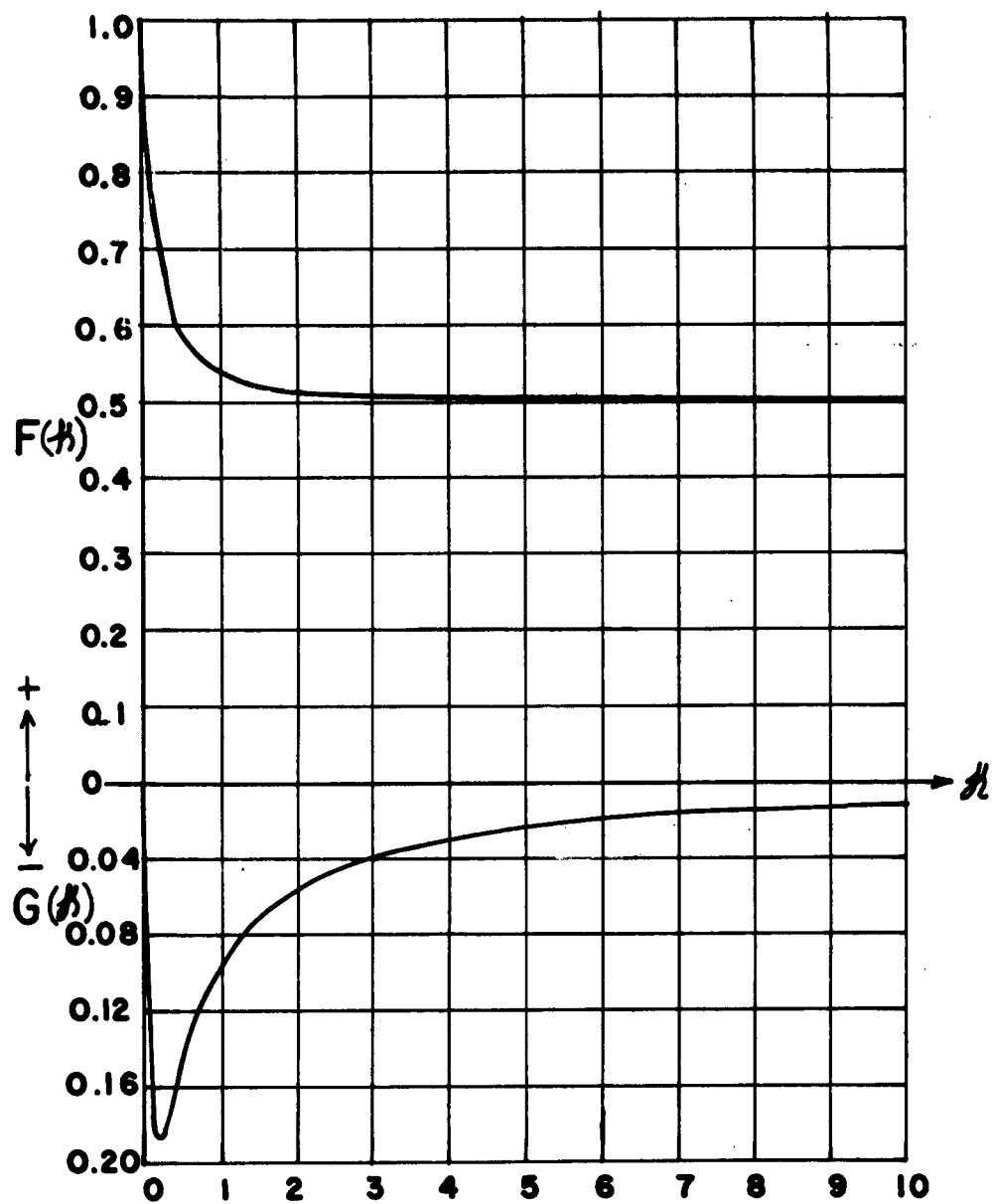


Fig. 12 Theodorsen Function, $G(h) = F(h) + iG(h)$

In this case Eqs. (9) and (10) become:

$$c_p = \frac{9}{4} \pi \rho b^3 HV \quad (9a)$$

$$K_p = \frac{1}{2} \pi \rho b^2 HV^2 \quad (10a)$$

Viscous Moment

The viscous moment is a damping moment due to the finite fluid viscosity. It is actually related to the relative fluid-plate velocity but will be assumed here to be given by the linear relationship:

$$M_{\text{viscous}} = M_v = -c_v \dot{\alpha} \quad (11)$$

Forcing Moment

This is the moment which must be present in order to initiate plate motion. It arises from the fluctuations in pressure distribution on the plate resulting from flow separation at the trailing edge and hence will likely be modified by the magnitude of the motion which it initiates.

Let $M_{\text{forcing}} = M$. Equation (1) can now be written:

$$(I_s + I_p) \ddot{\alpha} + (c_s + c_v + c_p) \dot{\alpha} + (K_s + K_p) \alpha = M \quad (12)$$

From purely dimensional considerations, the simplest form of the forcing moment is:

$$M = m_f \frac{1}{2} \rho H (2b)^2 V^2 \quad (13)$$

in which m_f = forcing moment coefficient. When the forcing moment is periodic as in the case of excitation by vortex shedding, the moment coefficient is conveniently written in the complex form:

$$m_f = m_{f0} e^{i(2\pi f_v t + \phi)} \quad (14)$$

in which:

- f_v = frequency of vortex shedding from one side of the plate in cps,
- ϕ = phase angle between forcing moment and the motion α ,
- and
- t = time in seconds.

Equation (12) is then written:

$$\begin{aligned} & (I_s + I_p)\ddot{\alpha} + (c_s + c_v + c_p)\dot{\alpha} + (K_s + K_p)\alpha \\ & = m_{fo} \frac{1}{2} \rho H (2b)^2 V^2 e^{i(2\pi f_v t + \phi)} \end{aligned} \quad (15)$$

Under conditions of steady ambient flow and small amplitude simple harmonic vibrations, the coefficients, I_s , I_p , c_s , c_v , c_p , K_s , and K_p may be expected to be independent of time and plate motion. Assuming m_{fo} to be independent of time, equation (15) represents the damped forced vibration of a linear single degree of freedom system. The solution of the equation (15) is well known. The vibrational frequency is equal to the forcing frequency, i.e.

$$f_a = f_v = f \quad (16)$$

and

$$\alpha = \alpha_o e^{i2\pi f t} \quad (17)$$

Letting:

$$I_t = I_s + I_p \quad (18a)$$

$$c_t = c_s + c_v + c_p \quad (18b)$$

$$K_t = K_s + K_p ,$$

the amplitude response is given by:

$$\alpha_o = \frac{m_{fo} \frac{1}{2} \rho H (2b)^2 V^2}{[I_t^2 (\omega_n^2 - \omega^2)^2 + c_t^2 \omega^2]^{1/2}} \quad (19)$$

and the phase angle by:

$$\phi = \arctan \frac{c_t \omega}{K_t - I_t \omega^2} = \arctan \frac{\frac{c_t \omega}{I_t \omega_n^2}}{1 - \left(\frac{\omega}{\omega_n}\right)^2} \quad (20)$$

in which the fundamental structural resonant frequency, ω_n , is given by:

$$\omega_n = 2\pi f_n = \left(\frac{K_t}{I_t}\right)^{1/2} \quad (21)$$

It should be noted that this frequency cannot be determined by direct experimental measurement since it involves the Theodorsen stiffness and inertia but excludes damping. It is also a well established fact that for stationary bodies the Strouhal number

$$S_t = \frac{f t}{V} \quad (22)$$

is a unique function of body thickness Reynolds number, R_t . Above a moderate value of R_t (≈ 500 for circular cylinders) the Strouhal number for stationary bodies is approximately constant. Thus, with the simplified model presented above, resonant vibrations are expected $\frac{f t}{S_t}$ when the free stream velocity, V , approaches the value given by $V = \frac{f t}{S_t}$.

It has been discovered from previous investigations however (1) that the Strouhal number falls below its constant value in the vicinity of structural resonance where large vibrational amplitudes prevail. This fact illustrates the influence of the vibratory motion of the plate on the vortex shedding mechanism and thus on the forcing moment coefficient m_{f0} . In this case a dependence of the Strouhal number and the moment coefficient on the motion of the plate can lead to a non-linear equation of motion. The linear system described above cannot therefore be expected to give an exact representation of the vibration phenomenon but it can be used as a first approximation for the evaluation of the forcing moment coefficient from experimental data.

V. PRESENTATION AND DISCUSSION OF RESULTS

A. System Constants

As has been stated in Section IV the coefficients I_s , I_p , c_s , c_v , and K_s are independent of the free stream velocity and time and can be predetermined and are summarized in Table I.

The structural moment of inertia, I_s , for any spring-plate system has been computed from the geometry of the system (Table I). The moment of inertia of the plate itself accounts for 9/10 of the total structural moment of inertia.

In order to determine the natural frequencies and damping coefficients, free oscillation tests have been performed in air ($c_t = c_s$) and in still water ($c_{sv} = c_s + c_v$) and are described in detail in Appendix B. Such tests were performed for each plate-spring system at the beginning of the vibrational tests and for many systems at the end of the vibrational tests to check the dependability of the results. The natural frequencies in air at the end of the vibrational tests are in all cases slightly smaller than at the beginning of the tests. The damping in air at the end

of the vibrational tests is considerably higher than at the beginning. It should be kept in mind that at the beginning of the vibrational tests the whole mounting assembly had been cleaned and the bearings lubricated. At the end of the vibrational tests the lower portion of the shaft-bearing system was submerged in a small cavity of water and some dirt had accumulated over the bearings. Thus, apparent moment of inertia effects due to submergence of the lower shaft can account for the smaller natural frequencies at the end of the tests and the accumulated dirt around the bearings for the increased damping. In all cases the structural damping is very small; about 1/10 of the critical. The natural frequency in still water remained constant during the course of vibrational tests. A small difference is obtained only in the plate D - spring II system possibly due to a loosening of the spring-shaft connection. The relative total damping coefficient, $\frac{c_{sv}}{c_c}$, in still water is small but the absolute viscous damping coefficient, c_v , is larger than the corresponding structural coefficient, c_s .

The structural spring coefficient, K_s , was obtained from in-place static calibration as described in Appendix B. The apparent moment of inertia, I_p , for the vibrating plate can be predicted theoretically from potential flow theory as has been seen earlier (Equation 8). This formula gives an apparent moment of inertia for the tested plates:

$$I_p = 36.55 \times 10^{-4} \text{ lb.in.sec}^2.$$

Since in the present tests other structural parts of the plate-spring system are submerged, the true apparent moment of inertia should be larger than this theoretical value. The apparent moment of inertia of the plate-spring system is easily computed from the natural frequencies, f_n , determined experimentally in still air and in still water. Thus we have:

$$2\pi f_{n \text{ air}} = \omega_{n \text{ air}} = \left(\frac{K_s}{I_s}\right)^{1/2} \quad (23)$$

$$2\pi f_{n \text{ still water}} = \omega_{n \text{ still water}} = \left(\frac{K_s}{I_s + I_p}\right)^{1/2} \quad (24)$$

and

$$I_p = I_s \left(\left(\frac{f_{n \text{ air}}}{f_{n \text{ still water}}} \right)^2 - 1 \right) \quad (25)$$

The values of apparent moments of inertia computed in this fashion are tabulated for each plate-spring system in Table I. They agree very closely with the value predicted theoretically, being in general slightly larger.

B. Exploratory Tests

1. Experimental Procedure

Exploratory tests were performed with plate C - spring I to reveal the pertinent characteristics of the plate motion and of the wake structure.

The ambient free stream velocity range yielding measurable vibrational excitation of the plate was first defined. The following measurements were then made at several discrete velocities selected so as to cover this range:

- a) Vibrational amplitudes of all the significant harmonic components of the plate motion.
- b) Mean velocity distribution across the half width of the wake at a longitudinal station $x = 1.5t$ downstream of the trailing edge.
- c) Fluctuating total head spectral distribution at station $x = 1.5t$ and at the transverse position y/t at which the discrete component of the spectrum was a maximum. (See Fig. 13 for coordinate reference). The results obtained in these exploratory tests are presented and discussed in the following sections.

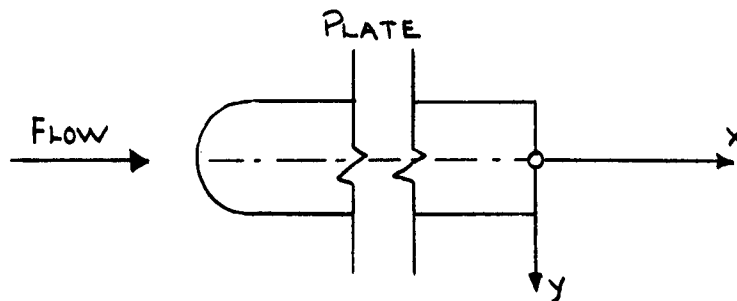


Fig. 13 Coordinate System

2. Vibrational Characteristics

The velocity range of significant vibrational excitation is from 5 fps to 9 fps for the system tested. Throughout the whole range of excitation the motion of the plate observed on the screen of the oscilloscope had the appearance of a sinusoid with continuously varying amplitude. For five velocities within the range of excitation the

frequencies, f_a , of vibration and their corresponding RMS amplitudes, \bar{a} , were picked up with the vibration analyzer. The results are tabulated in Table II. In all cases two frequencies were present, the fundamental, f_{a0} , and the third harmonic, f_{a3} . The RMS amplitude of the third harmonic, \bar{a}_3 , is much smaller than that of the fundamental, \bar{a}_0 , the ratio of amplitudes, \bar{a}_3/\bar{a}_0 , increasing with increasing velocity and fundamental frequency.

3. Wake Characteristics

Mean velocity wake transverses were made for the same five ambient velocities with the plate vibrating. A trial was made to duplicate the ambient flow conditions (mean velocity and mean static pressure) which were obtained with the plate clamped stationary. The duplication of flow velocity was not very successful due to operational difficulties. Therefore the mean velocity traverses for the stationary plate do not correspond to exactly the same mean ambient velocity as for the vibrational tests. The mean velocity distributions obtained are presented in Fig. A1. In all cases the velocity defect near the centerline of the wake is larger for the vibrating than for the stationary plate. Within the accuracy of the measurements, the width of the wake is not affected by the motion of the plate, being in general the same in both cases.

Spectral analyses of the total head fluctuations were made for four ambient velocities with the plate vibrating. These spectra were obtained at $x = 1.5t$ and at the y/t at which the fundamental discrete component had maximum energy density. The normalized spectral distributions are presented in Figs. A2 through A5. These spectra illustrate the turbulent nature of the early wake and the strong discrete periodicities present. The frequencies at which discrete energy is concentrated in the spectra are tabulated together with the corresponding vibrational frequencies in Table II. It is seen that in all spectra a fundamental discrete frequency is present along with its second and third harmonics. The fundamental frequency is exactly the same as the fundamental frequency of plate vibrations. For this reason we will henceforth omit the subscripts distinguishing the wake and vibrational frequencies.

An estimate of the discrete energy was made by computing the area of the spectral peak at the fundamental discrete frequency and subtracting the continuous turbulent background. The energy in the fluctuating total head at the fundamental discrete frequency can be seen (Table II) to account for roughly 50% of the total energy of the spectrum at this location. The total head fluctuation spectra presented here for the vibrating plate show only quantitative differences when compared with the spectra obtained for the same plate clamped stationary in the flow (Ref. 4). These latter spectra are also shown in Fig. A2 and Fig. A4 to facilitate comparison.

TABLE II RESULTS OF EXPLORATORY TESTS

PLATE C SPRING I

V fps	$\overline{a_0}$ 10^3 rad	$\overline{a_3}$ 10^3 rad	Vibrational Frequencies		Discrete Frequencies in the Flow			Ratio of discrete energy at f_{v0} to total spectral energy
			$\overline{a_0}$ cps	$\overline{a_3}$ cps	f_{v0} cps	f_{v2} cps	f_{v3} cps	
6.30	0.656	0.025	67	201	67	---	---	---
6.60	2.240	0.152	69	207	69	138	207	0.64
7.20	1.900	0.208	72	218	72	144	216	0.58
7.50	1.040	0.117	74	220	74	148	220	0.47
8.00	1.160	0.135	74	220	74	145	212	0.41

4. Conclusions

The conclusions drawn from the preliminary tests served as a guide for the final tests.

a) The mounting assembly and sensing elements for recording the motion of the plate proved satisfactory in all respects.

b) Since the amplitude of the third vibrational harmonic is substantially smaller than the amplitude of the fundamental, the motion of the plate may be considered simple harmonic for the purpose of further analysis.

c) The RMS of the vibrational amplitude represents to an extremely good degree of accuracy the RMS of the amplitude of the fundamental vibrational frequency.

d) The large percentage of the discrete energy in the total head fluctuation spectra indicates that the RMS of the total head fluctuation can reflect in a qualitative manner changes in the discrete energy.

e) The similarity of the spectral measurements for the stationary and vibrating cases substantiate the concept that vibrations are initiated by pressure fluctuations resulting from the shedding of vortices in the wake.

f) The fundamental frequency of total head fluctuation in the wake is the same as the fundamental frequency of plate vibration.

C. Final Tests - Vibrational Measurements

1. Experimental Procedure

For each plate-spring system the torsion spring was calibrated in place. The natural frequency as well as the damping coefficient, c_s , of the system in still air (water tunnel empty) and in still water, $c_{sv} = c_s + c_v$, were determined experimentally with free oscillation tests. The ambient free stream velocity was increased by small increments ΔV and the following measurements were made.

a) The mean ambient velocity using the calibrated contraction meter of the water tunnel.

b) The frequencies of the vibrational motion of the plate using the vibration analyzer.

c) The RMS of the vibratory motion of the plate with the AC Balantine voltmeter.

The velocity was increased up to the point at which measurable vibrations ceased. The velocity was then decreased by small decrements ΔV and the same quantities were measured.

The above measurements were performed with the following plate-spring systems.

Plate A - spring I

Plate B - spring I, II

Plate C - spring I, II

Plate D - spring I, II

For plate D - spring I, II and plate B - spring I, the natural frequency and damping coefficient in air and in still water were redetermined experimentally at the end of the tests.

In all cases the vibratory motion of the plate was observed on the screen of the oscilloscope and the qualitative nature of the motion was recorded.

2. Qualitative Vibrational Characteristics

The fundamental vibrational frequency, f_0 (cps), as given by the vibration analyzer and the RMS of the vibrational amplitude, $\overline{a_0}$ (rad), are plotted versus the ambient velocity, V (fps), for each plate-spring system in Figs. A6 through A9.

The qualitative character of the vibrations is discussed in the present section.

Plate B

Measurable vibrations start at a certain velocity with a frequency smaller than the fundamental natural frequency of the plate-spring system. For a small range of increasing velocity the fundamental vibrational frequency varies linearly with the ambient free-stream velocity corresponding to a constant value of the Strouhal number, $S_t = f_0 t / V = 0.258$. The vibrational amplitude increases with increasing velocity and frequency over this range. In this range the only vibrational frequency present is the fundamental. Only in the upper end of this range does an extremely small (hardly detectable) third harmonic make its appearance. The vibrational frequency in this range is constant (called "stable" hereafter) as far as could be determined experimentally but the amplitude varies (unstable). The variation of the amplitude was reflected in fluctuations of the needle of the voltmeter and was observed also on the screen of the oscilloscope.

With a small increase of velocity above this range the amplitude of vibrations increases sharply and the fundamental vibrational frequency falls below the value predicted by the constant Strouhal number of the earlier range. A considerable range of velocities exist where large amplitudes are obtained while the Strouhal number decreases continuously with increasing velocity. The third harmonic is present throughout this range with increasing amplitude as the velocity increases. In this range both the frequency and the vibrational amplitude are stable (see Figs. A10 and A11). Audible noise was present.

Increasing the velocity further, a velocity is reached at which the vibrations become intermittent with amplitude variable as much as 10 fold (see Figs. A12 and A13). The amplitude of the third harmonic seems to attain its maximum value at this point.

For still larger velocities, very small vibrations are obtained at frequencies indicating an increasing Strouhal number with increasing velocity. Thus three velocity ranges can be distinguished, as was reported previously by Ipsen et al. (1):

(1) Range I in which the Strouhal number remains constant with sinusoidal vibrations of varying amplitude.

(2) Range II in which the Strouhal number falls below its constant value with large stable vibrational amplitudes and increasing amplitude of the third harmonic with increasing velocity.

(3) Range III in which small varying amplitude vibrations are obtained and increasing Strouhal numbers. The vibrational characteristics described above are exhibited by plate B with both springs.

Plate D

Plate D exhibits vibrational behavior which is qualitatively similar to that of plate B. For plate D, however, there is a more gradual change in amplitude as the velocity is increased from range I to range II. Vibrational measurements in the range III were not made with plate D. The behavior of plate D in ranges I and II is illustrated in Figs. A14 through A17.

Plate C

Throughout the whole range of excitation the vibrational amplitude was unstable (see Figs. A18 and A19). The third harmonic was present but hardly detectable. Due to the small vibrational amplitudes obtained for this plate, the range of constant Strouhal number (Range I) could not be measured.

Plate A

Extremely small vibrational amplitudes were obtained. Throughout the whole range of measurable vibrational excitation the amplitude was unstable and the Strouhal number decreased slightly with increasing velocity.



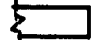

3. The Strouhal Number

Each plate exhibits its own variation of vibrational frequency with ambient free stream velocity, indicating the importance of trailing edge geometry in the vortex shedding mechanism. The Strouhal number was computed for plates B, D, tested with both springs, from the data taken in the range of linear dependence of the fundamental vibrational frequency on the velocity. An average value of the Strouhal number was defined for plate A from the data taken throughout the whole range of excitation. The Strouhal number was not computed for plate C due to the lack of experimental data in the velocity range I.

The Strouhal numbers for the three plates are tabulated in Table III together with the values obtained for the same plates by other investigators. The Strouhal numbers on lines (3)(4) are based on the fundamental frequency of total head fluctuation in the wake of stationary plates at a velocity of about 10 ft/sec. The values on line (3) agree very well with the present values, the difference being within the experimental error. The value on line (4) differs appreciably from that obtained for the present tests. This difference may result from the rougher plate surface and lower free-stream turbulence level in the present tests. The values in line (5) based on fundamental vibrational frequencies are not in good agreement with the present values although the trend is the same. Differences in plate alignment and free-stream turbulence level may be the cause of the noticed discrepancies.

The values of the Strouhal number for plates A, B, and D differ substantially, reinforcing earlier findings (Ippen et al. (1), Heskestad (8)) that the trailing edge geometry influences the vortex shedding frequency to a great extent. This is understandable since the time required for the vortices to mature and be detached as discrete entities from the separated shearing layers depend strongly on the early wake boundary conditions. The work of Gongwer (11) and Eagleson et al. (4) shows the importance of separation point boundary layer thickness on the Strouhal number. Thus, until the detailed mechanism of vortex formation and discharge is understood, a universal Strouhal number cannot be formulated.

TABLE III

	Strouhal Number $S_t = \frac{f_o t}{V}$			
	Plate A	Plate B	Plate C	Plate D
1. Plate				
2. Present tests	0.241	0.258	----	0.213
3. Ref. (3)	0.237	0.251	0.223	----
4. Ref. (2)	----	----	----	0.255
5. Ref. (1)	0.249	0.275	0.246	0.230

It has been stated in section V-C-2 that the vibrational Strouhal number decreases with increasing velocity in the velocity range II and then increases again in the velocity range III. The maximum and minimum values of the vibrational Strouhal number obtained for the different plates are:

Plate A	$S_{t \text{ max}} = 0.251$	$S_{t \text{ min}} = 0.234$
Plate B	$S_{t \text{ max}} = 0.258$	$S_{t \text{ min}} = 0.185$
Plate C	$S_{t \text{ max}} = 0.257$	$S_{t \text{ min}} = 0.214$
Plate D	$S_{t \text{ max}} = 0.213$	$S_{t \text{ min}} = 0.106$

The larger the drop in Strouhal number from range I to range II the larger the range of velocities in which large vibrational excitation occurs. It is in the velocity range II where large amplitudes are obtained. It is thus suggested that the decrease of Strouhal number in the range II is the result of dynamic changes imposed by the motion of the plate. It is the plate-spring system rather than the flow velocity which controls the frequency in this range. The decrease in Strouhal number seems too large to be attributed to the small possible transverse shift of separation points caused by the plate motion.

The frequency versus velocity relation in range II for each plate shows a similarity for the two tested springs. It seems to be independent of the absolute magnitude of the vibrational amplitudes.

Of interest is that for plates A, B, and C the fundamental vibrational frequency obtained at a certain velocity seems to be independent of the way the velocity was reached (increasing or decreasing velocity). For plate D an hysteresis effect is obvious for both springs. With decreasing velocity the fundamental vibrational frequency at a certain velocity is smaller than that obtained with increasing velocity. The differences are small, in general less than 1 cps and are more pronounced in the vicinity of the lower end of range II while diminishing on the upper end. It should be noted that plates A, B, and C have more or less fixed separation points while the trailing edge of plate D gives the possibility of forward or backward shift of the separation points. It is thus more likely that the frequency hysteresis effect is due to possible shift of the separation points.

4. Vibrational Amplitude versus Ambient Velocity

In Figs. A6 through A9 the RMS of the vibrational amplitude, \bar{a}_0 (rad), is plotted versus the ambient velocity, V (fps). From these figures the effect of trailing edge geometry on the vibrational amplitudes and velocity range of excitation is strikingly clear. Plates B and D exhibit maximum amplitudes of the same order of magnitude and much larger than for plates C and A. A common characteristic of plates B and D is that the trailing edge extends into the early wake beyond the separation points.

In all cases the maximum amplitude for every plate is smaller when tested with spring II than with spring I.

The amplitude distributions are dissimilar when compared from plate to plate but show a marked similarity for the same plate and the two springs tested. Thus a unique presentation of the results in a non-dimensional form is possible. Figs. A20 through A22 present a single curve for each plate of the dimensionless amplitude, $\bar{a}_0/\bar{a}_{0\max}$, versus the dimensionless velocity, V/V_r , V_r being the velocity at which $\bar{a}_{0\max}$ occurs for each plate-spring system. This presentation suggests the unique importance of the velocity and trailing edge geometry on the vibrational behavior of each plate.

A careful examination of the results obtained indicates that the vibrational amplitude of each plate-spring system at a certain velocity is practically independent of the way the velocity was reached. Some differences may exist at the transition from range I to range II.

5. Reproducibility of Results

Confidence in the quantitative value of experimental measurements is lost if the measurements are not repeatable. Thus upon completion of the final experiments the plate B - spring II system was re-tested. Natural frequencies and damping coefficients for the two tests

with this system have already been presented in Table I with a difference less than the estimated experimental error. The vibrational test results are presented in Fig. A23 together with the results obtained previously. No comment is necessary.

6. The Response Curves

In Figs. A24 through A27 the vibrational results are presented in the more conventional form of amplitude response curves. The RMS of the vibrational amplitudes, \bar{a}_o (rad), are plotted versus the dimensionless frequency, f_o/f_n . The maximum amplitude for all plate-spring systems occurs in the vicinity of the corresponding natural frequency, in general at a frequency slightly larger than the natural one. The figures show a rapid rise of amplitude left of resonance for plates B and C which is especially noticeable with spring I. No such behavior is shown for plate D for which the increase of amplitude is more gradual. For all plates the amplitudes obtained in the vicinity of and to the "right" (higher frequencies) of resonance are independent of the way the particular velocity was reached. It should be noted that stable vibrations were obtained in this region for plates B and D. At the "left" (lower frequencies) of resonance larger amplitudes are obtained in general with decreasing velocity than with increasing velocity. This is especially noticeable with plate D for which the frequency also exhibited an hysteresis effect. This region corresponds to velocity range I and the transition from range I to II where varying amplitude vibrations were obtained.

In order to eliminate the explicit role of velocity in the forcing moment expressed as $M_o = m_{fo} \frac{1}{2} \rho H (2b)^2 V^2$, the experimental data are presented in Figs. A28 through A31 in a reduced dimensionless form of $(\bar{a}_o/V^2)/(\bar{a}_o/V^2)_{\max}$ vs. f_o/f_n . The reduced response curves indicated that for all plates the reduced maximum amplitude occurs at the natural frequency of the system, small deviations being within the experimental error. The general characteristics of the reduced response curves are otherwise the same as those presented in Figs. A24 through A27. The hysteresis effect is now more clearly shown.

7. The Forcing Moment Coefficient

Equation (19) served as the basis for the computation of the forcing moment coefficient m_{fo} from the obtained experimental results.

$$a_o = \frac{m_{fo} \frac{1}{2} \rho H (2b)^2 V^2}{[I_t^2 (\omega_n^2 - \omega_o^2)^2 + c_t^2 \omega_o^2]^{1/2}} \quad (19)$$

in which $\omega_n^2 = (\frac{K_s + K_p}{I_t})$, $K_p = \frac{1}{2}\pi\rho b^2 HV^2$, and ω_0 is the fundamental

vibrational frequency. An evaluation of the term K_p for the range of velocities producing measurable vibrational excitation in the present tests indicates that $K_p \ll K_s$. Thus, K_p can be neglected and $\omega_n^2 \approx K_s/I_t$, ω_n being the undamped natural frequency of the plate-spring system in still water. The error introduced in ω_n by neglecting the K_p term is of the same order as the experimental error in determining the natural frequency in still water (i.e. ± 1 cps). The total damping coefficient is given by:

$$c_t = c_{sv} + \frac{9}{4}\pi\rho b^3 HV. \quad (18b)$$

c_{sv} is the structural plus viscous damping coefficient of the system and was assumed independent of the velocity V and the motion of the plate. It is assumed equal to the damping coefficient obtained by the free oscillation tests in still water (see Table I). The term $(9/4)\pi\rho b^3 HV$ represents the damping coefficient introduced in the system by the Theodorsen solution of the flat plate oscillating in a uniform stream of incompressible fluid. Evaluation of this term indicates that it is of great importance and is much larger than the term c_{sv} .

$$\text{Letting } c_p = (9/4)\pi\rho b^3 HV = CV, \quad (26)$$

we can write:

$$m_{fo} = \frac{\alpha_o [I_t^2 (\omega_n^2 - \omega_o^2)^2 + (c_{sv} + CV)^2 \omega_o^2]^{1/2}}{\frac{1}{2} \rho H (2b)^2 V^2} \quad (27)$$

All the quantities in the right member of the above expression are known and m_{fo} can be easily computed. For each plate-spring system a mean smooth curve was drawn in the $\bar{\alpha}_o$ versus f_o and f_o versus V graphs and from these curves values of $\bar{\alpha}_o$ and V were obtained for use in the computation of m_{fo} at selected frequencies. (Use of a smoothed curve rather than the actual data points is a convenience which will be justified later). Since the RMS of α_o (i.e. $\bar{\alpha}_o = \alpha_o/\sqrt{2}$) was readily available, the RMS of m_{fo} (i.e. $\bar{m}_{fo} = m_{fo}/\sqrt{2}$) was computed. Calculations of \bar{m}_{fo} were performed at equal intervals of $\Delta(\omega_n/\omega_o)$ at the left of resonance and of $\Delta(\omega_o/\omega_n)$ at the right of resonance.

Computations of \bar{m}_{fo} were made for plates B, C, D, and both springs. The experimental results for plate A were not considered accurate enough for quantitative correlations since in this case the electrical signal representing $\bar{\alpha}_o$ was of the same order of magnitude as the background noise of the electronic instruments used for vibrational measurements. For every frequency, ω_o , at which \bar{m}_{fo} was computed, the corresponding quantity $2b\omega_o\bar{\alpha}_o/V$ was also computed. This dimensionless quantity represents the ratio of the RMS transverse velocity of the plate

at the trailing edge to the ambient free stream velocity. For all plate-spring systems the computed \overline{m}_{f0} is plotted versus the corresponding $V^* = 2b\omega_0\overline{\alpha}_0/V$ quantity and is shown in figures A32, A33.

The correlation of \overline{m}_{f0} with $2b\omega_0\overline{\alpha}_0/V$ indicates characteristics of great importance for the understanding of the vibrational problem. A large increase of \overline{m}_{f0} occurs with increasing values of $2b\omega_0\overline{\alpha}_0/V$ indicating a strong interaction between forcing moment and motion of the plate. For small values of $2b\omega_0\overline{\alpha}_0/V$, at left of resonance and in the velocity range I where the Strouhal number remains constant for plates B, D, \overline{m}_{f0} varies linearly with $2b\omega_0\overline{\alpha}_0/V$. Thus \overline{m}_{f0} in this range can be written:

$$\overline{m}_{f0I} = C_{1I} + C_{2I} \left(\frac{2b\omega_0\overline{\alpha}_0}{V} \right) \quad (28)$$

The values of C_{1I} and C_{2I} are essentially the same for both plates B, D, with either spring. The value of C_{1I} is of great physical importance indicating that with no vibrations small forcing moments are present which initiate the motion of the plate. In the vicinity of resonance and to the right of resonance, in the velocity range II where the Strouhal number falls below its initial constant value, the rate of increase of \overline{m}_{f0} with increasing $2b\omega_0\overline{\alpha}_0/V$ is decreased. Here too, the \overline{m}_{f0} show a linear dependence on $2b\omega_0\overline{\alpha}_0/V$ but with a smaller slope than in range I. In this range the \overline{m}_{f0} can be written:

$$\overline{m}_{f0II} = C_{1II} + C_{2II} \left(\frac{2b\omega_0\overline{\alpha}_0}{V} \right) \quad (29)$$

For both plates B, D and for both springs, the C_{1II} and C_{2II} values are essentially the same. The experimental results indicate a larger scatter for plate B than for plate D. This is mainly due to the sharper response curve of plate B and to larger error introduced in the computation of \overline{m}_{f0} from the experimental inaccuracy of ω_n . For plate C no experimental results were available in range I. In range II the slope, C_{2II} , is exactly the same as that for plates B and D while the value C_{1II} indicates a difference between the two springs.

Disregarding the minor differences in the behavior of the various plates, it can be said that two ranges of \overline{m}_{f0} can be distinguished corresponding to the two velocity ranges, I, II, of vibrational excitation:

$$\text{Range I: } \overline{m}_{f0I} = C_{1I} + C_{2I} \left(\frac{2b\omega_0\overline{\alpha}_0}{V} \right) \quad (28)$$

$$\text{Range II: } \overline{m}_{fo_{II}} = C_{1II} + C_{2II} \left(\frac{2b\omega_o \overline{\alpha}_o}{V} \right) \quad (29)$$

with C_{1I} , C_{2I} , and C_{2II} the same for all plates and springs; and C_{1II} almost the same. These values are tabulated in Table IV.

Introducing the above expressions in the amplitude relation (19) we have:

$$\text{Range I: } \overline{\alpha}_o = \frac{(C_{1I} + C_{2I} \left(\frac{2b\omega_o \overline{\alpha}_o}{V} \right)) \frac{\rho}{2} H(2b)^2 V^2}{[I_t^2 (\omega_n^2 - \omega_o^2)^2 + (c_{sv} + CV)^2 \omega_o^2]^{1/2}} \quad (30)$$

$$\text{Range II: } \overline{\alpha}_o = \frac{(C_{1II} + C_{2II} \left(\frac{2b\omega_o \overline{\alpha}_o}{V} \right)) \frac{\rho}{2} H(2b)^2 V^2}{[I_t^2 (\omega_n^2 - \omega_o^2)^2 + (c_{sv} + CV)^2 \omega_o^2]^{1/2}} \quad (31)$$

TABLE IV

		NOMINAL VALUES OF MOMENT COEFFICIENT CONSTANTS					
Plate	Spring	C_{1I}	C_{2I}	C_{1II}	C_{2II}	C_I lbs-sec ²	C_{II} lbs-sec ²
B	I	0.0025	2.425	0.0090	1.765	0.00783	0.00569
B	II	0.0025	2.425	0.0090	1.765	0.00783	0.00569
C	I	-----	-----	0.0078	1.765	0.00783	0.00569
C	II	-----	-----	0.0042	1.765	0.00783	0.00569
D	I	0.0025	2.425	0.0090	1.765	0.00783	0.00569
D	II	0.0025	2.425	0.0090	1.765	0.00783	0.00569

Theodorsen Damping Coefficient, $C = \frac{2}{4} \pi \rho b^3 H = 0.00569 \text{ lb. sec}^2$ (Eq. 26)

Solving explicitly for $\overline{\alpha}_o$ we have:

$$\text{Range I: } \overline{\alpha}_o = \frac{C_{1I} \frac{\rho}{2} H(2b)^2 V^2}{[I_t^2 (\omega_n^2 - \omega_o^2)^2 + (c_{sv} + CV)^2 \omega_o^2]^{1/2} - C_{2I} \frac{\rho}{2} H(2b)^3 V \omega_o} \quad (32)$$

$$\text{Range II: } \bar{\alpha}_o = \frac{C_{1II} \frac{\rho}{2} H(2b)^2 v^2}{[I_t^2 (\omega_n^2 - \omega_o^2)^2 + (c_{sv} + CV)^2 \omega_o^2]^{1/2} - C_{2II} \frac{\rho}{2} H(2b)^3 v \omega_o} \quad (33)$$

Let:

$$C_{2I} \frac{\rho}{2} H(2b)^3 = C_I \quad (34)$$

and

$$C_{2II} \frac{\rho}{2} H(2b)^3 = C_{II} \quad (35)$$

Then:

$$\text{Range I: } \bar{\alpha}_o = \frac{C_{1I} \frac{\rho}{2} H(2b)^2 v^2}{[I_t^2 (\omega_n^2 - \omega_o^2)^2 + (c_{sv} + CV)^2 \omega_o^2]^{1/2} - C_I v \omega_o} \quad (36)$$

$$\text{Range II: } \bar{\alpha}_o = \frac{C_{1II} \frac{\rho}{2} H(2b)^2 v^2}{[I_t^2 (\omega_n^2 - \omega_o^2)^2 + (c_{sv} + CV)^2 \omega_o^2]^{1/2} - C_{II} v \omega_o} \quad (37)$$

From these two expressions it is obvious that the coefficients, C , C_I , and C_{II} have the same dimensions. A quantitative evaluation of C , C_I , and C_{II} yields the important result that $C_I > C$ and $C_{II} \approx C$. (See Table IV.) The two last expressions for $\bar{\alpha}_o$ (equations 36 and 37) will constitute the basis for further discussion of the vibrational behavior.

In order to check the hysteresis effect on the relationship of moment coefficient versus $2b\omega_o\bar{\alpha}_o/V$, the following computations were made for plate D-spring II for which the hysteresis is more pronounced. A smooth curve was drawn in the $\bar{\alpha}_o$ versus f_o graph through points obtained with increasing velocity, and a second one through points obtained with decreasing velocity. The \bar{m}_{f_o} and the corresponding $2b\omega_o\bar{\alpha}_o/V$ were then computed using points on the two smoothed curves and they are presented in Fig. A34 together with the results obtained from the mean curve. No substantial difference is indicated and the approach followed in the \bar{m}_{f_o} computation is thus justified.

8. Range I - The Frequency Range of Increasing Vibrational Amplitudes.

It has been derived in the previous section that in range I the amplitude is given by the expression:

$$\bar{a}_o = \frac{C_{1I} \frac{\rho}{2} H(2b)^2 V^2}{[I_t^2 (\omega_n^2 - \omega_o^2)^2 + (c_{sv} + CV)^2 \omega_o^2]^{1/2} - C_{1I} V \omega_o} \quad (36)$$

In this range the Strouhal number remains constant for each plate. Thus, the velocity is given by the expression:

$$V = \frac{\omega_o t}{2\pi S_t} \quad (38)$$

Substituting for V in (36) we get:

$$\bar{a}_o = \frac{C_{1I} \frac{\rho}{2} H(2b)^2 \left(\frac{\omega_o t}{2\pi S_t}\right)^2}{[I_t^2 (\omega_n^2 - \omega_o^2)^2 + (c_{sv} + C(\frac{\omega_o t}{2\pi S_t}))^2 \omega_o^2]^{1/2} - C_{1I} (\frac{t}{2\pi S_t}) \omega_o^2} \quad (39)$$

Let:

$$[I_t^2 (\omega_n^2 - \omega_o^2)^2 + (c_{sv} + C(\frac{\omega_o t}{2\pi S_t}))^2 \omega_o^2]^{1/2} = F_1(\omega_o) \quad (40)$$

and

$$C_{1I} (\frac{t}{2\pi S_t}) \omega_o^2 = F_2(\omega_o) \quad (41)$$

Thus, the denominator of the equation (39) is $F_1(\omega_o) - F_2(\omega_o)$. Physical reality makes it necessary that the denominator, $F_1(\omega_o) - F_2(\omega_o)$, be larger than zero so that finite amplitudes are obtained. Since $C_{1I} > C$, in the vicinity of resonance $F_1(\omega_o)$ can be smaller than $F_2(\omega_o)$ depending on the value of c_{sv} . In this case the relation (36) no longer holds and some dynamic adjustment must occur. Experiment has shown this adjustment to involve a change from $C_{1I} > C$ to $C_{1I} = C$, while the Strouhal number falls below its constant value. Thus, we have a classical Eigenvalue problem defined by the relation:

$$F_1(\omega_o) - F_2(\omega_o) = 0 \quad (42)$$

A qualitative representation of this equation is shown in Figure 14.

Depending on the actual value of c_{sv} the curve $F_1(\omega_o)$ may intersect the curve $F_2(\omega_o)$ at two points, ω_L and ω_U (Eigenvalues), at one point, or may not intersect $F_2(\omega_o)$ at any point for large values of c_{sv} .

The equation $F_1(\omega_o) - F_2(\omega_o) = 0$ is written:

$$\left[I_t^2 (\omega_n^2 - \omega_o^2)^2 + \left(c_{sv} + C \left(\frac{\omega_o t}{2\pi S_t} \right)^2 \omega_o^2 \right)^{1/2} \right] = C_I \left(\frac{t}{2\pi S_t} \right) \omega_o^2 \quad (43)$$

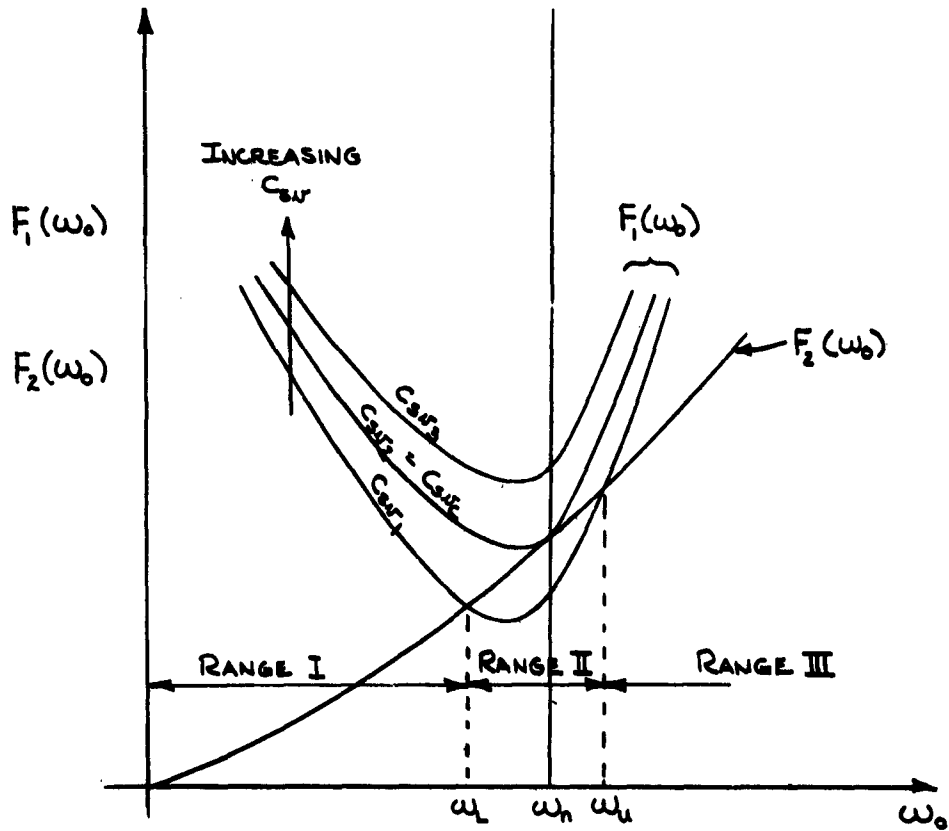


Fig. 14 Graphical Representation of Equation, $F_1(\omega_o) - F_2(\omega_o) = 0$.

In the present tests, the value of c_{sv} is much smaller than the Theodorsen term, CV , in range I and as a first approximation can be neglected for the general discussion of equation (43). Thus, equation (43) can be written:

$$I_t^2(\omega_n^2 - \omega_o^2)^2 + C^2\left(\frac{t}{2\pi S_t}\right)^2 \omega_o^4 \approx C_I^2\left(\frac{t}{2\pi S_t}\right)^2 \omega_o^4 \quad (44)$$

or, solving for the ratio $\frac{\omega_n}{\omega_o}$:

$$\left(\frac{\omega_n}{\omega_o}\right)^2 \approx 1 \pm \frac{t}{2\pi S_t I_t} \sqrt{C_I^2 - C^2} \quad (45)$$

Since $C_I > C$ two real solutions for ω_o are obtained. These two Eigenvalues are called the lower and upper critical frequencies, ω_L and ω_U , and hence define the frequency limits of range II. Using the above expression and the actual values of S_t and I_t for plates B and D, the ω_L and ω_U were computed for both springs. The values of ω_o thus obtained agree very well (see Table V) with the experimentally determined frequencies which bound range II. These experimental critical frequencies were determined from Figs. A7 and A9. The lower critical frequency and velocity were defined by the point at which the Strouhal number first leaves its constant value. The upper critical point was selected by the velocity at which the vibrational amplitude abruptly decreased. While the relationship $V = \omega_o t / 2\pi S_t$ does not hold for ω_U , the value obtained from the above equation agrees extremely well with the experimental value. Eq. (45) thus predicts accurately the range of frequency over which large amplitudes are obtained.

It is of great interest to notice here that the importance of the trailing edge configuration in the vibrational behavior enters into equation (45) through the "steady-state" Strouhal number S_t and C_I . The larger the Strouhal number the smaller the range of $\omega_U - \omega_L$ where large vibrations occur. The nominal value of C_I is independent of the trailing edge, however wake studies (4) have implied a variability in the steady state moment coefficients.

An exact solution of equation (43) by trial incorporating the actual values of c_{sv} for each plate-spring system, gives values of ω_L and ω_U only slightly different from the ones obtained by the simplified equation (45). See Table V.

Experimental results obtained with the same plates reported in Ref. (1) were available covering a much larger range of ω_n . Using equation (45) and the values of ω_n and S_t from Ref. (1) for plates B and D and the value of C_I obtained from the present analysis, values of ω_L and ω_U were computed and compared with the experimental values of

TABLE V CRITICAL FREQUENCIES

Plate	Spring	<u>Equation (45)</u>		<u>Equation (43)</u>		<u>Experimental</u>	
		f_L cps	f_u cps	f_L cps	f_u cps	f_L cps	f_u cps
B	I	66.9	78.5	67.6	77.1	69	76.5
B	II	69.3	81.1	70.3	79.8	74	80.8
D	I	65	79	66	77.2	65.6	79.2
D	II	69	83.9	70.4	81.8	69.1	83

frequencies at which the Strouhal number falls below its constant value left of resonance and the point where vibrations become intermittent at the right of resonance. All the results are summarized in Fig. A35. The predicted and experimental values are in extremely good agreement. This agreement suggests that the value of C_I obtained from the present tests performed over a quite narrow range of natural frequency (f_n from 70 cps to 75 cps) is applicable for a much wider range of natural frequencies and thus of velocities, at least for the same test plates.

9. The Critical Value of c_{sv}

It has been discussed in the previous section that for large values of c_{sv} , the curve $F_2(\omega_0)$ may not intersect the curve $F_1(\omega_0)$. Since the range (II) of large amplitude vibrations would then be absent, it is of practical importance to determine the limiting value of c_{sv} for which the equation $F_1(\omega_0) - F_2(\omega_0) = 0$ has only one real, positive root. This is done most easily by returning to the equation of motion, Eq. (15), and substituting the assumed solution, Eq. (17). Again neglecting $G(K)$ as small we obtain:

$$-I_t \omega_0^2 \bar{a}_0 + i c_t \omega_0 \bar{a}_0 + K_t \bar{a}_0 = [C_{1I} + C_{2I} \frac{2b\omega_0 \bar{a}_0}{V}] 2\rho b^2 H V^2 e^{i\phi} \quad (46)$$

Taking the imaginary part of Eq. (46) and solving for \bar{a}_0 :

$$\bar{a}_0 = \frac{2C_{1I}\rho b^2 H V^2 \sin \phi}{\omega_0 [c_t - C_{1I} V \sin \phi]} \quad (47)$$

The denominator of Eq. (47) will have a single root when $\sin \phi = 1$. From Eq. (20) this can be seen to occur when $\omega_0 = \omega_n$. Thus, the minimum

value of c_{sv} in order to avoid large amplitude vibrations is obtained from:

$$c_t = C_I V \quad (48)$$

or

$$c_{sv_c} = (C_I - C) V \quad (49)$$

and finally:

$$c_{sv_c} = \frac{\omega_n t}{2\pi S_t} (C_I - C) \quad (50)$$

Referring to the critical damping of the system, $c_c = 2 I_t \omega_n$, we have

$$\frac{c_{sv_c}}{c_c} = \frac{t(C_I - C)}{4\pi I_t S_t} \quad (51)$$

The values of c_{sv_c}/c_c for plates B and D have been computed using Eq. (51) and the experimental values of I_t , S_t and C_I . They are tabulated in Table VI in comparison with the relative damping actually experienced in the tests.

TABLE VI CRITICAL VALUES OF c_{sv}

	c_{sv}/c_c	c_{sv_c}/c_c
Plate B - Spring I	0.82%	3.07%
Plate B - Spring II	0.99%	3.00%
Plate D - Spring I	1.50%	3.80%
Plate D - Spring II	1.87%	3.90%

For values of $c_{sv} \geq c_{sv_c}$ the high rate of increase of moment coefficient with the self-excitation parameter, applicable in Range I, should persist over the entire range of vibrational excitation. The Strouhal number should thus retain its "steady-state" value and due to the higher damping, much smaller vibrational amplitudes should be obtained.

10. Range II - The Velocity Range of Large Vibrational Amplitudes

The development of section V-C-8 has made possible the prediction of the range of frequency $\omega_u - \omega_L$, around the natural frequency of the plate-spring system, for which large vibrations occur, i.e. range II. To complete the analysis, the functional relationship of ω_o

and V within this range of frequency must be established. We have already seen that at some critical value of the free stream velocity, the vibrational amplitude tends to infinity. This can lead to one of two results:

- a) structural failure resulting from unlimited growth of vibrational amplitude.
- b) large but finite vibrational amplitudes resulting from the coming into play of some amplitude limiting phenomenon.

The present experimental results indicate clearly that the amplitudes in Range II are self-limiting, which implies the existence of some non-linear damping mechanisms not accounted for in the analytical model in use here. Nevertheless, certain aspects of the Range II behavior which have considerable engineering significance may be determined without a detailed understanding of the amplitude-limiting mechanism.

From vortex street considerations Roshko (44) writes the mean body circulation, $\bar{\Gamma}_b$, as

$$\bar{\Gamma}_b = \left(\frac{s}{V}\right)^2 \frac{\pi V^2}{\omega_0} \quad (52)$$

in which V_s is the velocity along the separation streamline. Assuming application of the lifting force at the quarter-chord point, the vortex-induced moment resulting from this circulation may be written

$$\bar{M}_V = \rho V \bar{\Gamma}_b H b / 2 = \rho H \left(\frac{b}{4}\right) \left(\frac{s}{V}\right)^2 \frac{2\pi V^3}{\omega_0} = \bar{m}_{f_0} 2\rho b^2 H V^2 \quad (53)$$

or

$$\left(\frac{s}{V}\right)^2 = \frac{8b}{t} S_t \bar{m}_{f_0} \quad (54)$$

When the plate vibrates in response to this vortex-induced forcing moment, the velocity, V_s , along the separation stream line will be augmented due to the transverse velocity of the trailing edge, V_{TE} . For bodies of constant thickness, V_s should be of the general form

$$V_s^2 \sim V^2 + V_{TE}^2 \quad (55)$$

For vibration about the leading edge (as is the case being considered here) V_{TE} is given by

$$V_{TE} = 2b\omega_0 \alpha_0 \quad (56)$$

Under these conditions

$$\left(\frac{\bar{v}}{v}\right)^2 \sim 1 + \frac{2b\omega_o \bar{a}_o}{V} \sim 1 + v^* \quad (57)$$

When transverse vibration does not exist ($v^* = 0$) we may reasonably expect $(\bar{v}_s/v)^2$ to be constant and Eq. (54) becomes, in Range I:

$$\left(\frac{\bar{v}}{v}\right)^2_{\alpha_I=0} = S_t \left(\frac{8b}{t}\right) C_{1I} \quad (58)$$

Extrapolating the Range II behavior to $v^* = 0$ we obtain in a similar fashion:

$$\left(\frac{\bar{v}}{v}\right)^2_{\alpha_{II}=0} = S_t' \left(\frac{8b}{t}\right) C_{1II} \quad (59)$$

in which

$$S_t' = \frac{(\omega_o - \omega_L) t}{2\pi (V - V_L)} \quad (60)$$

and V_L is given by the constant Strouhal number of Range I as

$$V_L = \frac{\omega_L t}{2\pi S_t} \quad (61)$$

Under the assumption that the proportionality of Eq. (57) is constant at least in the absence of vibration:

$$\left(\frac{\bar{v}}{v}\right)^2_{\alpha_I=0} = \left(\frac{\bar{v}}{v}\right)^2_{\alpha_{II}=0} \quad (62)$$

and Eqs. (58), (59) give:

$$S_t' = S_t \frac{C_{1I}}{C_{1II}} \quad (63)$$

The range of applicability of Eq. (63) is bounded at one end by:

$$\omega_o = \omega_L \quad (\text{Predicted by Eq. 43})$$

$$\text{and } V = V_L \quad (\text{Predicted by Eq. 61})$$

and at the other end by

$$\omega_o = \omega_u \quad (\text{Predicted by Eq. 43})$$

$$\text{and } V = V_u$$

Putting $\omega_0 = \omega_u$ in S_t' , Eq. (63) gives a predictor for V_u :

$$V_u = \frac{\mu_L t}{2\pi S_t} \left[1 + \frac{C_{1II}}{C_{1I}} \left(\frac{\omega_u}{\omega_L} - 1 \right) \right] \quad (64)$$

The values of V_u given by Eq. (64) are compared below with the values indicated experimentally for plates B and D. V_u was defined experimentally as the velocity at which the vibrational amplitude abruptly decreases (see Figs. A7 and A9). Note that when the nominal values of C_{1I} and C_{1II} are used in Eq. (64) the prediction for plate D is in considerable error. Examination of Fig. A33 shows that the actual value of C_{1I} for plate D may be only 1/2 the nominal value or 0.00125. Predictions using this latter value are also given below.

UPPER CRITICAL VELOCITY, V_u

	Plate	Spring	Experimental V_u fps.	Theoretical V_u (Eq. 64) fps.	C_{1I}	C_{1II}
1.	B	I	8.6	8.2	0.0025	0.0090
2.	B	II	9.1	8.5	0.0025	0.0090
3.	D	I	15.8	10.3	0.0025	0.0090
4.	D	I	15.8	14.3	0.00125	0.0090
5.	D	II	16.6	11.3	0.0025	0.0090
6.	D	II	16.6	15.6	0.00125	0.0090

The predicted frequency - velocity relation for Range II using Eqs. 43, 61, 63 and 64 and the C's of lines 1, 2, 4 and 6 above are plotted as solid lines in Figs. A7 and A9.

Due to the extreme sensitivity of the Range II behavior to the values of these "steady-state" moment coefficients and to avoid the necessity for determining them, an alternative, empirical representation is offered:

It was observed that for each plate-spring system, the value of $\bar{\alpha}_0/V^2$ is approximately the same at the experimental values of ω_L and ω_u . This is shown in Table VII.

TABLE VII CRITICAL VELOCITY CRITERION

Plate	Spring	\bar{a}_o/V^2 at ω_L	\bar{a}_o/V^2 at ω_u
		$10^5 \text{ rad (sec}^2/\text{ft}^2)$	$10^5 \text{ rad (sec}^2/\text{ft}^2)$
B	I	6.8	8.4
B	II	8.4	7.6
D	I	2.75	2.75
D	II	2.0	2.0

Thus:

$$\bar{a}_o \text{ at } \omega_L = \frac{C_{LII} \frac{\rho}{2} H(2b)^2 V_L^2}{[I_t^2(\omega_n^2 - \omega_L^2)^2 + (c_{sv} + CV_L)^2 \omega_L^2]^{1/2} - CV_L \omega_L} \quad (65)$$

$$\bar{a}_o \text{ at } \omega_u = \frac{C_{LII} \frac{\rho}{2} H(2b)^2 V_u^2}{[I_t^2(\omega_n^2 - \omega_u^2)^2 + (c_{sv} + CV_u)^2 \omega_u^2]^{1/2} - CV_u \omega_u} \quad (66)$$

In order that

$$\left(\frac{\bar{a}_o \text{ at } \omega_L}{V_L^2} \right) = \left(\frac{\bar{a}_o \text{ at } \omega_u}{V_u^2} \right) \quad (67)$$

we should have:

$$\begin{aligned} & [I_t^2(\omega_n^2 - \omega_L^2)^2 + (c_{sv} + CV_L)^2 \omega_L^2]^{1/2} - CV_L \omega_L \\ & = [I_t^2(\omega_n^2 - \omega_u^2)^2 + (c_{sv} + CV_u)^2 \omega_u^2]^{1/2} - CV_u \omega_u \end{aligned} \quad (68)$$

With predetermined values of ω_L , ω_u , and V_L , the above equation can be solved for V_u since the left hand member is a known and easily computed quantity.

Let

$$[I_t^2(\omega_n^2 - \omega_L^2)^2 + (c_{sv} + CV_L)^2 \omega_L^2]^{1/2} - CV_L \omega_L = A \quad (69)$$

then

$$A = [I_t^2(\omega_n^2 - \omega_u^2)^2 + (c_{sv} + CV_u)^2 \omega_u^2]^{1/2} - CV_u \omega_u \quad (70)$$

or

$$A = (c_{sv} + CV_u) \omega_u \left[1 + \frac{I_t^2(\omega_n^2 - \omega_u^2)^2}{(c_{sv} + CV_u)^2 \omega_u^2} \right]^{1/2} - CV_u \omega_u \quad (71)$$

For values of $\frac{I_t^2(\omega_n^2 - \omega_u^2)^2}{(c_{sv} + CV_u)^2 \omega_u^2} \ll 1$, as is the case in these experiments,

$$\left[1 + \frac{I_t^2(\omega_n^2 - \omega_u^2)^2}{(c_{sv} + CV_u)^2 \omega_u^2} \right]^{1/2} \approx 1 + \frac{1}{2} \frac{I_t^2(\omega_n^2 - \omega_u^2)^2}{(c_{sv} + CV_u)^2 \omega_u^2} \quad (72)$$

or

$$A = c_{sv} \omega_u + CV_u \omega_u + \frac{1}{2} \frac{I_t^2(\omega_n^2 - \omega_u^2)^2}{(c_{sv} + CV_u) \omega_u} - CV_u \omega_u \quad (73)$$

and finally

$$V_u \approx \frac{1}{C} \left[\frac{1}{2} \frac{I_t^2(\omega_n^2 - \omega_u^2)^2}{(A - c_{sv} \omega_u) \omega_u} - c_{sv} \right] \quad (74)$$

The above expression indicates clearly that V_u strongly depends on c_{sv} . Thus inaccuracies in determining the c_{sv} value can greatly influence the computed value of V_u . Using equation (74), the values of ω_L and ω_u predicted by equation (43) and the experimental values of I_t , ω_n , and c_{sv} , the V_u was computed for plates B and D tested with both springs. Neglecting c_{sv} in equation (74) since values were not available, computations of V_u were also made with the available results reported in Ref. (1). All the results are presented in Fig. A36. For plate D the predicted V_u are

in general 5% larger than the experimental values while for plate B about 20% larger. Taking into account the extreme sensitivity of equation (74) to the values of $(\omega_n^2 - \omega_u^2)^2$ and c_{sv} the agreement between predicted and experimental values of V_u may be considered fairly satisfactory.

From an engineering point of view a rough estimate of the amplitudes in the velocity range II can then be obtained by approximating the ω_o, V relationship with a straight line within this range as is indicated in Fig. 15, and by employing equation (37) and the experimentally obtained values of c_{1II}, c_{2II} .

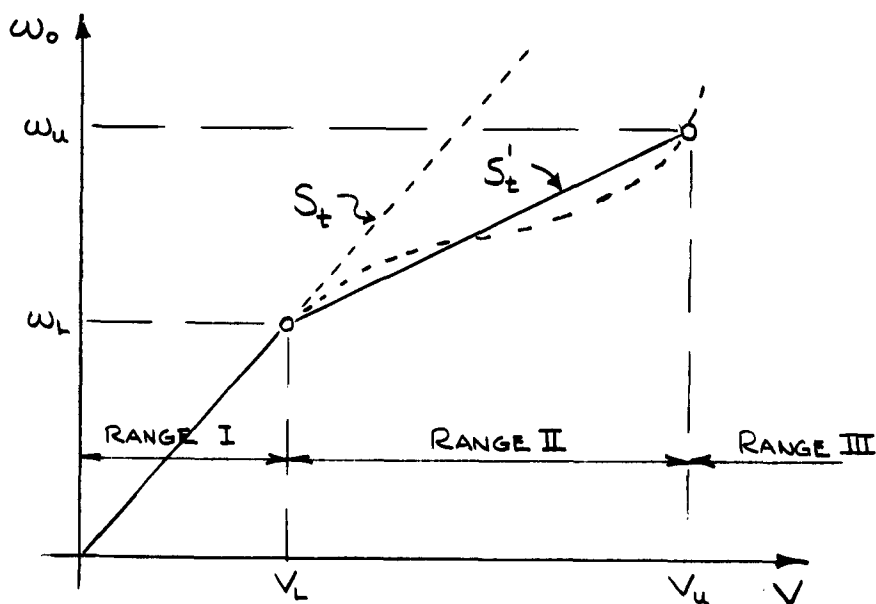


Fig. 15 Form of Frequency-Velocity Relationship in Range II

The amplitude at the natural frequency of the system is given according to equation (37) by:

$$\bar{a}_o = \frac{c_{1II} \frac{\rho}{2} H(2b)^2 V^2}{c_{sv} \omega_n} \quad (75)$$

and it is determined uniquely by V , c_{sv} , ω_n . For spring II the velocity at the corresponding ω_n is larger than for spring I, nevertheless the maximum amplitudes for spring II are in all cases smaller than for spring I. This indicates that the value for c_{sv} may increase with increasing velocity and amplitude of motion. While c_{sv} is small in the present test, compared with the Theodorsen damping term, it is of unique importance in the immediate vicinity of resonance where it determines the maximum amplitudes.

The presence of the third harmonic in the vibration signal of Ranges II and III, its dependence upon flow velocity and the regions of variable vibrational amplitude are additional evidence that the phenomenon under study is actually non-linear, at least when the amplitudes become large. The linear model employed in the present analysis cannot allow these effects. It is not surprising therefore that attempts to use this linear model to define the amplitude and frequency as unique functions of velocity and system constants are only moderately successful in Range II.

Other effects such as non-linearities of the spring may also be present for large amplitudes and in spite of their small significance in the shaping of the whole response curve can greatly affect the maximum amplitudes at resonance.

11. Range III - The Velocity Range of Small Varying Amplitude Vibrations

Thus far the discussion and analysis of the results have been restricted to the velocity ranges I and II. The trend of experimental data indicates that in range III the frequency tends to acquire the values predicted by the initial constant Strouhal number. This has been reported by Ippen et al. (1) but within the range of measurable vibrations in the present tests this does not occur. The Strouhal number increases above the minimum value obtained at ω_u , V_u , but still is much smaller than the initial constant value. It is of interest to study in some detail the moment coefficient diagram for an understanding of this behavior. (See Fig. 16).

It is seen that point d does not correspond to point b. Thus, range III is a transitional range corresponding to the interval db where the frequency is governed by the dynamics of the system as in range II, rather than by the velocity according to constant Strouhal relationship.

Once again, however, for engineering purposes, it may be assumed that when V_u is reached, the frequency will jump immediately to the value given by the constant initial Strouhal number and the velocity V_u . This is indicated by the solid vertical lines at V_u in Figs. A7 and A9. The Strouhal number then retains this constant value until, with increasing velocity, the second harmonic is approached and the whole process repeats itself.

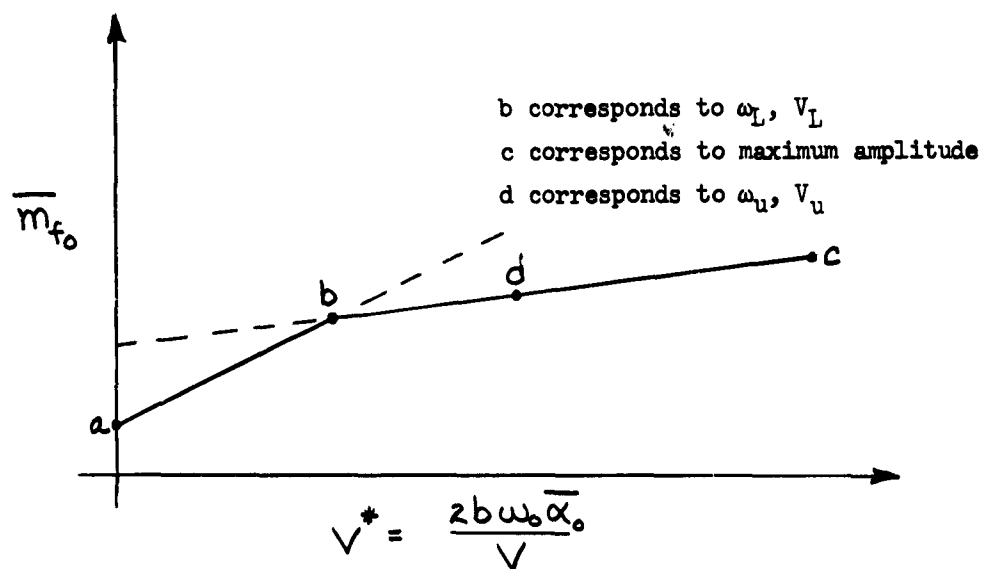


Fig. 16 Moment Coefficient

12. The Influence of Ambient Velocity on the Viscous Damping

In all of the previous development the damping coefficient in still water was considered to represent the structural plus viscous damping of the system. It was assumed that the viscous damping is independent of the velocity V and the motion of the plate. In order to check the influence of the velocity V on the viscous damping, the following tests were performed with plate B - spring II. It was possible to perform free oscillation tests with the water running in the water tunnel at the atmospheric pressure. The natural frequency and damping coefficient in still water and at two velocities smaller than the velocity at which vibrational excitation starts, were determined with free oscillation tests. The results obtained are shown below.

V fps	f_n cps	c_{sv}/c_c
0	80.0	0.98%
3.65	80.3	0.90%
4.92	81.2	1.03%

The few values of damping coefficient obtained show no systematic dependence on the velocity V insofar as it could be determined experimentally. The indicative small increase in natural frequency with

increasing velocity is much larger than that indicated by inclusion of the Theodorsen terms and is within the experimental error, thus no definite conclusion can be drawn.

An effort was made to perform free oscillation tests at velocities well above the range of vibrational excitation of plate B. No consistent results were obtained, the motion being irregular and of high frequency. From these limited tests it appears that for small amplitudes and velocities, the natural frequency and damping coefficient in still water are the correct values.

13. The Self-Excited Nature of the Vibrations

Analysis of the experimental results has indicated a strong interaction of forcing moment and plate motion. Increasing moments are associated with increasing amplitudes; thus the vibrations of the plates can be characterized as self-excited. Several phenomena can contribute to such strong dependence of the moment coefficient on the motion of the plate.

Discharge of Vorticity

For the stationary plate the rate of discharge of vorticity in the wake from each side of the plate is approximately:

$$\int_0^{\delta'} \frac{\partial u}{\partial y} u dy = \lambda_1 V^2,$$

λ_1 being a proportionality constant. For the oscillating plate with $\alpha = \alpha_0 \sin \omega t$, the fluid particles in the boundary layer acquire a transverse velocity, $v = x' \alpha_0 \omega \cos \omega t$, in which x' is the distance of the fluid particle in the boundary layer from the axis of oscillations. Thus the fluid particles acquire an additional periodic vorticity component $(\partial v / \partial x') = \alpha_0 \omega \cos \omega t$. The rate of discharge of this vorticity in the wake is

$$\int_0^{\delta'} \frac{\partial v}{\partial x'} u dy = \lambda_2 \alpha_0 \omega V \cos \omega t,$$

λ_2 being a proportionality constant. The total rate at which vorticity is discharged in the wake is then $\lambda_1 V^2 + \lambda_2 \alpha_0 \omega V \cos \omega t$. A part of this vorticity is diffused and annihilated with vorticity of opposite sign and the rest contributes to the formation of discrete vortices. The presence of the term $\lambda_2 \alpha_0 \omega V \cos \omega t$ may thus be the cause of vortices of larger strength as a result of the plate motion.

It is interesting to note that the intercept of the experimental moment coefficient for $\bar{\alpha}_0 = 0$ affords an estimate of the lift-producing circulation about the plate in the absence of self-excitation. From Eq. (53)

$$\bar{\Gamma}_b = 4 C_{l_I} b V \quad (76)$$

Assuming that the vortex is "shed" when $\Gamma_b(t) = \Gamma_{b_{\max}}$ and that the initial vortex strength, k_0 , is commensurate with this circulation:

$$k_0 = \frac{\Gamma_{b_{\max}}}{2\pi} = \frac{\bar{\Gamma}_b}{\sqrt{2}\pi} = \frac{4 C_{l_I} b V}{\sqrt{2}\pi} \quad (77)$$

In Table III of Ref. (4), values of $k_{1.5}$ (i.e., k at 1.5 plate thicknesses downstream of the trailing edge) are given for a velocity of 9.30 fps. as determined from wake measurements for these same plates with vibration prevented. A comparison of these values with k_0 (k at trailing edge) as given by Eq. (77) is of interest:

ESTIMATED VORTEX STRENGTHS AT $V = 9.30$ fps.

PLATE	C_{l_I}	k_0 (trailing edge), ft^2/sec . (From Eq. 77)	$k_{1.5}$ ($x/t = 1.5$), ft^2/sec (From Wake Meas. Ref. 4)
A	-	-	0.00127
B	0.0025	0.00175	0.00245
C	-	-	0.00117
D	0.0025	0.00175	0.00251
D	0.00125	0.00088	0.00251

Three-Dimensional Effects

Theoretical models for the determination of vortex induced forces acting on a body are usually based upon two-dimensional considerations (von Karman vortex street). It has to be understood, however, that the total moment acting on the plate is an integral quantity and that three-dimensional effects can greatly affect its magnitude. Roshko (31) reports on the three-dimensional structure of the wake behind a cylinder. His measurements indicate that the stable vortex street ($R < 150$) has a periodic spanwise structure with a wave length parallel to the cylinder of 18 diameters at $R = 80$. Unfortunately no available results exist in the voluminous wake literature concerning the three-dimensional structure of wakes at higher Reynolds number.

The three-dimensional effects are of extreme importance as is shown below.

The forcing moment per unit spanwise length of the plate at any spanwise position, z , can be expressed as

$$m_{fz} = \frac{1}{2} \rho (2b)^2 V^2 e^{i\omega t}.$$

The coefficient, m_{f0} , as determined by measurement of the net moment on the entire plate is then given by:

$$m_{f0} = \frac{\int_0^H m_{fz} dz}{H}$$

If m_{fz} is periodic such that H is an integral multiple of the spanwise wavelength then $m_{f0} = 0$.

If m_{fz} is periodic but H is not an integral multiple of the spanwise wavelength then m_{f0} may have any value up to the spatial RMS of m_{fz} .

For the stationary plate, the degree of two-dimensionality of the wake should depend strongly on body Reynolds number and perhaps to some degree on the trailing edge geometry. For an oscillating plate, the degree of two-dimensionality may logically be expected to increase with the amplitude of motion, at least when the frequency of oscillation is that of the wake motion as it is in the forced vibrations being considered here. The observed increase of moment coefficient with increase in the dynamic parameter:

$$V^* = \frac{2b\omega \bar{a}_0}{V}$$

may thus result from increases in two-dimensionality as well as from increases in local vortex strength.

Plates B and D with extending trailing edges exhibit large amplitudes and thus large values of V^* in the vicinity of resonance. It is thus possible that the extension of trailing edges beyond the separation points, and thus the provision of solid shielding between the shearing layers of opposite sign, greatly affects the strength of the shed vortices in addition to the two-dimensional structure of the wake. For plates A and C the trailing edge does not provide solid shielding of the shearing layers and larger annihilation of vorticity may take place in the early wake, resulting in vortices of smaller strength.

D. Final Tests - Wake Measurements

1. Experimental Procedure

For several plate-spring systems, several discrete velocities were selected within the velocity range of measurable vibrational excitation and at each velocity the amplitude and frequency of vibration were measured. Measurements of the RMS of the total head fluctuations, H'_t , were then made across the half-width of the wake at station $x = 1.5t$ utilizing the thermocouple voltmeter. Measurements were taken at sufficient transverse points so that a continuous distribution curve could be drawn. Three measurements of the RMS were made at every point and the average of them considered as the true RMS value. The discrete frequencies of the spectrum of $\sqrt{H'^2_t}$ were picked up with the vibration analyzer.

The plate-spring systems and the number of velocities for which transverse distributions of the total head fluctuation were made are indicated below.

Plate B - spring I	7 Runs
Plate C - spring I	3 Runs
Plate C - spring II	3 Runs
Plate D - spring I	10 Runs
Plate D - spring II	4 Runs

2. Interpretation of Wake Measurements

The response of the turbulence gage used for the fluctuating total head measurements is discussed in detail in Refs. (2), (3) and (43). It is shown in these references that, neglecting the probe response to the transverse components of turbulence, the RMS of the fluctuating component of the local instantaneous total head is given by:

$$\sqrt{H'^2_t} = \frac{\sqrt{e_m^2}}{G_a G_p K_G} \quad (78)$$

in which

e_m = amplified gage signal input to the measuring instruments
 G_a = amplifier gain
 G_p = preamplifier gain
 K_G = gage sensitivity in millivolts per foot of water

Under additional restrictive conditions, the principle one being that $\sqrt{u'^2} \ll u$, Ippen (42) has shown that Eq. (78) may be simplified to

$$\sqrt{H_t'^2} = \frac{\sqrt{\frac{e_m^2}{G_a G_p K_G}}}{g} \approx \frac{u \sqrt{u'^2}}{g} \quad (79)$$

which provides a means of studying the longitudinal turbulent velocity component, u' , provided the mean velocity, u , is known.

Under the conditions existing in the early wake, where the present measurements were made, the applicability of Eq. (79) is very questionable. A reduction of data from the preliminary tests performed with plate C - spring I and using Eq. (79) indicated local values of the relative turbulence $\sqrt{u'^2}/u$ as high as 1 on the wake centerline and about 0.1 at a transverse distance, $y/t = 1.1$. For this reason, no attempt to calculate $\sqrt{u'^2}$ from this reduced relation was felt justified and mean local velocity traverses were not made. The reduced formula will be used only for a general qualitative interpretation of the measurements taken.

The actual $\sqrt{H_t'^2}$ consists of two parts: a random turbulent background covering the continuous spectrum of frequencies and discrete components due to the "shedding of vortices". In these tests the discrete component at the fundamental vibrational frequency accounts usually for more than 50% of the total RMS as has been discussed in section V-B-3.

For an ideal vortex street (von Karman vortex street) with geometric configuration independent of the ambient velocity and of plate motion, the $\sqrt{u'^2}$ at any particular point in the wake will be proportional to the strength of the discrete vortices.

$$\sqrt{u'^2} \sim \text{vortex strength}$$

Under the assumption of similar velocity distribution in the wake it can be deduced that for a given x/t in the early wake $u \sqrt{u'^2} \sim V \sqrt{u'^2} \sim V \cdot (\text{Vortex strength}) \sim V \cdot (\text{circulation}) \sim \text{lift force} \sim \text{vortex-induced lift moment}$. For the qualitative arguments of the present discussion we will assume that

$$u \sqrt{u'^2} \sim \sqrt{H_t'^2}$$

in spite of the inaccuracy pointed out above. Thus it is concluded that the $\sqrt{H_t'^2}$ at any particular point in the wake is very roughly proportional to the lifting moment acting on the plate.

To avoid reliance upon a point measurement for comparative studies the integral of $\sqrt{H_t'^2} d(y/t)$ over the width of the wake will be used as a better index of a two-dimensional vortex-induced lifting moment than is $\sqrt{H_t'^2}$ at a single location.

3. Correlation of Wake Measurements with Vibrational Characteristics

The transverse distributions of the total head fluctuation in the wake of the plates (at midspan only) are presented in Figs. A37 through A40. The dimensionless total head fluctuation $(2g \sqrt{H_t'^2})/v^2$ has been plotted versus the dimensionless transverse distance y/t over the half width of the wake, δ . The quantity

$$m = \frac{2g \int_0^{\delta/t} \sqrt{H_t'^2} d(\frac{y}{t})}{v^2 \cdot \delta/t} \quad (80)$$

has been computed for every test velocity by numerical integration. The integral has been extended out to $y/t = 1.1$ since it was found in the preliminary tests that there the mean local velocity is almost equal to the free stream velocity. The computed values of m as well as the ambient velocity, amplitude and fundamental vibrational frequency are presented in the Figs. A37 through A40.

It is obvious from the developments of the previous section that the dimensionless quantity m should be roughly proportional to the two-dimensional forcing moment coefficient. Also, the effect of increasing two-dimensionality of the wake cannot be reflected in the coefficient m due to the single spanwise location of the measurements made. A study of the values of m reveals the following:

For plate D (Fig. A39) the value of m remains essentially constant. The extent of the influence of the plate motion on the strength of the vortices is illustrated best perhaps by Fig. A40 in which we can compare values of m for different \bar{a}_0 but at the same velocity. For a 3-fold variation in amplitude ($V = 6.37$ fps), m increases by a factor of only 1.6 yet from Fig. A34 the moment coefficient increases by a factor of 2.7. We are thus led to conclude that the sensitivity of moment coefficient to plate motion is at least as dependent upon other mechanisms such as increasing wake two-dimensionality or transverse redistribution of vorticity as it is upon local increase in the strength of discrete vorticity.

For plate B (Fig. A37), m undergoes a 1.7 fold variation. Again using the corresponding values of the self-excitation parameter, V^* , the moment coefficient is seen to increase by a factor of 7.2. For this plate, the increase in local vortex strength is clearly a minor effect.

For plate C (Fig. A38) m changes by a factor of 1.26 while \bar{m}_{f_0} experiences only a 1.16 fold variation. Due to the qualitative nature of the total head interpretations, speculations concerning the sign of this difference between m and \bar{m}_{f_0} are unwarranted but it appears as though increasing vortex strength may account for the entire increase in moment coefficient.

Although the above comparisons are only qualitative, the nature of the major inaccuracies in interpretation of the probe response are such as to give turbulent velocities which are too large. For this reason, the indication that at least certain of the plates become self-excited through increasing wake two-dimensionality bears emphasis by a tabulation of the factors just discussed:

Importance of Increasing Local Vortex Strength
in the Self-Excitation Mechanism

Plate	Maximum Factor of Variation in " m "	Corresponding Factor of Variation in \bar{m}_{f_0}	Apparent Major Self-Excitation Mech.
B	1.7	7.2	Two-dimensionality
C	1.6	2.7	Two-dimensionality and local vortex strength
D	1.26	1.16	Local vortex strength

It should also be noted that for all transverse positions discrete frequencies were present in the spectrum of $\sqrt{H'_t{}^2}$. The fundamental frequency was easily detected as were the second and third harmonics. The fundamental discrete frequency in the spectrum of $\sqrt{H'_t{}^2}$ was exactly the same as the fundamental frequency of the vibrating plate in all cases.

4. The Periodic Flow Field in the Wake

The electrical signal of H'_t was observed on the screen of the oscilloscope. Near the centerline of the wake the signal possessed periodicity but it was obscured by the heavy turbulent background. The periodicity was more clear as the probe was moved away from the centerline. From the investigation of the wake structure for stationary

plates (2)(3), it is known that the probe, at large values of y/t , responds to the free turbulence level. No discrete periodicities are present at this position with the stationary plates and the spectrum of $\sqrt{H'^2_t}$ is continuous. In the present case of the vibrating plate the signal of H'_t at the points $y/t = 1.82, 2.62, 5.42$ was periodic and almost sinusoidal with a very small turbulent background superimposed. This was observed for plates B and D which give large vibrational amplitudes. The RMS level of H'_t at these points is considerably higher than the corresponding level of the free turbulence. The free turbulence level in the water tunnel is $\sqrt{u'^2}/V = 3\%$ or 4% while the RMS of the H'_t at $y/t = 5.42$ gives an indicated value of $\sqrt{u'^2}/V = 25\%$ for plate B at resonance.

A special test was carried out with plate B - spring I when this observation was made. The total head fluctuation gage was placed at station $x/t = 1.5$, $y/t = 5.42$. The velocity in the water tunnel was increased by small increments and the RMS of H'_t was measured by the A.C. Voltmeter. The test covered the whole range of velocities where vibrational excitation occurs. The vibrational amplitude versus velocity relationship having been established, a direct comparison could be made between $\sqrt{H'^2_t}$ and the vibrational amplitude: It was discovered that for large amplitudes the $\sqrt{H'^2_t}$ at $y/t = 5.42$ is proportional to the vibrational amplitude. The same behavior is exhibited with plate D for large amplitudes.

Table VIII presents the values of $\sqrt{H'^2_t}$ at $y/t = 5.42$, the corresponding velocity, V , the RMS of vibrational amplitude, \bar{a}_0 , and the ratio $\bar{a}_0/\sqrt{H'^2_t}$ for plates B and D.

For plate B the values of $\sqrt{H'^2_t}$ at the transverse positions $y/t = 1.82, 2.62, 5.42$ remain almost constant with higher values sometimes at $y/t = 5.42$ as it is shown in Fig. A37. For plate D the $\sqrt{H'^2_t}$ decreases slightly from $y/t = 1.82$ to $y/t = 5.42$. For plate C the value of $\sqrt{H'^2_t}$ at $y/t = 1.82, 2.62, 5.42$ is larger than the free turbulence level but the periodicity is obscured by the turbulent background. The points $y/t = 1.82, 2.62, 5.42$ at the station $x/t = 1.5$ are outside of the conventionally described wake width.

From the complete expression for the total head fluctuation it is observed that two terms can make a significant contribution, u' and p' . It is thus likely that a fluctuating pressure field is created by the vibrating plate with $p' \sim \alpha = \alpha_0 \cos \omega_0 t$. In this case

$$\sqrt{H'^2_t} = \sqrt{\frac{u'^2}{g^2} + \frac{p'^2}{\gamma^2}} \quad (74)$$

TABLE VIII

Free Stream Total Head Fluctuations
and Vibrational Amplitudes

Plate B - Spring I

V fps	$\bar{\alpha}_0$ 10^3 rad	$\sqrt{H_t^2}$ at $y/t = 5.42$ ft. water	$\frac{\bar{\alpha}_0}{\sqrt{H_t^2}}$, $\frac{10^3 \text{ rad}}{\text{ft.w.}}$	
5.58	1.20	0.074	16.2	
5.67	2.50	0.104	24	
6.40	8.70	0.344	25.3	
6.70	9.25	0.382	24.2	
6.82	9.38	0.388	24.2	
7.13	9.05	0.374	24.2	
7.50	8.60	0.333	25.8	
7.88	8.00	0.317	25.2	
8.27	7.35	0.294	25.0	
8.80	0.90	0.118	7.6	
8.16	0.35	0.117	3.0	
5.72	3.61	0.131	27.5	
6.00	6.43	0.245	26.2	
6.47	9.15	0.301	30.4	
7.17	8.91	0.358	24.9	
7.50	7.98	0.320	24.9	
8.60	1.08 2.35	0.216	10.9	

Measurements of
 $\sqrt{H_t^2}$ made with
A.C. Balantine
Voltmeter.

Measurements of
 $\sqrt{H_t^2}$ made with
Thermocouple
Voltmeter.

Plate D - Spring I

6.37	0.86	0.084	10.2	
8.00	3.15	0.173	18.2	
9.29	4.87	0.245	19.85	
10.80	7.02	0.353	19.9	
11.75	7.92	0.353	22.4	
12.40	8.64	0.431	20.0	
13.65	8.89	0.465	19.1	
14.20	8.74	0.490	17.8	
15.05	8.06	0.490	16.45	
15.50	6.83	0.490	13.9	

Measurements of
 $\sqrt{H_t^2}$ made with
the Thermocouple
Voltmeter.

Plate D - Spring II

7.97	2.17	0.142	15.3	
10.8	5.39	0.314	17.1	
12.45	6.74	0.441	15.3	

As long as $\overline{p'^2}/\gamma^2 \gg u^2 \overline{u'^2}/g^2$, the $\sqrt{H'^2_t}$ at $y/t = 5.42$ is proportional to $\overline{\alpha}_0$. The importance of the term $u^2 \overline{u'^2}/g^2$ increases with increasing velocity. The above arguments are greatly supported by the experimental results.

A careful study of Table VIII reveals the following. For plate B in the small range of relatively low velocities where large amplitudes are obtained, the proportionality of $\sqrt{H'^2_t}$ to the vibrational amplitude is perfect, because the term $u^2 \overline{u'^2}/g^2$ is of minor importance compared with $\overline{p'^2}/\gamma^2$. To the left and right of resonance, with small amplitudes and thus increasing importance of the term $u^2 \overline{u'^2}/g^2$, the proportionality fails. For plate D, which exhibits large amplitudes at relatively high velocities, the importance of the term $u^2 \overline{u'^2}/g^2$ is greater than for plate B and the proportionality of $\sqrt{H'^2_t}$ to the vibrational amplitude holds only near resonance.

To see if the periodic pressure field created by the plate vibration is imposed upon the whole flow field, the total head fluctuation gage was placed at station $x/t = 10$ and $y/t = 5.42$. The $\sqrt{H'^2_t}$ at this position was found to be only 2/3 of the value obtained at $x/t = 1.5$ and $y/t = 5.42$. The signal of H'_t exhibited random characteristics with an almost complete absence of discrete periodicity. This observation indicates that the free-stream periodicities are likely the result of fluctuating local pressures caused by, and related in magnitude to, the local transverse velocity fluctuations. These latter fluctuations, near the plate, will be directly related to the magnitude of α_0 , while with distance downstream in the wake they are subject to viscous decay and degeneration into random turbulence.

It was thought of interest to investigate the phase difference between the motion of the plate and the periodic flow disturbance outside the wake. For this purpose a special test was performed with plate D - spring II. The total head fluctuation gage was placed at $x/t = 1.5$ and $y/t = 5.42$. The signals H'_t and α were connected to the two channels of the oscilloscope and were observed on the screen. For all tested velocities the signals were in phase as far as it could be determined experimentally. Fig. A41 presents pictures of the two signals under two of the test conditions. The observed phasing is what would be expected from the dynamic pressure changes accompanying an oscillating velocity field. That is, the pressure should be 90° out of phase with the fluid velocity and, close to the plate, the fluid velocity should be 90° out of phase with the plate motion which initiates it.

VI. SUMMARY AND CONCLUSIONS

The vibrational behavior and wake structure of four flat plates (chord = 2", thickness = 1/4") with different trailing edge geometry, mounted at zero mean angle of attack in a uniform flow field and allowing torsional oscillations about an axis containing the leading edge, has been investigated in a closed-jet water tunnel.

Measurements of the amplitude and frequency of the vibration and of the fluctuating total head in the wake were made over the range of ambient velocity producing measurable vibrational excitation.

An equation for the amplitude response of the plate-spring system is developed incorporating the hydrodynamic loads predicted by the linearized potential theory of Theodorsen and an unknown flow-induced forcing moment.

Using the experimental data and the above theoretical model the forcing moment coefficients were evaluated and correlated with the dynamic characteristics of the flow-plate system.

The following conclusions are drawn:

1. Similarity of normalized spectral distributions of total head fluctuations in the early wake of the same plate when stationary and when vibrating indicates that periodic vortex shedding provides the forcing mechanism in the flow-induced plate vibration studied.

2. The fundamental vibrational frequency coincides exactly, in all cases, with the fundamental discrete frequency in the total head fluctuation spectrum.

3. Large amplitude flow-induced vibrations are characterized by three distinct ranges of vibrational behavior:

Range I: "simple harmonic" motion with slowly varying small amplitude where a constant body-thickness Strouhal No. ($St = f_0 t/V$) prevails. This range ends at a frequency less than the resonant frequency.

Range II: periodic motion with large stable amplitude containing a third harmonic which grows with ambient velocity. Strouhal number (based on the fundamental frequency) continually decreases with ambient velocity in this range which ends at a frequency higher than the resonant frequency.

Range III: periodic motion of small, unstable amplitude. Strouhal number continually increases with ambient velocity.

4. The Range I Strouhal number appears to be the same as the steady body Strouhal number.

5. Vortex-induced forcing moments and plate motion are related uniquely for all plates tested through the self-excitation parameter, $V^* = 2b\omega_o\bar{\alpha}_o/V$. This parameter is the ratio of the RMS transverse velocity of the trailing edge to the mean ambient flow velocity. It is shown to be proportional to the ratio of separation stream line velocity to free stream velocity and hence is also proportional to wake pressure coefficient.

The form of this relationship is a piecewise linear variation in the forcing moment coefficient, \bar{m}_{f_o} , with the self-excitation parameter, V^* . Corresponding to the above Ranges:

$$\text{Range I: } \bar{m}_{f_o} = C_{1I} + C_{2I} V^* \quad (28)$$

$$\text{Range II: } \bar{m}_{f_o} = C_{1II} + C_{2II} V^* \quad (29)$$

6. The linear dependence of forcing moment of the self-excitation parameter yields the effect of a decreasing damping with increasing velocity. It leads to an eigenvalue problem defining the critical frequencies bounding Range II in terms of the system constants, the "moment slope", C_I , and the Range I Strouhal number, S_t , i.e.

$$\left[I_t^2 (\omega_n^2 - \omega_o^2)^2 + \left(c_{sv} + C \left(\frac{\omega_o t}{2\pi S_t} \right) \right)^2 \omega_o^2 \right]^{1/2} - C_I \left(\frac{\omega_o t}{2\pi S_t} \right) \omega_o = 0 \quad (43)$$

7. The ambient velocity, V_L , corresponding to the lower critical frequency, ω_L , (and the beginning of large amplitude motion) can be predicted precisely through use of the smaller root of Eq. (43) and the Range I Strouhal number, S_t .

$$V_L = \frac{\omega_L t}{2\pi S_t} \quad (61)$$

8. The ambient velocity, V_u , corresponding to the upper critical frequency, ω_u (and the end of large amplitude motion) can be predicted accurately enough for engineering purposes (+5 to 20%) by assuming the reduced amplitude, $\bar{\alpha}_o/V^2$, to be the same at ω_L and ω_u .

This yields:

$$V_u \approx \frac{1}{C} \left[\frac{1}{2} \frac{I_t^2 (\omega_n^2 - \omega_u^2)^2}{(A - c_{sv} \omega_u) \omega_u} - c_{sv} \right] \quad (74)$$

where

$$A = [I_t^2 (\omega_n^2 - \omega_L^2)^2 + (c_{sv} + CV_L)^2 \omega_L^2]^{1/2} - CV_L \omega_L \quad (70)$$

9. Controlled variation of the system parameters should allow design of a system in which Eq. (43) has only one root, i.e. where Range II is absent and thus large flow-induced vibrations are not incurred. This can perhaps be most practically accomplished by increasing the combined structural and viscous damping coefficient, c_{sv} , until

$$c_{sv} \geq \frac{\omega_n t}{2\pi S_t} (C_I - C) \quad (50)$$

For a fixed value of the damping, c_{sv} , the critical frequency range, $\omega_u - \omega_L$, can be reduced through an increase in the Strouhal number, S_t .

10. Wake measurements suggest that the large increase in moment coefficient, \bar{m}_{f0} , with increasing self-excitation parameter, V^* , may be due to either increasing two-dimensionality of the wake or to increasing local vortex strength depending upon the trailing edge geometry. For the plates tested the former phenomenon seems to govern when the trailing edge separation points are variable and the latter when separation points are fixed.

VII. APPENDICES

APPENDIX A: Experimental Results

APPENDIX B: Spring Calibration and Free Oscillation Tests

APPENDIX C: References

APPENDIX A

Experimental Results

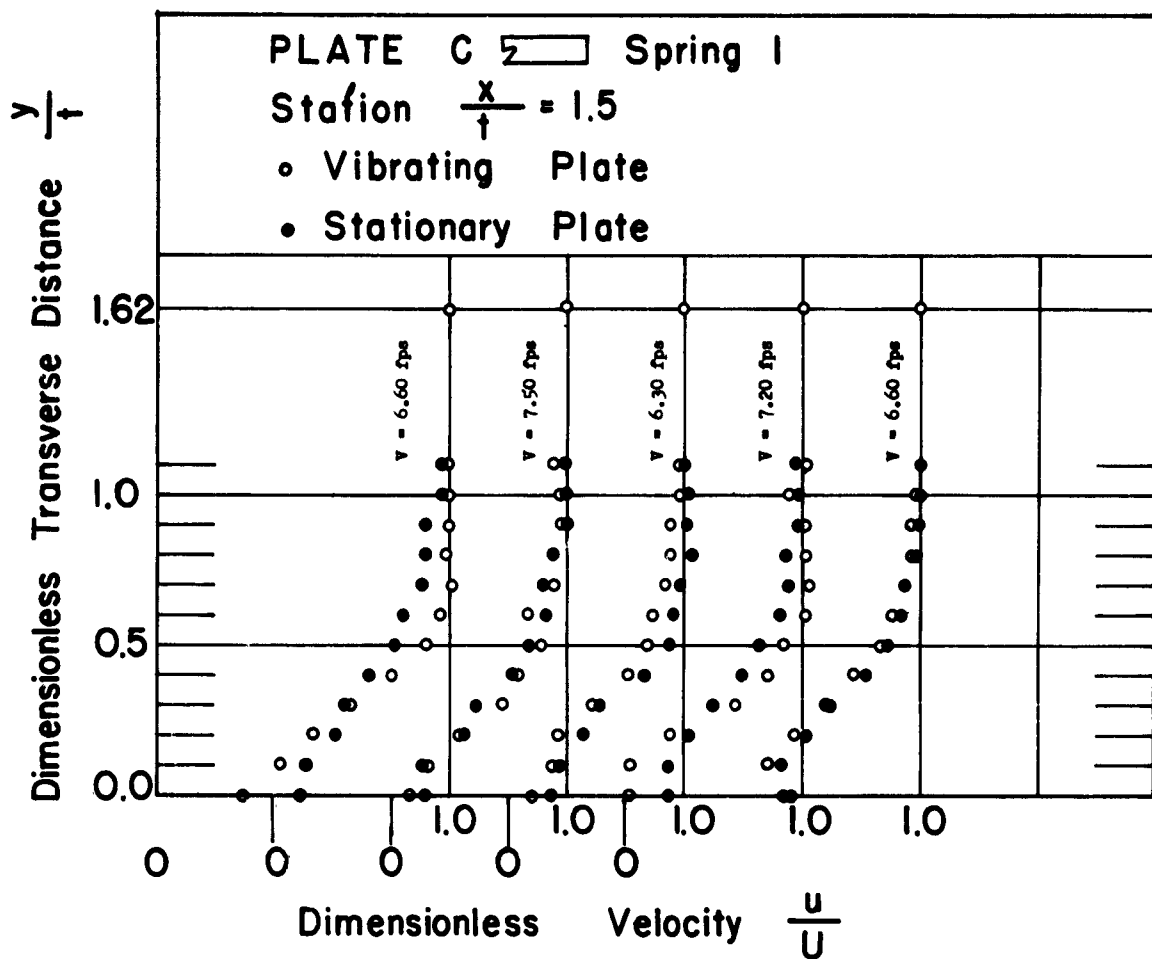


Fig. A1 Mean Velocity Distributions in the Wake

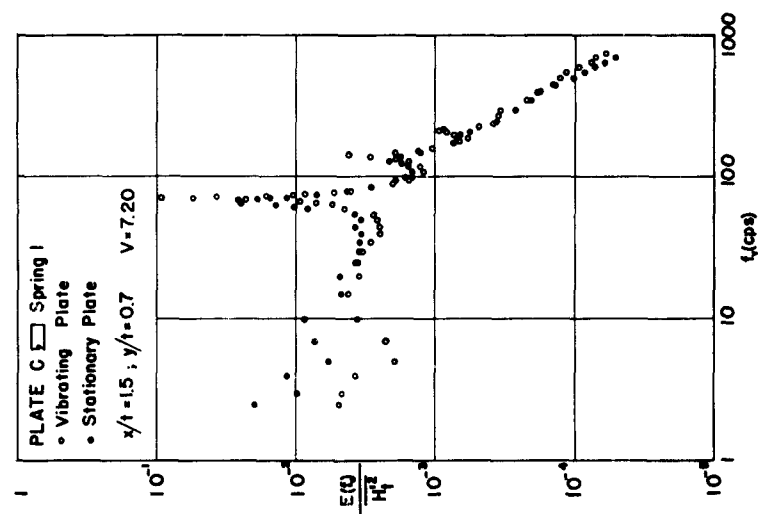


Fig. A3 Normalised Spectral Distributions of $[H_t^2]^{1/2}$

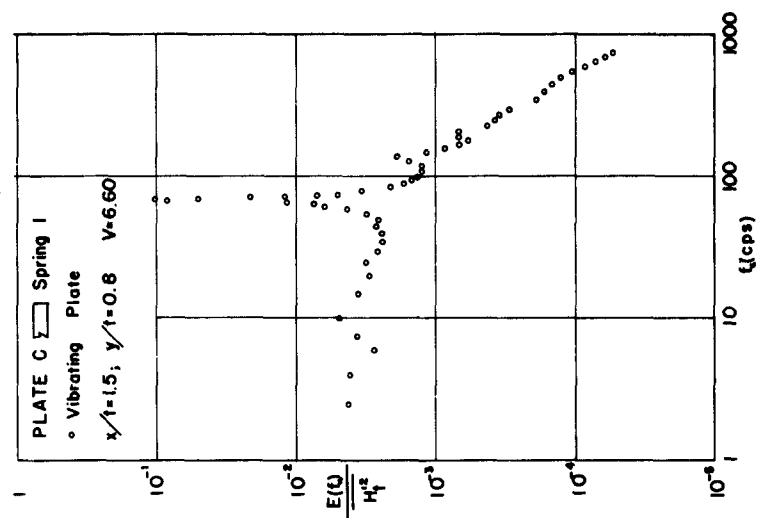


Fig. A2 Normalised Spectral Distributions of $[H_t^2]^{1/2}$

(Note: Units of velocity, V , are fps)

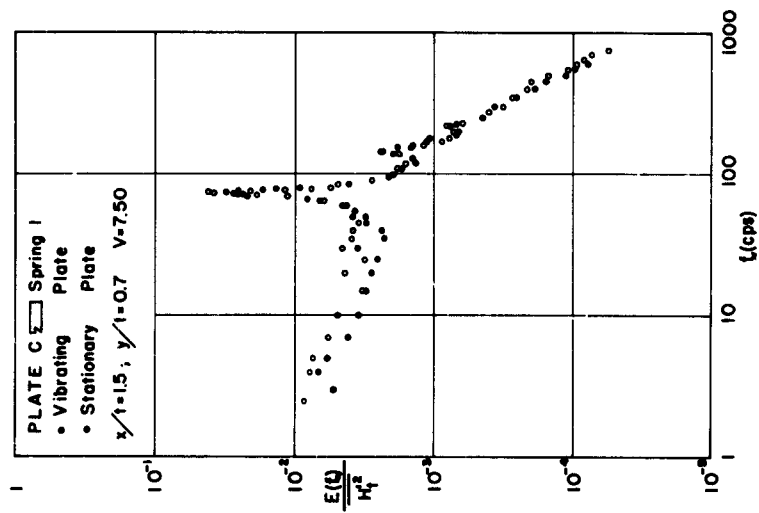


Fig. A4 Normalised Spectral Distributions of $[H_c^2]^{1/2}$

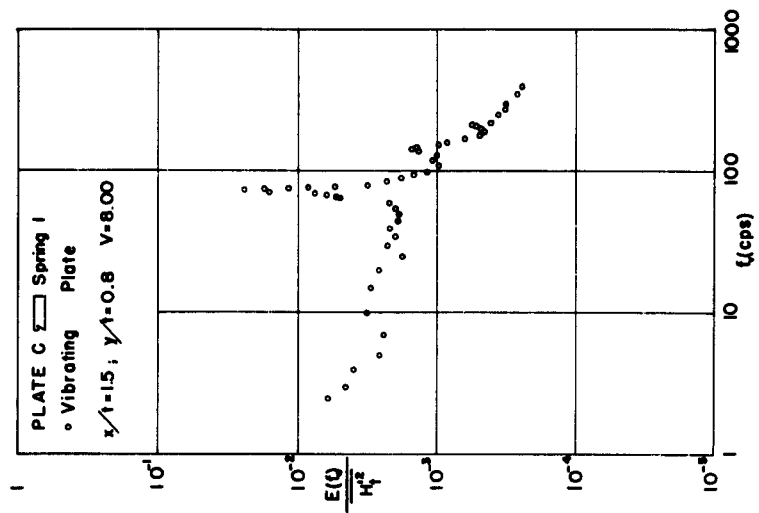


Fig. A5 Normalised Spectral Distributions of $[H_c^2]^{1/2}$

(Note: Units of velocity, V, are fps)

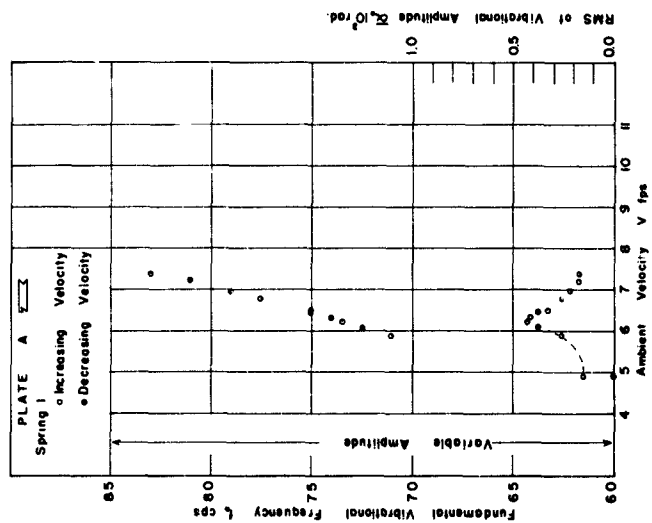


Fig. A6 Frequency-Amplitude vs. Ambient Velocity, Plate A

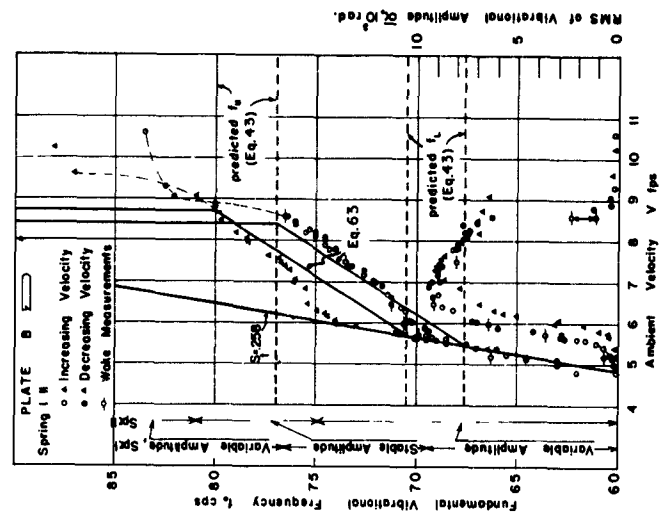


Fig. A7 Frequency-Amplitude vs. Ambient Velocity, Plate B

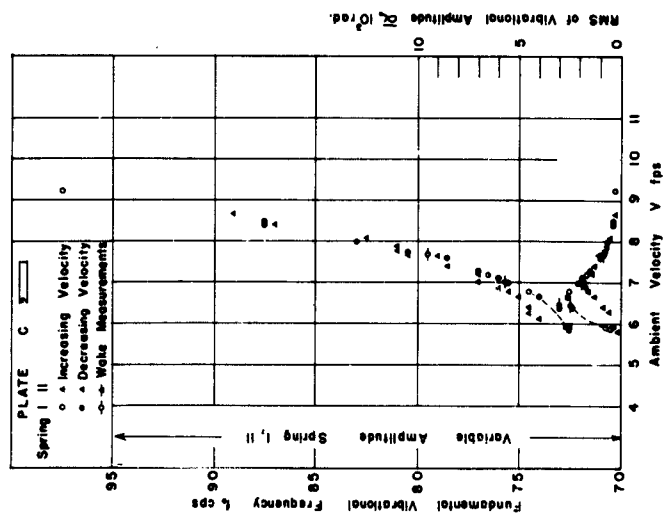


Fig. A8 Frequency-Amplitude vs. Ambient Velocity, Plate C

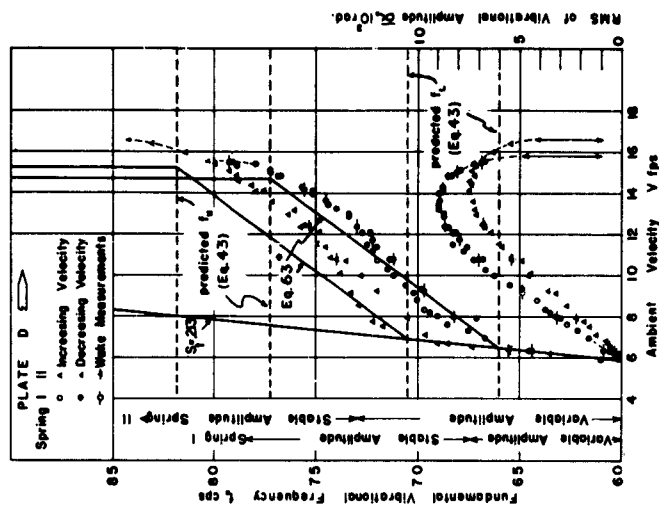


Fig. A9 Frequency-Amplitude vs. Ambient Velocity, Plate D

(*Using $C_{LI} = 0.00125$ in Eq. 63)

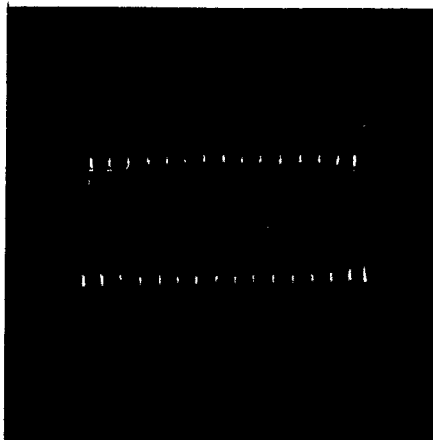


Fig. A10 Vibrational Signal
Plate B - Spring I
Range II
Stable Vibrations
 $V = 6.47 \text{ fps}$,
 $\bar{\alpha}_0 = 9.15 \cdot 10^{-3} \text{ rad.}$,
 $f_0 = 71.2 \text{ cps}$.

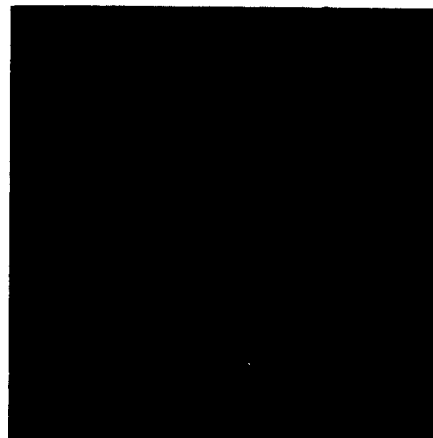


Fig. A11 Vibrational Signal
Plate B - Spring I
Range II
Stable Vibrations
 $V = 7.17 \text{ fps}$,
 $\bar{\alpha}_0 = 8.91 \cdot 10^{-3} \text{ rad.}$,
 $f_0 = 72.6 \text{ cps}$.



Fig. A12 Vibrational Signal
Plate B - Spring I
Point of Intermittancy
between Range II, III
 $V = 8.60 \text{ fps}$,
 $\bar{\alpha}_0 = 2.35 - 1.08 \cdot 10^{-3} \text{ rad.}$,
 $f_0 = 76.3 \text{ cps}$.



Fig. A13 Vibrational Signal
Plate B - Spring I
Point of Intermittancy
between Range II, III
 $V = 8.60 \text{ fps}$,
 $\bar{\alpha}_0 = 2.35 - 1.08 \cdot 10^{-3} \text{ rad.}$,
 $f_0 = 76.3 \text{ cps}$.

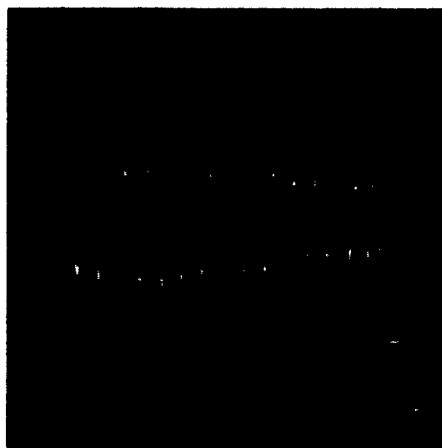


Fig. A14 Vibrational Signal
Plate D - Spring I
Range I
Unstable Vibrations
 $V = 6.37$ fps,
 $\bar{\omega}_0 = 0.86 \cdot 10^{-3}$ rad.,
 $f_0 = 64.4$ cps.



Fig. A15 Vibrational Signal
Plate D - Spring I
Range II
Stable Vibrations
 $V = 9.29$ fps,
 $\bar{\omega}_0 = 4.86 \cdot 10^{-3}$ rad.,
 $f_0 = 69.7$ cps.



Fig. A16 Vibrational Signal
Plate D - Spring I
Range II
Stable Vibrations
 $V = 9.29$ fps,
 $\bar{\omega}_0 = 4.86 \cdot 10^{-3}$ rad.,
 $f_0 = 69.7$ cps.



Fig. A17 Vibrational Signal
Plate D - Spring I
Range II
Stable Vibrations
 $V = 14.20$ fps,
 $\bar{\omega}_0 = 8.74 \cdot 10^{-3}$ rad.,
 $f_0 = 75.5$ cps.

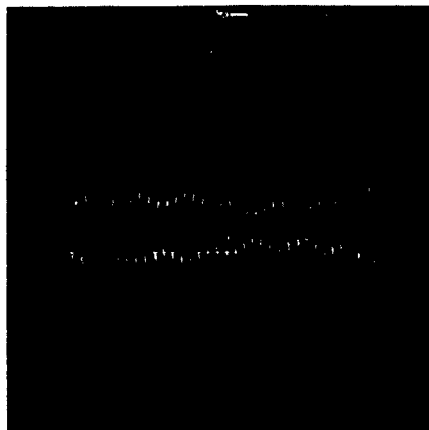


Fig. A18 Vibrational Signal
 Plate C - Spring II
 Unstable Vibrations of
 varying amplitude
 $V = 6.46 \text{ fps.}$
 $\overline{\alpha}_0 = 1.52 \cdot 10^{-3} \text{ rad.},$
 $f_0 = 74.5 \text{ cps.}$

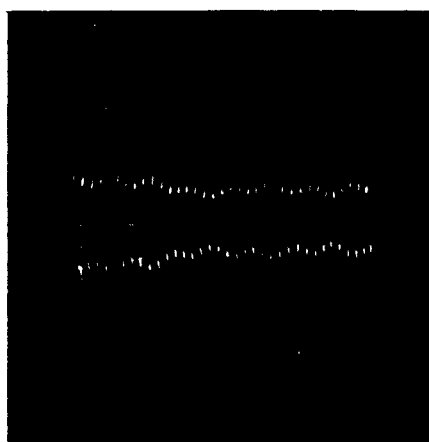


Fig. A19 Vibrational Signal
 Plate C - Spring II
 Unstable Vibrations of
 varying amplitude
 $V = 7.03 \text{ fps.}$
 $\overline{\alpha}_0 = 1.75 \cdot 10^{-3} \text{ rad.},$
 $f_0 = 77.0 \text{ cps.}$

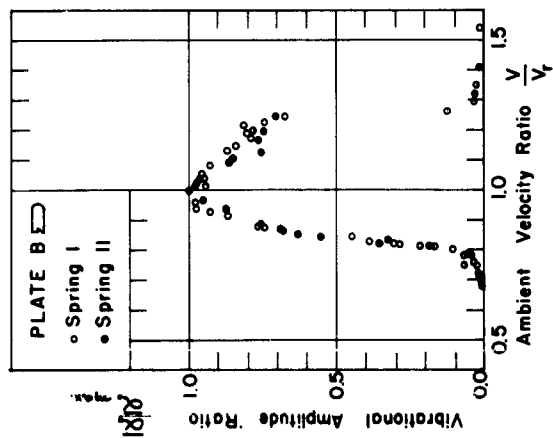


Fig. A20 Normalised Response Curve, Plate B

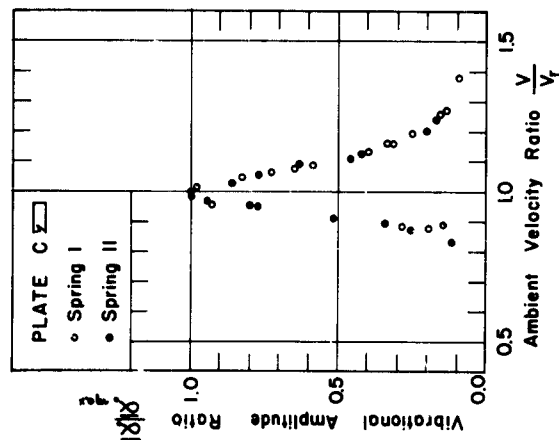


Fig. A21 Normalised Response Curve, Plate C

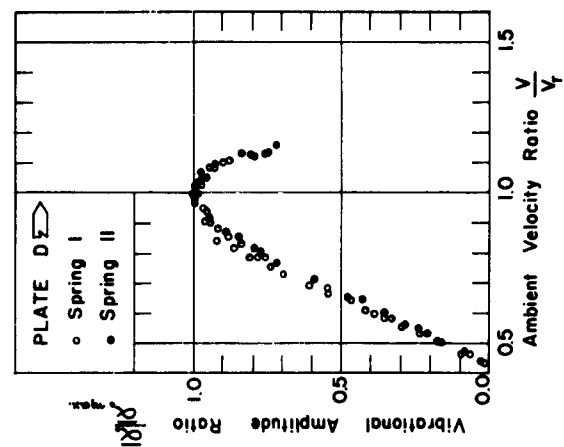


Fig. A22 Normalised Response Curve, Plate D

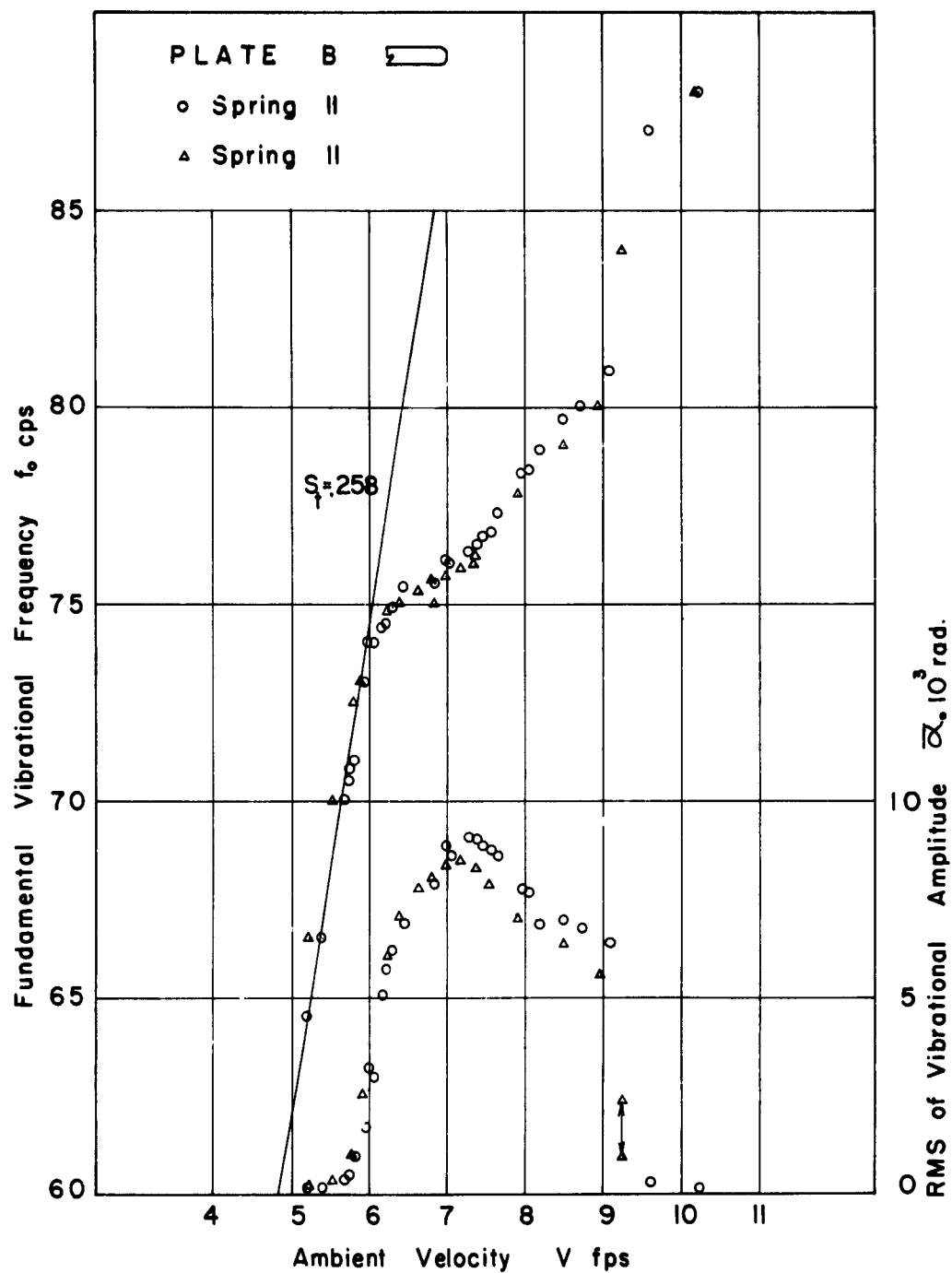


Fig. A23 Reproducibility of Results, Plate B - Spring II

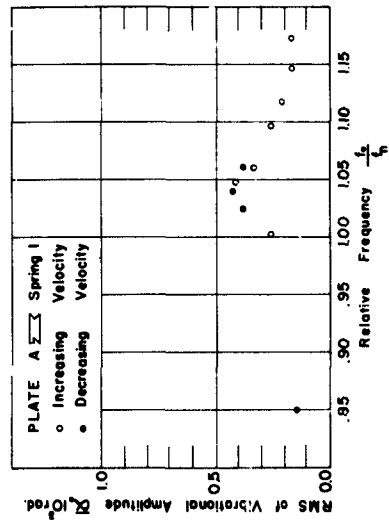


Fig. A24 Response Curve, Plate A

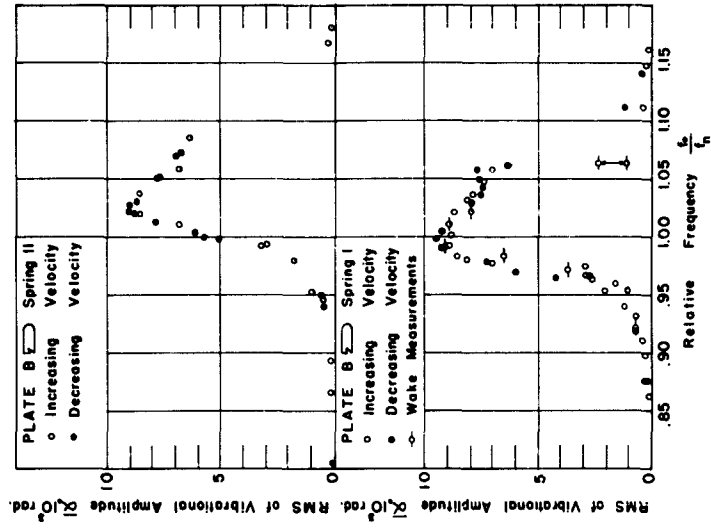


Fig. A25 Response Curve, Plate B

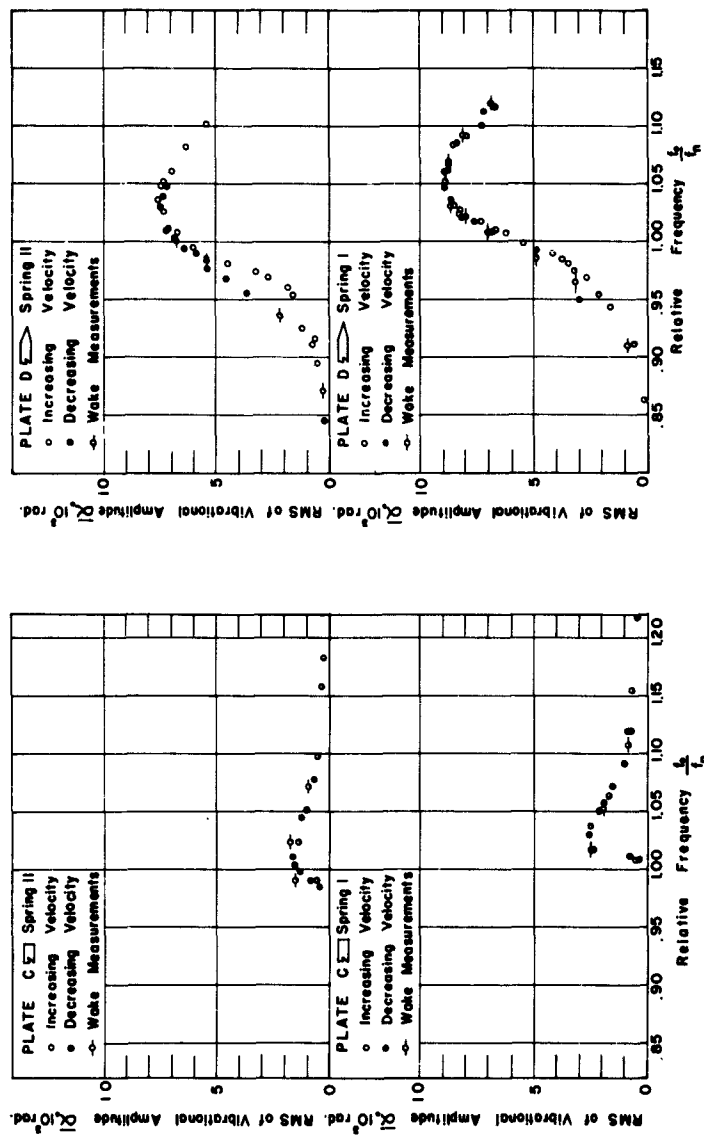


Fig. A26 Response Curve, Plate C

Fig. A27 Response Curve, Plate D

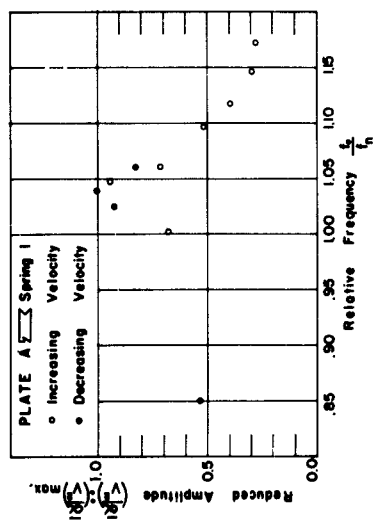


Fig. A28 Reduced Response Curve, Plate A

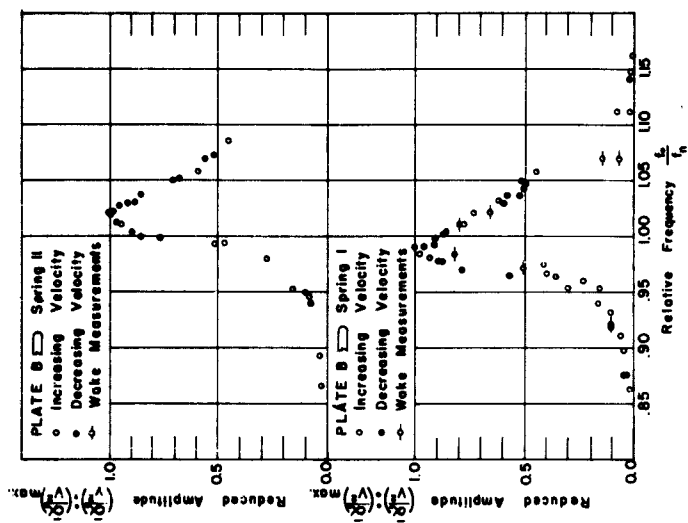


Fig. A29 Reduced Response Curve, Plate B

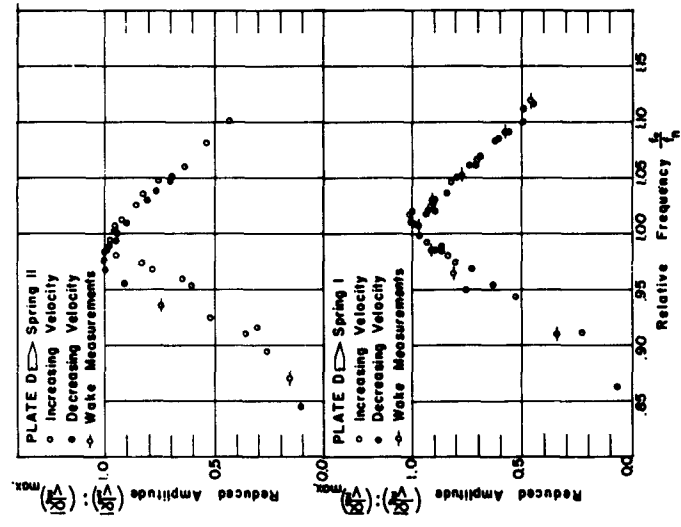


Fig. A31 Reduced Response Curve, Plate D

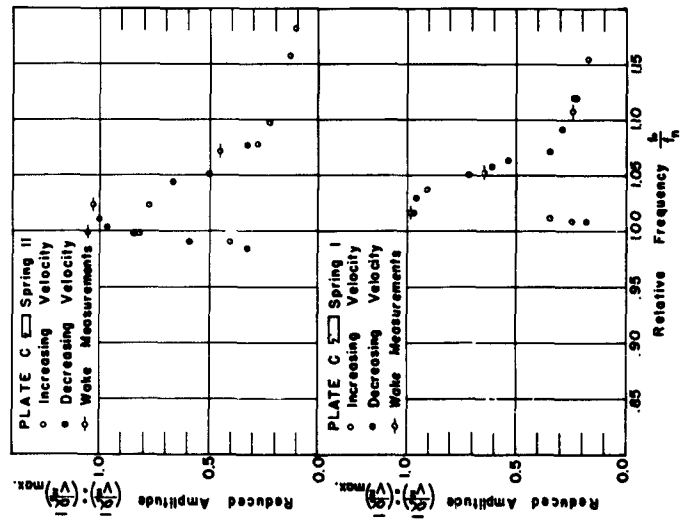


Fig. A30 Reduced Response Curve, Plate C

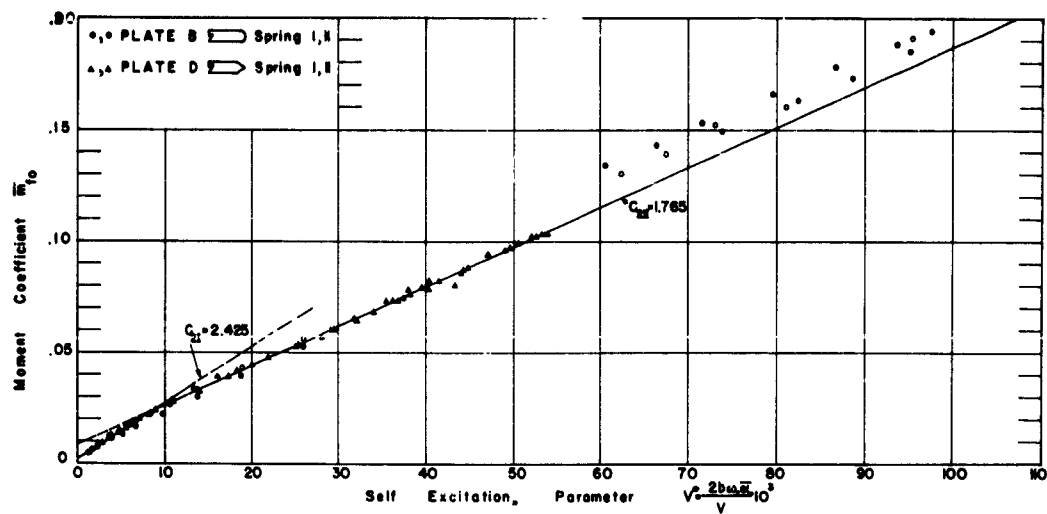


Fig. A32 The Moment Coefficient

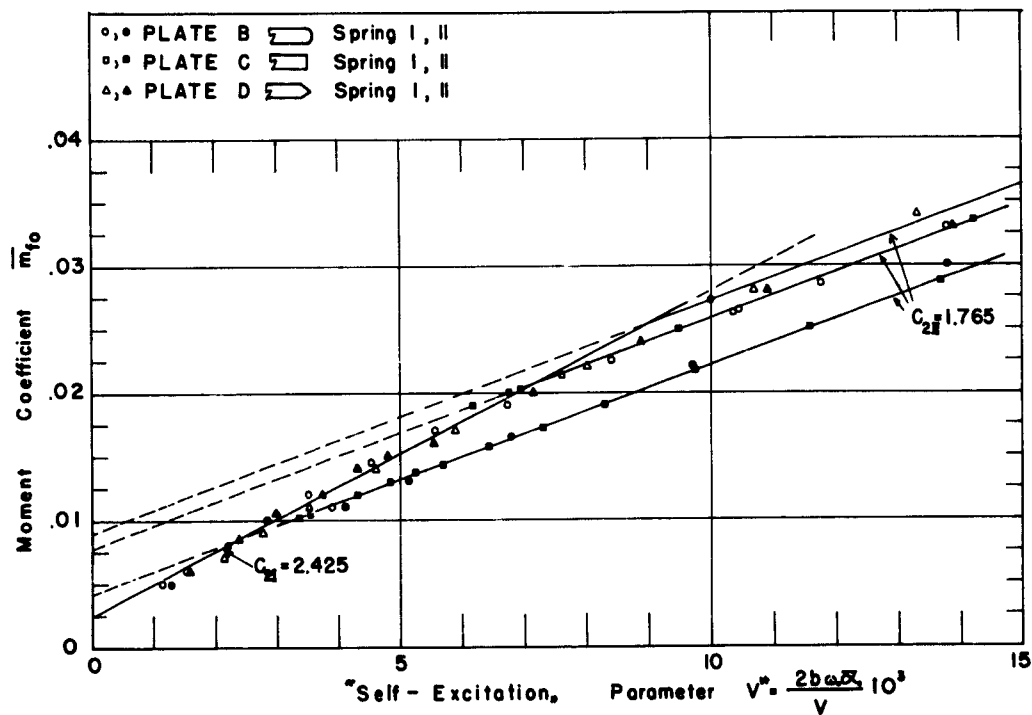


Fig. A33 The Moment Coefficient, Expanded Scale

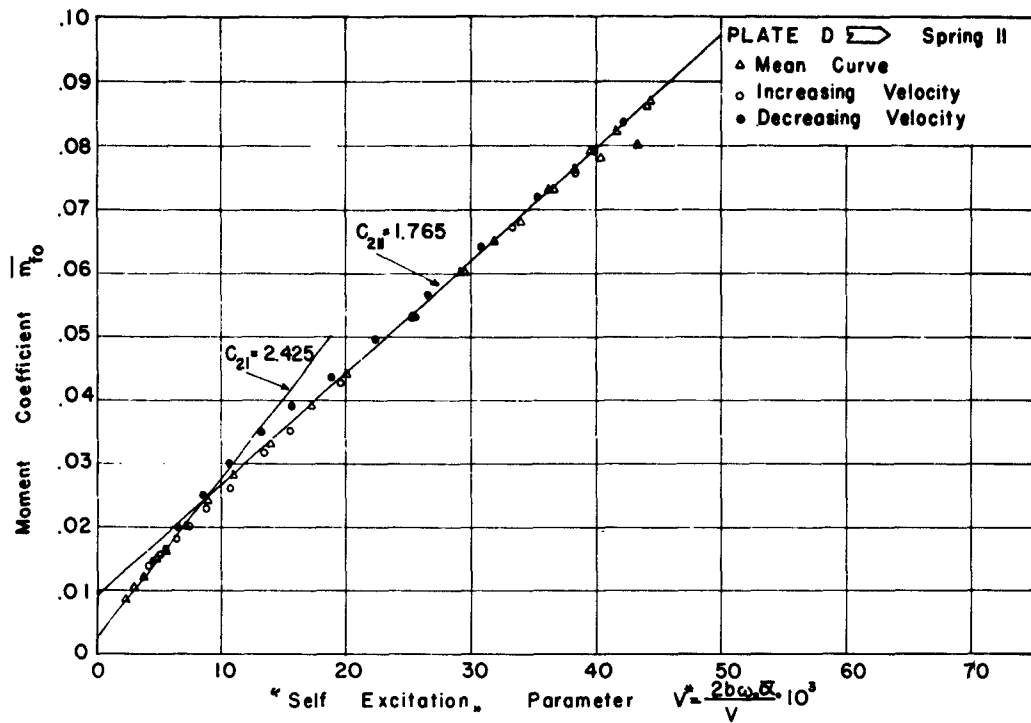


Fig. A34 The Moment Coefficient, Hysteresis Effect

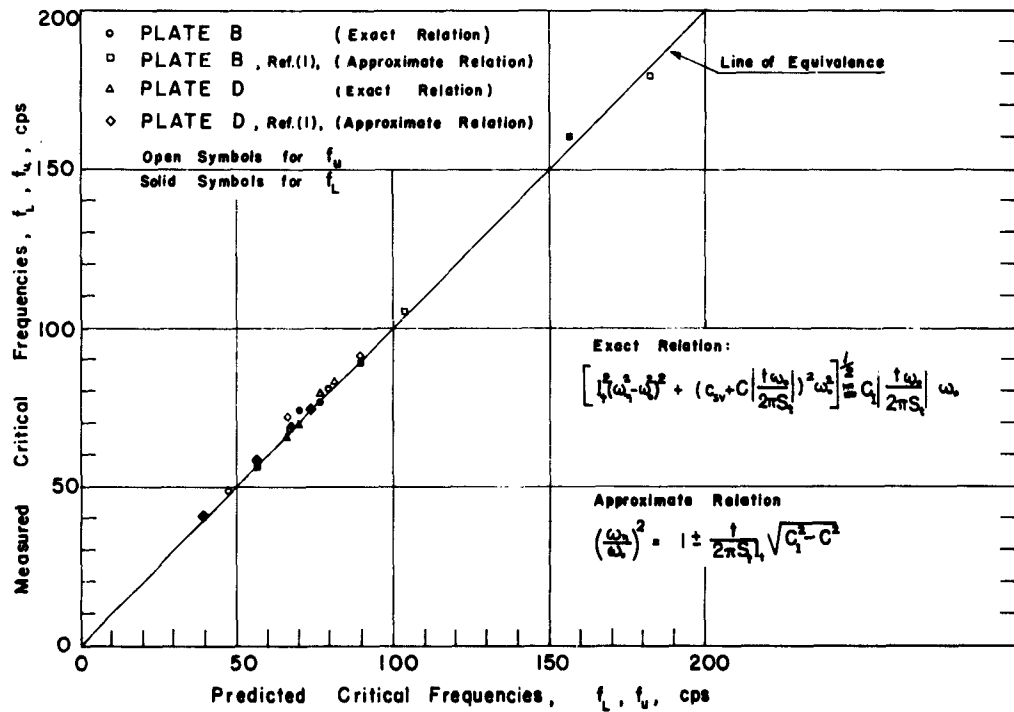


Fig. A35 Prediction of Critical Frequencies

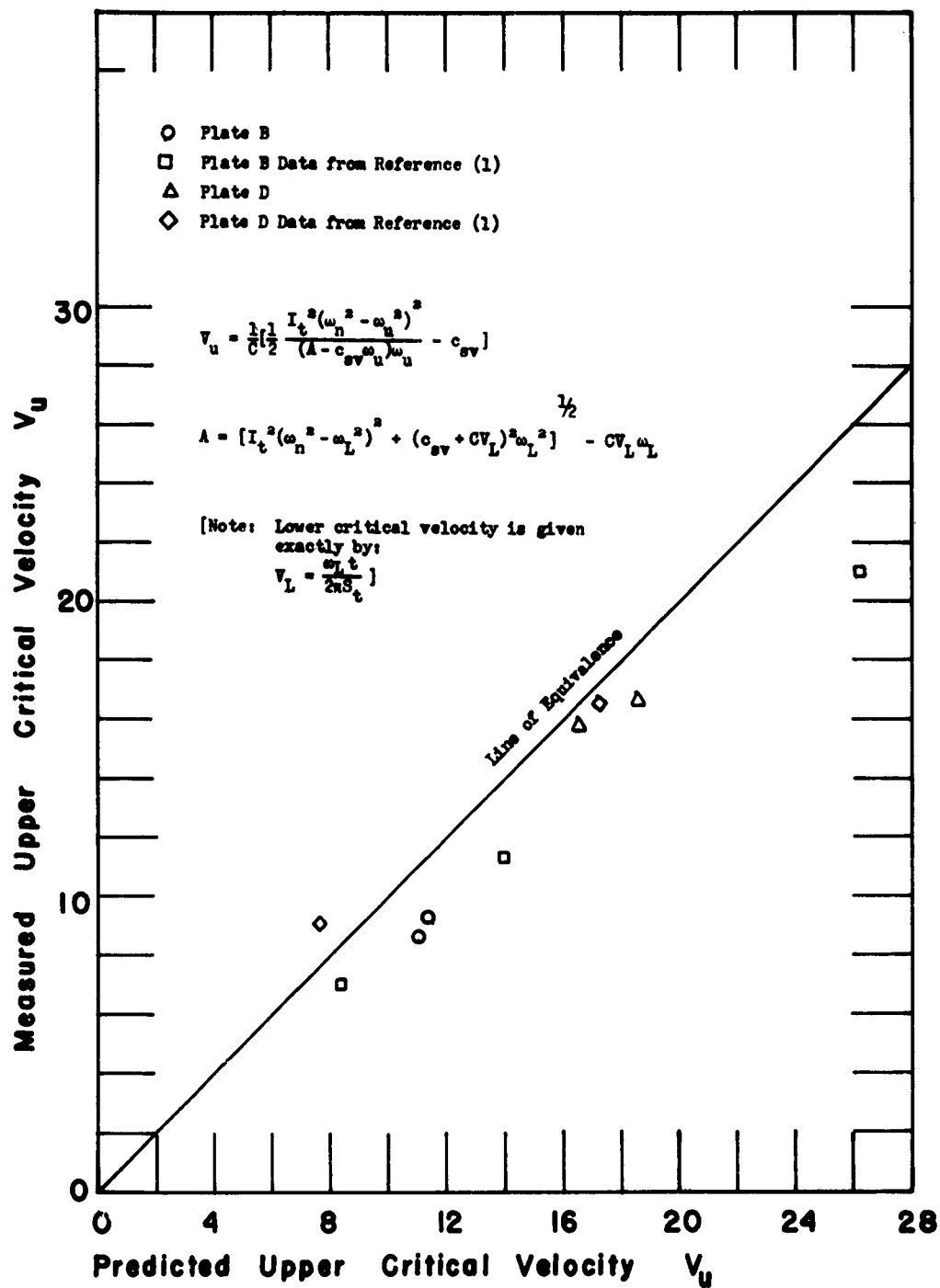


Fig. A36 Prediction of Critical Velocities

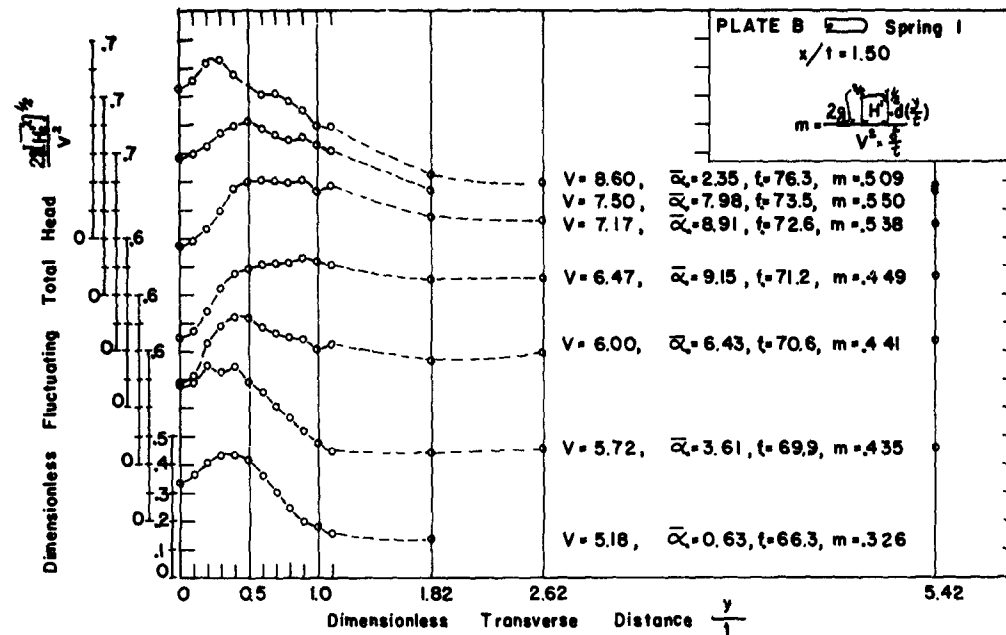


Fig. A37 Transverse Wake Profiles - Fluctuating Total Head, Plate B

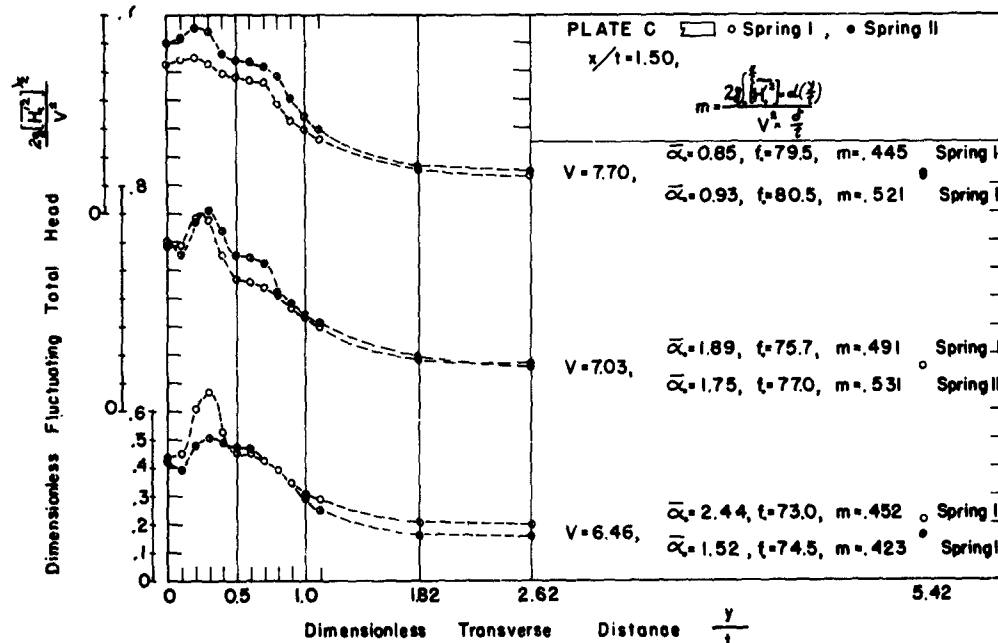


Fig. A38 Transverse Wake Profiles - Fluctuating Total Head, Plate C

(Note: In above figures, V in fps, $\bar{\alpha}_0$ in 10^{-3} rad., f_0 in cps)

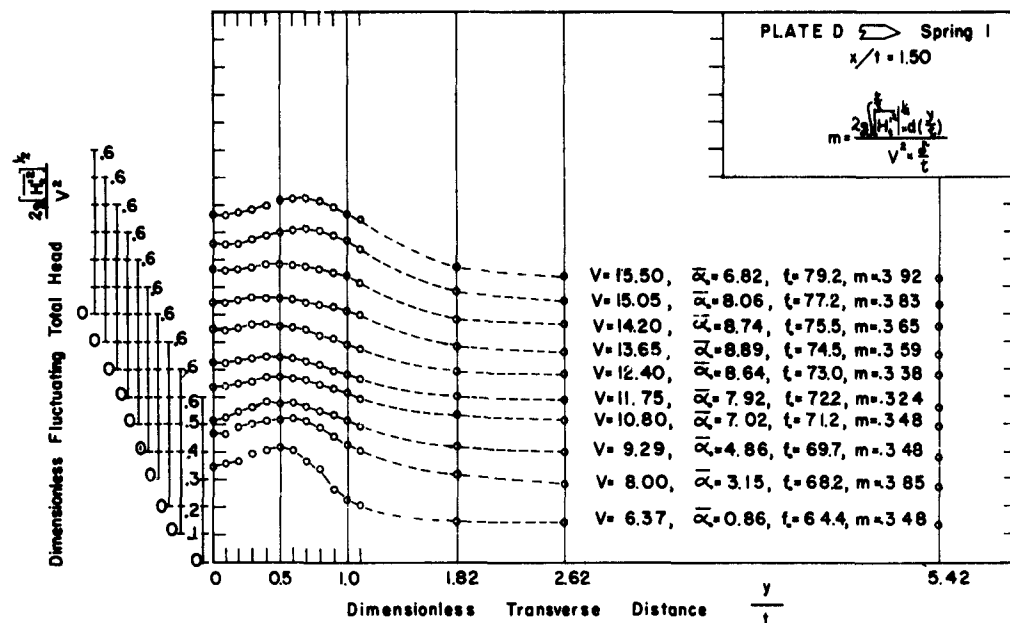


Fig. A-9 Transverse Wake Profiles - Fluctuating Total Head, Plate D

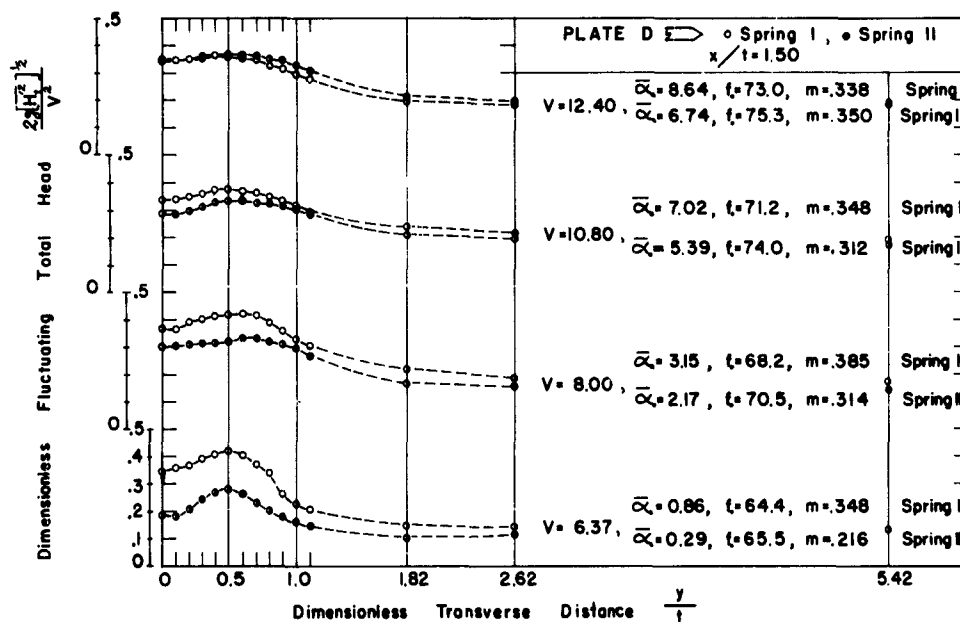


Fig. A-10 Transverse Wake Profiles - Fluctuating Total Head, Plate D

(Note: In above figures, V in fps, $\bar{\alpha}_0$ in 10^{-3} rad., f_0 in cps)



Plate D-Spring II

$V = 13.50 \text{ fps}$ $\bar{\alpha}_0 = 7.41 \cdot 10^{-3} \text{ rad.}$

$f_0 = 77.9 \text{ cps}$

Total Head Fluctuation

Gage at $\frac{Y}{t} = 5.42$



Plate D-Spring II

$V = 9.60 \text{ fps}$ $\bar{\alpha}_0 = 4.44 \cdot 10^{-3} \text{ rad.}$

$f_0 = 73.0 \text{ cps}$

Total Head Fluctuation

Gage at $\frac{Y}{t} = 5.42$

Fig. A41 Vibrational Signal vs. Total Head Fluctuation Signal

APPENDIX B

Spring Calibration and Free Oscillation Tests

1. Spring Calibration

It can be shown theoretically (43) that the unbalanced voltage, ΔE , (in millivolts) across a 4 active arm strain gage bridge arrayed for torsion measurement, is related to the excitation voltage, E , (in volts) and the angular deflection, α , (in radians) by the expression:

$$\Delta E = G_s E \alpha$$

in which G_s is the torsion spring calibration constant in millivolts per radian per volt of excitation.

G_s was determined experimentally by an in-place calibration. To accomplish this, the set-screws which fasten the plate shaft to the spring were replaced by two long stainless steel rods threaded at one end to insure the shaft-to-spring rigidity. Applying a force to one rod caused the other to deflect. This deflection was measured to the nearest 0.001 inch with a micrometer at a distance of 10 inches from the spring axis. The bridge output was amplified 500 or 1000 times and measured with a D.C. voltmeter.

Each spring was tested in both directions to check its symmetrical behavior and with increasing and decreasing deflection to check any hysteresis. Each spring was calibrated in place at the beginning and at the end of vibrational tests with every plate-spring system in order to check possible spring fatigue. Fig. B1 shows one of the calibration graphs obtained.

The spring sensitivity G_s for each plate-spring system is indicated below.

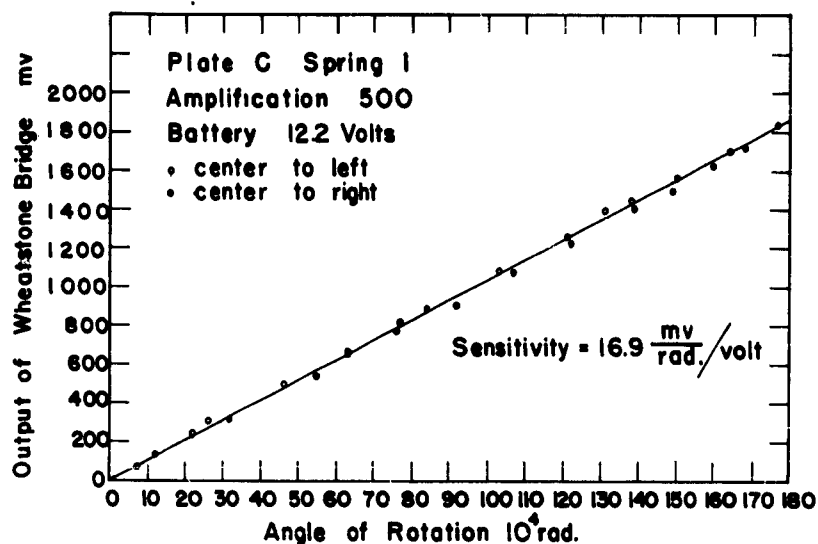
Exploratory Tests

Plate C - Spring I $G_s = 16.9 \frac{\text{mv}}{\text{rad-volt of Batt.}}$

Final Tests

G_s in $\frac{\text{mv}}{\text{rad-volt of Battery}}$

<u>Plate</u>	<u>Spring I</u>	<u>Spring II</u>
B	17.2	18.13
D	17.34	18.27
C	16.78	18.26
A	16.78	-----



B1 Sample of Spring Calibration

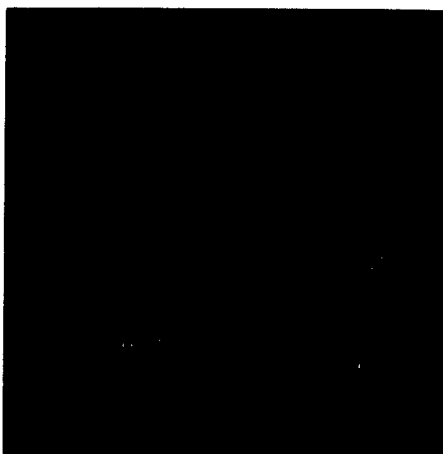


Plate D - Spring II
 Beginning of Tests

$$f_n \text{ air} = 153 \text{ cps.}$$

$$\frac{c_s}{c_c} = 1.042 \%$$

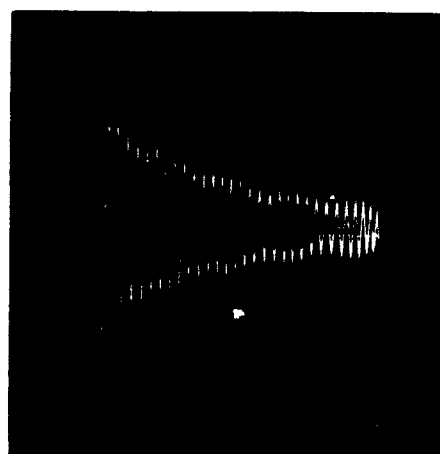


Plate B - Spring I
 Beginning of Tests

$$f_n = 75.8 \text{ cps.}$$

$$\frac{c_{sv}}{c_c} = 1.05 \%$$

B2 Free Oscillation Test in Air

B3 Free Oscillation Test in Still Water

Simultaneous measurement of the force applied to produce the deflections allows determination of the structural spring constant, K_s .

2. Free Oscillation Tests

In order to determine the plate-spring system constants, free oscillation tests were performed in air (water tunnel empty) and in still water:

Free oscillation tests in air:

Assuming linear damping, the equation of motion for the plate-spring system in air is:

$$I_s \ddot{\alpha} + c_s \dot{\alpha} + K_s \alpha = 0$$

Under the initial conditions:

$$\alpha = \alpha_0 \text{ and } \dot{\alpha} = 0 \text{ at } t = 0,$$

the solution of the above equation yields

$$\omega_n \text{ in air} = \sqrt{\frac{K_s}{I_s} - \frac{c_s^2}{4I_t^2}}$$

$$\text{or for } \frac{c_s^2}{4I_t^2} \ll \frac{K_s}{I_s} :$$

$$\omega_n \text{ in air} \approx \sqrt{\frac{K_s}{I_s}}$$

Free oscillation tests in still water:

Again assuming linear damping, the equation of motion for the plate-spring system in still water is:

$$(I_s + I_p) \ddot{\alpha} + (c_s + c_v) \dot{\alpha} + K_s \alpha = 0$$

or

$$I_t \ddot{\alpha} + c_{sv} \dot{\alpha} + K_s \alpha = 0$$

Under the initial conditions:

$$\alpha = \alpha_0 \text{ and } \dot{\alpha} = 0 \text{ at } t = 0,$$

the solution yields:

$$\omega_n \text{ in still water} = \sqrt{\frac{K_s}{I_t} - \frac{c_{sv}^2}{4I_t^2}}$$

$$\text{or for } \frac{c_{sv}^2}{4I_t^2} \ll \frac{K_s}{I_t} :$$

$$\omega_n \text{ in still water} \approx \sqrt{\frac{K_s}{I_t}}$$

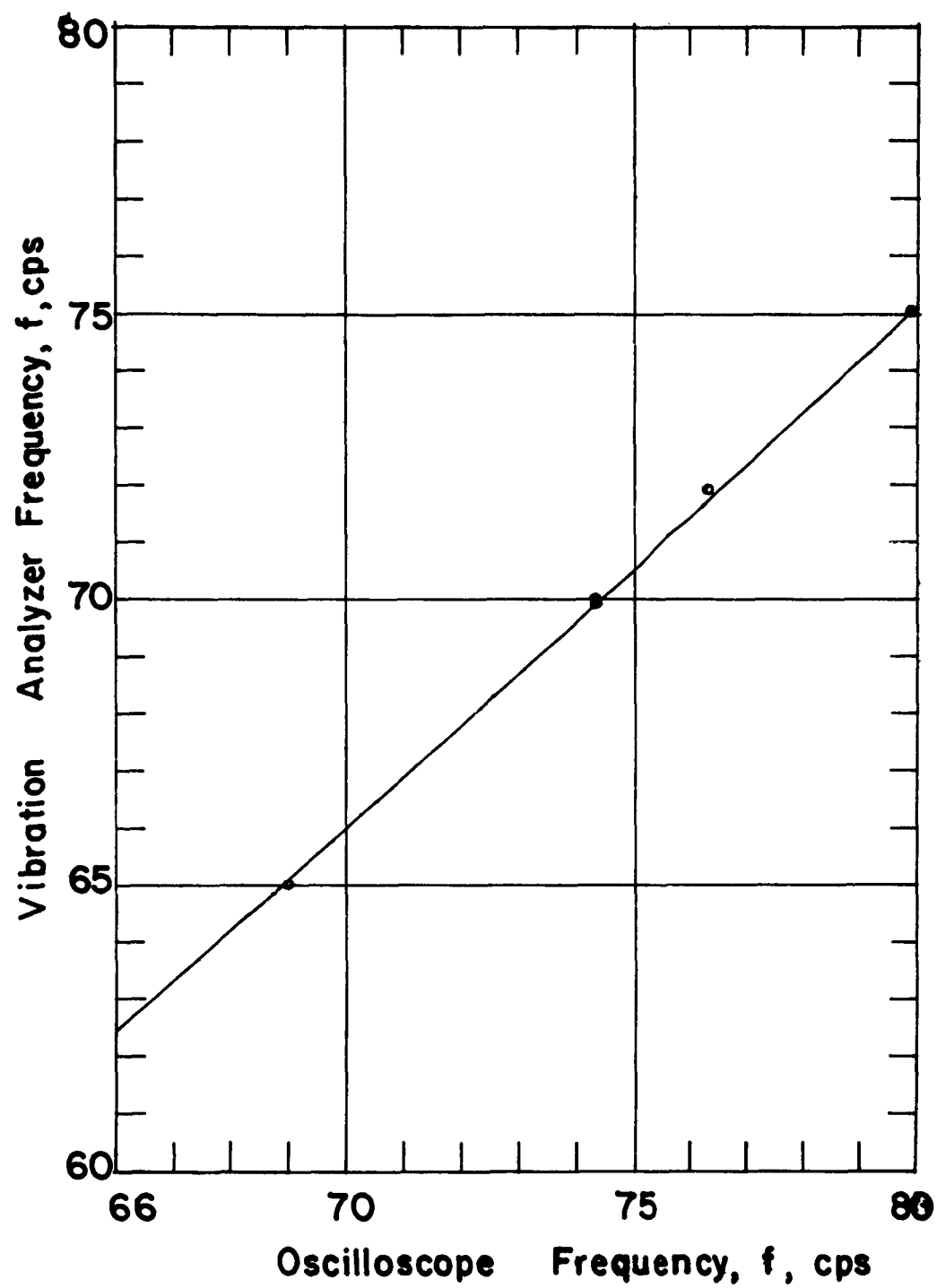
For the tests in air the plate was very easily deflected and suddenly released by striking it. The decaying oscillation was photographed by using a polaroid camera fitting on the screen of the oscilloscope. For the tests in still water it was impossible to strike the plate; instead the spring itself was given a deflection and then suddenly released.

Figures B2, B3 are samples of the free damped oscillations obtained.

Knowing the sweep rate of the oscilloscope signal the frequency of oscillation was easily obtained from the pictures. Several pictures were taken for each plate spring system and the average value of frequency f_n in air and f_n in still water was considered the true value. The experimental error in determining the frequency from the pictures is about 1.5%.

The damping coefficients c_s and c_{sv} were also obtained from the free oscillation pictures by the conventional method of determining the average logarithmic decrement for successive oscillations. For each plate-spring system, the coefficients were determined from several pictures and averaged. Although the assumption of linear damping proved satisfactory, the individual coefficients showed a scatter of up to 10% of the average value.

During the course of experiments it was discovered that the frequency recorded by the vibration analyzer and the oscilloscope were not exactly the same. Therefore a calibration test of the oscilloscope versus the vibration analyzer was performed. A sinusoidal electrical signal from a signal generator was fed to the vibration analyzer and the oscilloscope simultaneously. From pictures taken the frequency given by the oscilloscope was determined and plotted versus the frequency obtained by the vibration analyzer. A linear relationship was established as is shown in Fig. B4. The graph, B4, was used to reduce the natural frequencies obtained by the oscilloscope to the corresponding vibration analyzer frequencies.



B4

Calibration of Oscilloscope versus Vibration Analyzer

APPENDIX C

References

1. Ippen, A.T., Toebes, G.H., Eagleson, P.S.: "The Hydroelastic Behavior of Flat Plates as Influenced by Trailing Edge Geometry", MIT Hydro. Lab., T.R. 36, April 1960.
2. Eagleson, P.S., Huval, C.J., Perkins, F.E.: "Turbulence in the Early Wake of a Fixed Flat Plate", MIT Hydro. Lab., T.R. 46, February 1961.
3. Petersen, E.J., Sylvester, G.D.: "An Investigation of the Early Wake Behind Submerged Flat Plates as Influenced by Trailing Edge Configuration", Thesis for the Naval Engineer degree, MIT Course XIII, May 1961 (unpublished).
4. Eagleson, P.S., Daily, J.W., Grace, R.A.: "The Effects of Trailing Edge Geometry and Chord Length on the Early Wake of Stationary Flat Plates", MIT Hydro. Lab. R 51, April 1962.
5. Dockstader, E.A., Swiger, W.F., Ireland, E.: "Resonant Vibrations of Steel Stacks", Trans. ASCE, Vol. 121, 1956.
6. Parmakian, J., Jacobson, R.S.: "Measurement of Hydraulic-Turbine Vibration", Trans. ASME, Vol. 74, 1952.
7. Donaldsen, R.M.: "Hydraulic-Turbine Runner Vibrations", Trans. ASME, Vol. 78, 1956.
8. Heskestad, G., Olberts, D.R.: "Influence of Trailing Edge Geometry on Hydraulic-Turbine Blade Vibration Resulting from Vortex Excitation", Proc. ASME, paper No. 59-Hyd. 7, May 1959.
9. Conn, J.F.C.: "Marine Propeller Blade Vibrations", Inst. of Eng. and Shipb. Scot., 1939.
10. Hughes, W.L.: "Propeller Blade Vibrations", N.E.C. Inst. of Eng. and Shipb. Scot., Vol. 65, 1949.
11. Gongwer, G.A.: "A Study of Vanes Singing in Water", J. of Applied Mech., Vol. 19, No. 4, 1952.
12. Dickey, D.L., Woodruff, G.B.: "The Vibrations of Steel Stacks", Proc. ASCE, Sep. No. 540, Nov. 1954.

13. Penzien, J.: "Wind Induced Vibration of Cylindrical Structures", Proc. ASCE, Paper 1191, 1957.
14. Marris, A.W., Brown, O.G.: "Hydrodynamically Excited Vibrations of Cantilever-Supported Probes", ASME Paper No. 62-Hyd. 7, 1962.
15. Price, P.: "Suppression of the Fluid Induced Vibration of Circular Cylinders", Proc. ASCE, Paper 1030, July 1956.
16. Weaver, W., Jr.: "Experimental Investigation of Wind-Induced Vibrations in Antenna Members", MIT Lincoln Lab., Group Report No. 75-4, August 1959.
17. Baird, R.C.: "Wind Induced Vibration of a Pipe-Line Suspension Bridge and its Cure", Trans. ASME, Vol. 77, No. 6, August 1955.
18. Shannon, J.F., Arnold, R.M.: "Statistical and Experimental Investigations on the Singing Propeller Problem", Trans. Inst. of Eng. and Shipb. Scot., Vol. 82, 1939.
19. Kirchhoff, G.: "Zur Theorie freier Flüssigkeitsstrahlen", J. Reine Angew. Math. 70, 289-298, 1869.
20. Karman, Th. von: "Über den Mechanismus des Widerstandes den ein bewegter Körper in einer Flüssigkeit erfährt", Gott. Nachr., 547-556, 1912.
21. Karman, Th. von, Rubach, M.: "Über den Mechanismus des Flüssigkeits- und Luftwiderstandes", Phys. Zeit. 13, 49-59, 1912.
22. Rosenhead, L.: "The Spread of Vorticity in the Wake Behind a Cylinder", Proc. R. S. of London, Ser. A, Vol. 127, 1930.
23. Tyler, E.: "Vortices Behind Aerofoil Sections and Rotating Cylinders", Phil. Mag., Ser. 7, Vol. 5, 1928.
24. Fage, A., Johansen, F.C.: "On the Flow of Air Behind an Inclined Flat Plate of Infinite Span", Proc. Roy. Soc. London, Ser. A, Vol. 116, 1927.
25. Taneda, S.: "Oscillation of the Wake Behind a Flat Plate Parallel to the Flow", J. Phys. Soc. Japan, Vol. 13, No. 4, 1958.
26. Goldstein, S.: "Modern Developments in Fluid Dynamics", Oxford University Press, London, Vol. 2, 1938.
27. Hooker, S.G.: "On the Action of Viscosity in Increasing the Spacing Ratio of a Vortex Street", Proc. Roy. Soc. London, Ser. A, Vol. 154, 1936.

28. Birkhoff, G.: "Formation of Vortex Streets", J. Appl. Phys., Vol. 24.
29. Heisenberg, W.: "Die absoluten Dimensionen der Karmanschen Wirbelbewegung", Phys. Zeit. 23, 1922.
30. Prandtl, L., Tietjens, D.G.: "Applied Hydro- and Aero-Elasticity", Dover Press, 1957.
31. Roshko, A.: "On the Development of Turbulent Wakes from Vortex Streets", NACA Rep. 1191, 1954.
32. Tyler, E.: "Vortex Formation Behind Obstacles of Various Sections", Phil. Mag., Ser. 7, Vol. 11, 1931.
33. Fage, A., Johansen, F.C.: "The Structure of Vortex Sheets", Phil. Mag., Ser. 7, Vol. 5, 1928.
34. Delany, N.K., Sorensen, N.E.: "Low Speed Drag of Cylinders of Various Shapes", NACA, T.N. 3038, Nov. 1953.
35. Makovsky, M.S.: "Vortex Induced Vibration Studies", DTMB Navy Dept., Report 1190, 1958.
36. McGregor, D.M.: "An Experimental Investigation of the Oscillating Pressures on a Circular Cylinder in a Fluid Stream", University of Toronto A.T.N., 14, 1957.
37. Gerrard, J.H.: "Measurement of the Fluctuating Pressure on the Surface of a Circular Cylinder", Aeronautical Research Council, 19, 844, F.M. 2637, 1958.
38. Theodorsen, T.: "General Theory of Aerodynamic Stability and the Mechanism of Flutter", NACA, R 496, 1935.
39. Toebes, G.H., Perkins, F.E., Eagleson, P.S.: "Design of a Closed Jet, Open Circuit Water Tunnel for the Study of Wake Mechanics", MIT, T.N. 3, Hydro. Lab., April 1958.
40. Perkins, F.E., Eagleson, P.S.: "The Development of a Total Head Tube for High Frequency Pressure Fluctuations in Water", MIT Hydro. Lab., T.N. 5, July 1959.
41. Bisplinghoff, R.L., Ashley, H., Halfman, R.L.: "Aeroelasticity", Addison-Wesley Publishing Co. Inc., 1957.
42. Ippen, A.T., Tankin, R.S., Raichlen, R.: "Turbulence Measurements in Free Surface Flow with an Impact Tube-Pressure Transducer Combination", MIT Hydro. Lab. T.R. 20, 1955.

43. Noutsopoulos, G.K.: "Flow-Induced Vibrations of Flat Plates: Moment Coefficients and Wake Structure", ScD. Thesis, MIT Department of Civil Engineering, Sept. 1962.
44. Roshko, A.: "On the Drag and Shedding Frequency of Two-Dimensional Bluff Bodies", NACA TN 3169, Washington, July 1954.

APPROVED DISTRIBUTION LIST FOR
UNCLASSIFIED TECHNICAL NOTES ISSUED UNDER
CONTRACT Nonr-1841 (21)

Government Agencies

Commanding Officer and Director David Taylor Model Basin Washington 7, D. C. Attn: Code 513	(75)	Director Naval Research Laboratory Washington 25, D. C. Attn: Code 2021	(1)
Chief of Naval Research Department of the Navy Washington 25, D. C. Attn: Code 438	(3)	Documents Service Center Armed Services Technical Information Agency Arlington Hall Station Arlington 12, Virginia	(10)
Commanding Officer Office of Naval Research Branch Office 495 Summer Street Boston, Massachusetts	(1)	Chief, Bureau of Naval Weapons Department of the Navy Washington 25, D.C. Attn: Research Division	(2)
Commanding Officer Office of Naval Research Branch Office The John Crerar Library Bldg. 86 East Randolph Street Chicago 1, Illinois	(1)	Office of Ordnance Research Department of the Army Washington 25, D. C.	(1)
Commanding Officer Office of Naval Research Branch Office 346 Broadway New York 13, New York	(1)	Commander Air Research and Development Command Andrews Air Force Base Washington 25, D. C. Attn: Fluid Mechanics Division	(1)
Commanding Officer Office of Naval Research Branch Office 1030 East Green Street Pasadena 1, California	(1)	Director of Research National Aeronautics and Space Administration Langley Field, Virginia	(1)
Commanding Officer Office of Naval Research Branch Office 1000 Geary Street San Francisco 9, California	(1)	Director National Bureau of Standards Washington 25, D. C. Attn: Fluid Mechanics Branch Library	(1) (1)

	<u>Institutions</u>
Commanding Officer Office of Naval Research Navy No. 100, Fleet Post Office New York, New York	Stevens Institute of Technology Davidson Laboratory 711 Hudson Street Hoboken, New Jersey
(1)	(1)
Commander Naval Ordnance Test Station 3202 E. Foothill Blvd. Pasadena 8, California	California Institute of Tech. Division of Engineering Pasadena 4, California
(1)	(1)
Director U.S. Waterways Experiment Station Box 631 Vicksburg, Mississippi	Brown University Graduate Division of Applied Mathematics Providence 12, Rhode Island
(1)	(1)
Office of the Chief of Engineers Department of the Army Engineering Division, Civil Works Washington 25, D. C.	Stanford University Applied Mathematics and Statistics Laboratory Stanford, California
(1)	(1)
Beach Erosion Board U.S. Army Corps of Engineers 5201 Little Falls Road Washington 16, D. C.	Massachusetts Institute of Technology Department of Naval Architecture Cambridge 39, Massachusetts
(1)	(1)
Director Woods Hole Oceanographic Institute Woods Hole, Massachusetts	Ordnance Research Laboratory The Pennsylvania State University University Park, Pennsylvania
(1)	(1)
Commanding Officer and Director U.S.N. Underwater Sound Laboratory Fort Trumbull New London, Connecticut	Applied Mechanics Reviews Southwest Research Institute 8500 Culebra Road San Antonio 6, Texas
(1)	(1)
Chief, Bureau of Ships Department of the Navy Washington 25, D. C.	Institute of Fluid Mechanics University of Maryland College Park, Maryland
(1)	(1)
Attn: Research Division Code 341B, Ship Research Branch	Library, Institute of Aeronautical Sciences, Inc. 2 East 64th Street New York 21, New York
(1)	(1)
Code 345, Ship Silencing Branch	
(1)	
Code 430 (Preliminary Design)	
(1)	
Code 421 Technical Information Section	Librarian Society of Naval Architects and Marine Engineers 74 Trinity Place New York 6, New York
(3)	(1)
Code 320 Lab. Manage- ment	
(1)	